



ROMA TRE UNIVERSITÀ DEGLI STUDI

CORSO DI DOTTORATO XXVI CICLO

**Quark masses and pseudoscalar
decay constants with $N_f = 2 + 1 + 1$
twisted mass lattice QCD**

Author:
Lorenzo Riggio

Supervisor:
Prof. Vittorio Lubicz

October 2013

Contents

Introduction	iii
1 Flavor Physics	1
1.1 The Standard Model and the quark masses	1
1.2 The Cabibbo Kobayashi Maskawa Matrix	8
1.2.1 Definition & parametrization	8
1.2.2 CKM Unitarity relations	11
1.3 Leptonic decay constants	14
1.3.1 f_K/f_π and f_K	16
1.3.2 f_D and f_{D_s}	18
2 Lattice QCD	19
2.1 Lattice regularization	19
2.1.1 Fermionic Action	20
2.1.2 Regularization of Yang-Mills theory	23
2.2 Improvement	26
2.3 Twisted Mass Action	28
2.3.1 Automatic $O(a)$ improvement	31
2.3.2 Tuning to maximal twist	32
2.3.3 Twisted mass with non degenerate quarks	33
2.4 Numerical simulations	34
2.4.1 Integration of the fermionic degrees of freedom	34
2.4.2 Montecarlo method for the gauge configurations	35
2.4.3 Error analysis	35
2.4.4 Systematic effects	37
2.5 Two-point correlation functions	40

3	Quark Masses	45
3.1	Simulation details	46
3.1.1	The Action	46
3.1.2	Lattice set up used in this analysis	47
3.2	Analysis of the 2-point PS correlators	50
3.3	Average up and down quark mass	52
3.3.1	Analyses of the pion mass in units of r_0	54
3.3.2	Analyses of the pion mass in units of M_{ss}	60
3.3.3	Results in the pion sector.	64
3.4	Strange quark mass	70
3.4.1	Analyses of the kaon mass in units of r_0	72
3.4.2	Analyses of the kaon mass in units of M_{ss}	74
3.4.3	Results for the kaon sector	75
3.5	Determination of the ratio m_s/m_{ud}	79
3.6	Determination of the ratio m_u/m_d	81
3.7	Charm quark mass	83
3.7.1	Analyses of D and D_s meson masses in units of r_0	85
3.7.2	Analyses of D and D_s meson masses in units of M_{cs}	86
3.7.3	Results in the D sector	88
3.8	Determination of the ratio m_c/m_s	93
4	Leptonic decay constants	97
4.1	f_{K^+} and the ratio f_{K^+}/f_{π^+}	97
4.1.1	Analyses of f_K in units of r_0	100
4.1.2	Analyses of f_K in units of M_{ss}	105
4.1.3	Results for f_{K^+} and f_{K^+}/f_{π^+}	107
4.1.4	Analyses of the ratio f_K/f_π	111
4.2	f_{D_s}, f_D and the ratio f_{D_s}/f_D	113
4.2.1	Analyses of Φ_{D_s} in units of r_0	115
4.2.2	Analyses of Φ_{D_s} in units of M_{cs}	117
4.2.3	Analyses of the ratios Φ_{D_s}/Φ_D and $(f_{D_s}/f_D)/(f_K/f_\pi)$	117
4.2.4	Results for f_{D_s}, f_D and f_{D_s}/f_D	121
	Conclusions	125

Introduction

In this thesis we present an accurate lattice determination of the average up/down, strange and charm quark masses and of the decay constants f_K , f_K/f_π , f_D and f_{D_s} , using the gauge configurations produced by the European Twisted Mass (ETM) Collaboration. These decay constants in combination with the experimental measurements of appropriate leptonic decay rates provide the knowledge of the CKM matrix elements $|V_{ud}|$, $|V_{us}|$, $|V_{cd}|$ and $|V_{cs}|$.

The precise knowledge of the quark masses and of the CKM matrix elements plays a fundamental role both in testing the Standard Model (SM) and in the search for new physics (NP).

The Standard Model (SM) is the modern theory that describes the fundamental interactions among elementary particles.

So far the SM has proven remarkably successful in reproducing the experimental data. During the past forty years, many experiments have tested it obtaining very good agreement with theoretical predictions. Furthermore, in the last year a new particle with mass around 125 GeV and showing Higgs boson properties has been observed by ATLAS and CMS [1, 2]. After years of intense experimental search, it could be the Higgs boson of the SM, the last missing particle of the model to be discovered.

Despite its success in describing with high precision a wide variety of experimental results, there are several reasons to believe that the SM is not the final theory of particle interactions, but a low-energy approximation of a more fundamental theory.

The fact that the SM does not provide a description for the gravitational interaction is perhaps the most evident limit of the theory. Other missing pieces in the puzzle include: the instability of the Higgs mass to radiative corrections, the lack of a mechanism explaining the baryogenesis, the absence of a candidate for the dark matter, and its failure to truly unify all the fundamental forces together.

Beyond these issues, questions related with the flavor structure of the SM still remain unanswered. In particular, the fact that the model only parametrizes the observed hierarchy of particles mass and mixing angles through free parameters (limiting to the quark sector only: 6 masses, 3 angles and 1 complex phase), without providing an explanation for it.

These questions may find an answer in a more fundamental theory that manifest itself at some higher scale.

The search for new physics can be carried out by investigating directly higher and higher energies in particle accelerators as LHC, or looking at the indirect effects of new physics at lower scales, occurring through quantum loops. These effects should manifest as small corrections to the Standard Model predictions.

In the perspective of highlighting and quantifying the effects of new physics testing the predictions of the Standard Model, a dominant role is played by flavor physics, which, because of its highly non trivial structure, is particularly sensitive to higher scales.

This requires the precise knowledge of the parameters of the (hadronic) flavor sector which are the quark masses and the CKM matrix elements.

As far as the quark masses are concerned, on the theoretical side, explaining and understanding their hierarchical structure remains an open and fascinating challenge. On the phenomenological side, since several important observables depend on the quark masses, a precise determination of these values is crucial to constrain the SM.

The extraction of the values of the CKM matrix elements on the other hand, performed combining experimental inputs with theoretical calculations, represents the most tighten test of the Standard Model. In particular the decay constants calculated in this work can be used to test the unitarity constraints of the first two row of the CKM matrix.

In the determination of the quark masses and decay constants lattice QCD (LQCD) plays a primary role as it is a non-perturbative approach based on first principles only. It consists in simulating QCD itself by formulating the Lagrangian on a discrete and finite Euclidean space-time which allows for a numerical computation of the path integrals via Montecarlo methods. The finite volume, the lattice spacing and generally the lower bound on the simulated light quark masses, which are limited by the current available computing power, introduce errors which have to be well under control and accounted for.

Thanks to the increased computational power as well as to the algorithm and action improvements of the last decade, LQCD simulations have made significant progresses

reaching a remarkable level of precision. In particular, this is due to the so-called unquenched calculations, where the contribution of loops of dynamical sea quarks is taken into account. As a matter of fact, most of the recent lattice determinations of quark masses have been performed with either two (up and down) [3, 4] or three (up, down and strange) [5]-[12] dynamical sea quarks.

In this thesis we present a lattice calculation using the gauge configurations produced by the European Twisted Mass (ETM) Collaboration with four flavors of dynamical quarks ($N_f = 2 + 1 + 1$), which include in the sea, besides two light mass degenerate quarks, also the strange and the charm quarks with masses close to their physical values. Such a setup is the closest one to the real world, adopted till now only by the ETM [13, 14] and the MILC [15] Collaborations.

The thesis is organized as follows

- In Chapter 1 I will first discuss the flavor sector of the SM and its free parameters, paying a particular attention to the CKM flavor mixing matrix. I will then move to leptonic decays, introducing the leptonic decay constants, which are one of the subject of the present work together with the precise determination of up, down, strange and charm quark masses. In particular, the central role of the decay constants in the determination of CKM matrix elements will be emphasized in specific cases.
- Chapter 2 will be dedicated to the introduction of the calculation method employed in this work: lattice QCD. After a general introduction I will present the Twisted Mass action used by the ETM Collaboration and, in the second part, I will give some details on the numerical analysis discussing the statistical and systematic error treatment. Before closing this chapter, I will also discuss the relation between the two-point correlation functions, which are the basic ingredient of our numerical analysis, and the meson masses and matrix elements.

Chapter 3 and 4 present the main original works performed in this thesis

- In Chapter 3, after discussing the details of the simulation, I will present our determination of the quark masses obtained analysing pseudoscalar meson masses. The chapter will be divided in three section describing respectively the calculation of the average up/down quark mass m_{ud} , of the strange quark mass m_s and the

charm quark mass m_c . Our determination of the ratio m_u/m_d , m_s/m_{ud} and m_c/m_s will also be discussed.

- In Chapter 4 I will present our analysis of the leptonic decay constants. The first part of this chapter will be focused on the kaon sector and on the determination of the kaon decay constant f_K and the ratio f_K/f_π , while the second part will concern the D sector and the determination of the decay constants f_D and f_{D_s} , along with ratio f_{D_s}/f_D .

Finally, I will present some conclusions and comment on future perspective.

The main results obtained in this work are summarized below

- Quark masses

The final results obtained for the quark masses in the $\overline{\text{MS}}$ scheme are:

$$\begin{aligned} m_{ud}(2 \text{ GeV}) &= 3.70(17) \text{ MeV} , \\ m_s(2 \text{ GeV}) &= 99.2(3.9) \text{ MeV} , \\ m_c(m_c) &= 1.350(46) \text{ GeV} , \end{aligned} \tag{1}$$

where the errors are the sum in quadrature of the statistical and systematic uncertainties. We also obtain preliminary results for the following ratios of quark masses

$$\begin{aligned} \frac{m_u}{m_d} &= 0.486(54) , \\ \frac{m_s}{m_{ud}} &= 26.65(30) , \\ \frac{m_c}{m_s} &= 11.65(12) , \end{aligned} \tag{2}$$

which are independent of both the renormalization scheme and scale.

- Decay constants

The final results we obtained for the decay constants are:

$$\begin{aligned} f_{K^+} &= 154.4(2.1) \text{ MeV} , \\ \frac{f_{K^+}}{f_{\pi^+}} &= 1.183(17) \end{aligned} \tag{3}$$

$$\begin{aligned} f_{D_s} &= 242.1(8.3) \text{ MeV} , \\ f_D &= 201.9(8.0) \text{ MeV} , \\ \frac{f_{D_s}}{f_D} &= 1.199(25) \end{aligned} \tag{4}$$

Chapter 1

Flavor Physics

In this chapter we discuss some aspects of flavor physics in the SM focusing on the issues which are more relevant for the present work. We will first discuss the SM lagrangian and its free parameters which in the quark sector are the particle masses and the entries of the Cabibbo Kobayashi Maskawa (CKM) matrix which regulates the mixing between different flavors of quarks.

Then we will show how, combining experimental measurements with the non perturbative determinations provided by Lattice QCD, it is possible to precisely determine these parameters.

1.1 The Standard Model and the quark masses

The standard model of electroweak and strong interaction is a gauge theory invariant under the symmetry group $SU(3)_C \otimes SU(2)_L \otimes U(1)_Y$.

$SU(3)_C$ is the group associated to the color symmetry, on which the description of the theory of the strong interaction, the quantum chromodynamics (QCD), is based. The group $SU(2)_L \otimes U(1)_Y$ describes the electromagnetic and weak interactions involving gauge (W^\pm, Z^0, γ) and matter fields. The electroweak theory is an example of what is called a “chiral” theory, i.e. a theory in which the *left-handed* and *right-handed* components of the fermionic field undergoes different transformation properties; this is what is meant by the letter L , which suggests that the interactions described by $SU(2)_L$ gauge group involve only the *left-handed* components.

Y , instead, labels the weak hypercharge group $U(1)_Y$. The hypercharge is related

to the electric charge Q and to the third component of weak isospin by the relation $Q = T_3 + Y/2$.

The electroweak gauge symmetry is spontaneously broken by the vacuum expectation value (VEV) different from zero of the Higgs field in the electromagnetic subgroup with the following path

$$SU(3)_C \otimes SU(2)_L \otimes U(1)_Y \rightarrow SU(3)_C \otimes U(1)_Q. \quad (1.1)$$

Spontaneous symmetry breaking permits to generate mass terms, proportional to the Higgs VEV, for those gauge bosons associated to the broken symmetries (the so called *Higgs mechanism* [16, 17]). In other words, the spontaneous breaking of the symmetries associated to the W^\pm, Z^0 (i.e. $SU(2)_L$ and $U(1)_Y$) produces the necessary mass term for the electroweak gauge bosons, while leaving $SU(3)_C \otimes U(1)_Q$ unbroken guaranties that the gluon and the photon remain massless.

The fermionic matter contents of the SM is made up by the known leptons and quarks organized in three families. In the electroweak sector of the theory, the fermionic fields are organized in a particular way: *left-handed* components (in the interaction eigenstates basis) are grouped in $SU(2)_L$ doublets, while the *right-handed* components of quark fields and of the three charged leptons are $SU(2)_L$ singlets.

$$\begin{aligned} L_L^1 &= \begin{pmatrix} \nu_e \\ e^- \end{pmatrix}_L, \quad L_L^2 = \begin{pmatrix} \nu_\mu \\ \mu^- \end{pmatrix}_L, \quad L_L^3 = \begin{pmatrix} \nu_\tau \\ \tau^- \end{pmatrix}_L; \\ l_R^1 &= (e^-)_R, \quad l_R^2 = (\mu^-)_R, \quad l_R^3 = (\tau^-)_R; \\ Q_L^1 &= \begin{pmatrix} u \\ d' \end{pmatrix}_L, \quad Q_L^2 = \begin{pmatrix} c \\ s' \end{pmatrix}_L, \quad Q_L^3 = \begin{pmatrix} t \\ b' \end{pmatrix}_L; \\ u_R^1 &= (u)_R, \quad u_R^2 = (c)_R, \quad u_R^3 = (t)_R; \\ d_R^1 &= (d')_R, \quad d_R^2 = (s')_R, \quad d_R^3 = (b')_R; \end{aligned} \quad (1.2)$$

The chiral nature of the electroweak interaction forbids the presence of mass terms

in the lagrangian for fermions, as can be easily seen from the behavior of a fermionic mass term under a generic gauge group transformation:

$$\mathcal{L}_m = m (\bar{f}_L f_R + \bar{f}_R f_L) \rightarrow \mathcal{L}'_m = m (\bar{f}_L U_L^\dagger U_R f_R + \bar{f}_R U_R^\dagger U_L f_L) \neq \mathcal{L}_m, \quad (1.3)$$

with $U_L \neq U_R$. It is known however that, in a gauge invariant theory, it is possible to obtain mass terms for fermions, once again, through the spontaneous gauge symmetry breaking, using the VEV of the Higgs scalar doublet.

The Standard Model lagrangian can be summarized as:

$$\mathcal{L}_{SM} = \mathcal{L}_{fermions} + \mathcal{L}_{gauge} + \mathcal{L}_{Higgs} + \mathcal{L}_Y. \quad (1.4)$$

The fermionic Lagrangian has the following structure

$$\mathcal{L}_{fermions} = \sum_{i=1}^3 \left[\sum_{\psi=Q_L, u_R, d_R} \bar{\psi}_i \not{D} \psi_i + \sum_{\psi=L_L, l_R} \bar{\psi}_i \not{D} \psi_i \right] \quad (1.5)$$

where, to ensure the gauge invariance under $SU(3)_C \otimes SU(2)_L \otimes U(1)_Y$ we introduced the covariant derivative D_μ , defined as

$$D^\mu = \partial^\mu + ig_s \frac{\lambda_a}{2} G_a^\mu + ig \frac{\sigma_b}{2} W_b^\mu + ig' Y B^\mu \quad (1.6)$$

with G_a^μ the eight gluon fields, W_b^μ the three weak interaction bosons and B^μ the single hypercharge boson. λ_a and σ_b are the Gell-Mann matrices and the Pauli matrices respectively. Obviously, the terms proportional to g and g_s are present only if the field is not a singlet of $SU(2)_L$ and $SU(3)_C$. The covariant derivative thus introduces the interactions between fermionic and gauge fields.

The physical mediator of the electroweak interactions are related to W_μ^i and B_μ by the following relations

$$W_\mu = (W_\mu^1 + iW_\mu^2)/\sqrt{2} \quad (1.7)$$

and

$$\begin{pmatrix} W_\mu^3 \\ B_\mu \end{pmatrix} = \begin{pmatrix} \cos \theta_W & \sin \theta_W \\ -\sin \theta_W & \cos \theta_W \end{pmatrix} \begin{pmatrix} Z_\mu \\ A_\mu \end{pmatrix} \quad (1.8)$$

where θ_W is the Weinberg angle.

The electroweak interaction lagrangian between matter and gauge fields emerge considering non-kinetic terms in the covariant derivatives, which can be of two kinds:

$$\mathcal{L}_{int}^{EW} = \mathcal{L}_{CC} + \mathcal{L}_{NC} , \quad (1.9)$$

charged currents couplings to W^\pm bosons and *neutral currents* one to γ and Z^0 bosons. In particular one finds that charged current interactions are described by

$$\mathcal{L}_{CC} = \frac{g}{2\sqrt{2}} (J_\mu^\dagger W^\mu + W_\mu^\dagger J^\mu) , \quad (1.10)$$

with

$$J_\mu^\dagger = \sum_{i=1,3} (\bar{u}_L^i \gamma_\mu d_L^i + \bar{l}_L^i \gamma_\mu \nu_L^i) , \quad (1.11)$$

where we have indicated with i the family index for both lepton and quark fields. For neutral currents interactions one has

$$\mathcal{L}_{NC} = -e J_{em}^\mu A_\mu + \frac{g}{2 \cos \theta_W} J_Z^\mu Z_\mu , \quad (1.12)$$

where

$$\begin{aligned} J_{em}^\mu &= \sum_f Q_f \bar{f} \gamma^\mu f, \\ J_Z^\mu &= \sum_f \bar{f} \gamma^\mu (v_f - a_f \gamma_5) f, \end{aligned} \quad (1.13)$$

with

$$v_f = T_3^f - 2Q_f \sin^2 \theta_W , \quad a_f = T_3^f . \quad (1.14)$$

In these expressions Q_f and T_3^f represents, respectively, the electric charge and the third components of weak isospin (different from zero only for *left-handed* fermions); we have also indicated with g and e the $SU(2)_L$ and $U(1)_Q$ coupling constants, respectively.

	ν_L^l	l_L^-	l_R^-	u_L	d_L	u_R	d_R
Q	0	-1	-1	2/3	-1/3	2/3	-1/3
T_3	1/2	-1/2	0	1/2	-1/2	0	0
Y	-1	-1	-2	1/3	1/3	4/3	-2/3

Table 1.1: *Electroweak quantum numbers for leptons and quarks. We have indicated with Q the electric charge, T_3 the third component of weak isospin and with Y , the weak hypercharge.*

In table 1.1 we have collected all the electroweak quantum numbers for the different fermions.

The gauge kinetic term, \mathcal{L}_{gauge} , in the Lagrangian (1.4) reads

$$\mathcal{L}_{gauge} = -\frac{1}{4} [G_{\mu\nu}^a G_a^{\mu\nu} + W_{\mu\nu}^i W_i^{\mu\nu} + B_{\mu\nu} B^{\mu\nu}] \quad (1.15)$$

where $G_{\mu\nu}^a$ and $W_{\mu\nu}^i$ are defined as follows

$$F_{\mu\nu}^a \doteq \partial_\mu A_\nu^a - \partial_\nu A_\mu^a - g f^{abc} A_\mu^b A_\nu^c, \quad (1.16)$$

where f^{abc} are the structure constants of the corresponding gauge group, and while for $B_{\mu\nu}$ holds

$$B^{\mu\nu} = \partial^\mu B^\nu - \partial^\nu B^\mu \quad (1.17)$$

Finally, we describe the so called Higgs sector of the Standard Model lagrangian. It contains a complex scalar field, ϕ , which is an $SU(2)_L$ doublet:

$$\phi = \begin{pmatrix} \phi^+ \\ \phi^0 \end{pmatrix}. \quad (1.18)$$

described by the following lagrangian

$$\mathcal{L}_{Higgs} = |D\phi|^2 - V(\phi, \phi^\dagger) \quad (1.19)$$

with a potential $V(\phi, \phi^\dagger)$ defined as

$$V(\phi, \phi^\dagger) = +\mu^2 \phi^\dagger \phi + \frac{1}{2} \lambda (\phi^\dagger \phi)^2, \quad (1.20)$$

with $\lambda > 0$. In this framework, spontaneous symmetry breaking happens if the potential minimum occurs for values of the ϕ field which are different from zero. From the shape of the potential $V(\phi, \phi^\dagger)$ it is easy to see that this will happen if $\mu^2 < 0$.

The field component with VEV different from zero is the neutral one and this imply that the vacuum is invariant under $U(1)_Q$. In particular, one can parametrize the Higgs doublet as a VEV part plus a part which oscillates around the minimum v ,

$$\phi(x) = U(x) \frac{1}{\sqrt{2}} \begin{pmatrix} 0 \\ v + h(x) \end{pmatrix}, \quad (1.21)$$

where $h(x)$ is a real field whose VEV is zero and $U(x) \in (SU(2) \otimes U(1)_Y)$. $U(x)$ can be cancelled making the inverse gauge transformation $U(x)^{-1}$ which brings us in the so called *unitary* gauge. In this gauge, the field ϕ becomes

$$\phi(x) = \frac{1}{\sqrt{2}} \begin{pmatrix} 0 \\ v + h(x) \end{pmatrix}. \quad (1.22)$$

If we look at the covariant derivative in the lagrangian (1.19), which now reads

$$|D\phi|^2 \rightarrow \frac{1}{2} \partial_\mu h \partial^\mu h + (v + h)^2 \left[\frac{g^2}{4} W_\mu^\dagger W^\mu + \frac{g^2}{8 \cos^2 \theta_W} Z_\mu Z^\mu \right] \quad (1.23)$$

it is clear that the non vanishing VEV has generated a mass term for the W^\pm and the Z leaving the photon massless.

Let us now describe the Standard Model lagrangian term which is responsible for the fermionic masses, which is the so called Yukawa lagrangian \mathcal{L}_Y . Assuming there are no right handed neutrinos, this term is the most general one describing the coupling of the Higgs doublet with fermionic fields

$$\mathcal{L}_Y = -\lambda_l^{ij} \bar{L}_L^i \phi e_R^j - \lambda_d^{ij} \bar{Q}_L^i \phi d_R^j - \lambda_u^{ij} \bar{Q}_L^i \phi u_R^j + h.c., \quad (1.24)$$

where the field $\bar{\phi}$ is defined as $\bar{\phi}^\alpha = \epsilon^{\alpha\beta} \phi_\beta^*$, with $\epsilon^{\alpha\beta}$ is the $SU(2)_L$ antisymmetric tensor and α, β are isospin indices. The complex-valued matrices λ_l, λ_u and λ_d are 3×3 matrices and $i, j = 1, 2, 3$ are generation indices.

After the spontaneous symmetry breaking the Yukawa lagrangian becomes

$$\mathcal{L}_Y = - \left(1 + \frac{H}{v} \right) \left[\bar{d}_L M'_d d_R + \bar{u}_L M'_u u_R + \bar{l}_L M'_l l_R + h.c. \right] \quad (1.25)$$

where also in this case the non vanishing VEV of ϕ has introduced mass terms through the M' which are generic 3×3 complex matrices.

It is always possible to diagonalize M'_i by means of a redefinition of the fermionic fields. A generic, complex valued matrix can always be rewritten in terms of a diagonal matrix D_i with positive eigenvalues and two unitary matrices

$$D_i = U_L M_i U_R^\dagger \quad (1.26)$$

so that, rescaling the fields as for example

$$u_L \rightarrow U_{uL} u_L, \quad u_R \rightarrow U_{uR} u_R, \quad (1.27)$$

the Yukawa term written in terms of the mass eigenstates reads

$$\mathcal{L}_Y = - \left(1 + \frac{H}{v} \right) \left[\bar{d}'_L D_d d'_R + \bar{u}'_L D_u u'_R + \bar{l}'_L D_l l'_R + h.c. \right] \quad (1.28)$$

where the diagonal matrices D_i now contain the masses of the fermions of the theory

$$D_d = \text{diag}(m_d, m_s, m_b) \quad D_u = \text{diag}(m_u, m_c, m_t) \quad D_l = \text{diag}(m_e, m_\mu, m_\tau) \quad (1.29)$$

It is useful to emphasize that particle masses introduced here, which are related to the Yukawa couplings and to VEV of field ϕ , are free parameters of the SM in the sense that the theory does not provide a prediction for their values nor an explanation of their observed hierarchical structure. Naturally, all fermion masses would be expected to be of the order of the VEV v , as well as the weak gauge boson masses. Only for the top quark, however, this expectation is realized in nature.

In the next session we will introduce the other free parameters of the SM in the quark sector that control the flavor mixing, namely the CKM matrix elements.

1.2 The Cabibbo Kobayashi Maskawa Matrix

In this section we will continue the brief overview on the Standard Model flavour sector by describing the quark flavour mixing matrix, also known as *Cabibbo-Kobayashi-Maskawa* matrix.

This matrix enters the Lagrangian because weak interactions in the quark sector are not flavour diagonal in the mass eigenstates basis.

1.2.1 Definition & parametrization

In the previous section we applied the transformation (1.27) to the fermionic fields in order to diagonalize the mass matrices M_i in the Yukawa lagrangian. It is then necessary to investigate the consequences of these transformation in the other part of the SM lagrangian. In what follows we will only focus on the quark sector being the one related to the present work.

Let us first note that the matrices U cancel out in all kinetic terms and in the interaction terms between quarks and gluonic fields, because they are both chirally conserving and flavour diagonal. The interaction terms with the electromagnetic (A_μ) and the neutral weak mediator (Z^0) fields remain unchanged too, for the same reason.

The only effect of the rotation is thus present in the charged weak currents which transform as

$$J^{\mu\dagger} = \frac{1}{\sqrt{2}}\bar{u}_L\gamma^\mu d_L \rightarrow \frac{1}{\sqrt{2}}\bar{u}_L\gamma^\mu U_{u_L}^\dagger U_{d_L} d_L. \quad (1.30)$$

From this expression expression one defines the unitary *Cabibbo-Kobayashi-Maskawa* (CKM) [18, 19] flavour mixing matrix as

$$U_{u_L}^\dagger U_{d_L} = V_{CKM}. \quad (1.31)$$

This matrix connects the interaction eigenstates (d', s', b') with the mass eigenstates (d, s, b):

$$\begin{pmatrix} d' \\ s' \\ b' \end{pmatrix} = \begin{pmatrix} V_{ud} & V_{us} & V_{ub} \\ V_{cd} & V_{cs} & V_{cb} \\ V_{td} & V_{ts} & V_{tb} \end{pmatrix} \begin{pmatrix} d \\ s \\ b \end{pmatrix}. \quad (1.32)$$

The mass eigenstates are different from the interaction ones and the charged current interactions mix different flavours with weight V_{ij} in the mass eigenstates basis. It is worthwhile to underline that within the Standard Model the only flavour changing mechanism is represented by this matrix and that there are no flavour changing neutral currents (FCNC) whose absence is ensured by the unitarity of V_{CKM} .

In the case of three quark generations, the CKM matrix is a 3×3 unitary complex matrix which depends on nine real numbers ($9 \times 2 = 18$ real parameters with 9 unitarity constraint relations). Exploiting the quark fields phase redefinition freedom ($6 - 1 = 5$ arbitrary phases) one concludes that V_{CKM} depends only on 4 real parameters, three angles and one phase, which, together with fermion masses, constitute the free parameters of the flavour quark sector of the Standard Model.

Once the number of the independent physical parameters of this matrix is known, one can introduce a set of different parametrization for that matrix. The most natural choice consists in writing the matrix as a product of three different rotations

$$V_{CKM} = \begin{pmatrix} 1 & 0 & 0 \\ 0 & c_{23} & s_{23} \\ 0 & -s_{23} & c_{23} \end{pmatrix} \begin{pmatrix} c_{13} & 0 & s_{13}e^{-i\delta} \\ 0 & 1 & 0 \\ -s_{13}e^{i\delta} & 0 & c_{13} \end{pmatrix} \begin{pmatrix} c_{12} & s_{12} & 0 \\ -s_{12} & c_{12} & 0 \\ 0 & 0 & 1 \end{pmatrix}, \quad (1.33)$$

which leads to

$$V_{CKM} = \begin{pmatrix} c_{12}c_{13} & s_{12}c_{13} & s_{13}e^{-i\delta} \\ -s_{12}c_{23} - c_{12}c_{23}s_{13}e^{i\delta} & c_{12}c_{23} - s_{12}s_{23}s_{13}e^{i\delta} & s_{23}c_{13} \\ s_{12}s_{23} - c_{12}c_{23}s_{13}e^{i\delta} & -c_{12}s_{23} - s_{12}c_{23}s_{13}e^{i\delta} & c_{13}c_{23} \end{pmatrix}, \quad (1.34)$$

where $s_{ij} = \sin \theta_{ij}$, $c_{ij} = \cos \theta_{ij}$ (and θ_{12} is the Cabibbo angle) and δ is the phase. What is important to emphasize is that if $\delta = 0$ the matrix V_{CKM} becomes real and one has no CP violation in the quark sector too.

Another interesting feature of the matrix is that for a complex phase to be present in the Standard Model the number of quark generations must be at least three. In the old Cabibbo version of the theory, which involved only two generations (u, d) and (c, s), the mixing matrix was a real rotation in flavour space and there was no room for CP violation. Moreover in order for CP violation to appear, it is necessary that all quark masses are different because, if this is not the case, by means of suitable unitary transformation, one could redefine the quark fields eliminating the CP violating phase. It can be shown that the *necessary* condition for having CP violation is

$$(m_t^2 - m_c^2)(m_t^2 - m_u^2)(m_u^2 - m_c^2)(m_b^2 - m_s^2)(m_b^2 - m_d^2)(m_d^2 - m_s^2) \times J_{CP} \neq 0 \quad (1.35)$$

where we have introduced the Jarlskog parameter [20]

$$J_{CP} = s_{12}s_{13}s_{23}c_{12}c_{23}c_{13}^2 \sin \delta . \quad (1.36)$$

J_{CP} can be thought as a quantitative estimate of the size of CP violation in the SM, and it has been measured to be $J_{CP} = 3.12(9) \cdot 10^{-5}$ [21].

The weak interaction mixes flavors according to a specific hierarchy: the diagonal elements of the matrix (1.32) describe transitions *within* the same generation and are larger ($\sim O(1)$) than off diagonal elements ($\sim O(10^{-1})$ to $\sim O(10^{-3})$), which represent transitions *between* different generations, one has $s_{13} \ll s_{23} \ll s_{12} \ll 1$.

The hierarchical structure of the CKM matrix has been pictorially represented in figure 1.1, where transitions within the same generation are represented with bold black lines, while transitions between different generations are represented with dashed and dotted lines of different colors.

A specific CKM matrix parametrization, which explicitly shows this hierarchical structure has been proposed by Wolfenstein [22] and can be obtained by setting

$$s_{12} = \lambda , \quad s_{23} = A\lambda^2 , \quad s_{13}e^{-i\delta} = A\lambda^3(\rho - i\eta) . \quad (1.37)$$

Expanding the matrix elements in powers of λ , neglecting terms $O(\lambda^4)$ one has

$$V_{CKM} = \begin{pmatrix} 1 - \frac{\lambda^2}{2} & \lambda & A\lambda^3(\rho - i\eta) \\ -\lambda & 1 - \frac{\lambda^2}{2} & A\lambda^2 \\ A\lambda^3(1 - \rho - i\eta) & -A\lambda^2 & 1 \end{pmatrix} + \mathcal{O}(\lambda^4) . \quad (1.38)$$

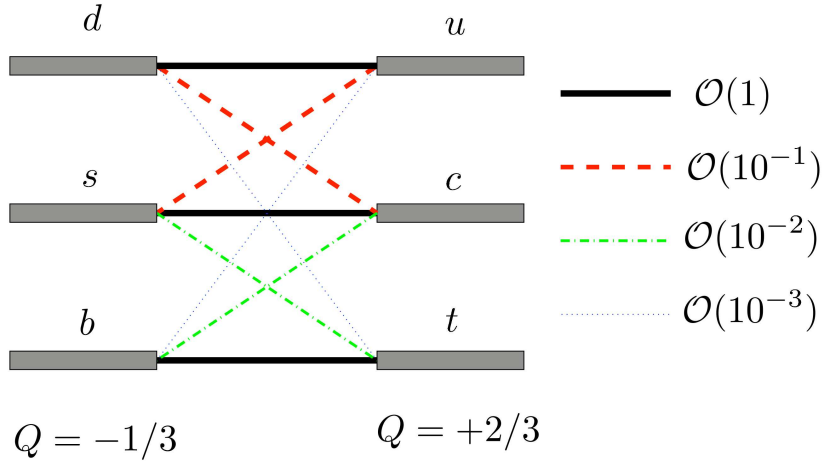


Figure 1.1: The hierarchy of charged currents flavour mixing transition.

1.2.2 CKM Unitarity relations

Other important information on the CKM matrix can be extracted performing the so called *unitarity triangle* analysis. This kind of analysis is based on the unitarity of V_{CKM}

$$V_{CKM}^\dagger V_{CKM} = V_{CKM} V_{CKM}^\dagger = 1. \quad (1.39)$$

It consists of nine relations between the matrix elements. Since different entries of CKM matrix can be independently determined, it is possible to test SM by verifying whether such relations are satisfied. These relations can be divided in two classes: three normalization relations and six orthogonality relations.

The normalization relations requires that the sum of squared entries of each rows (or columns) must be equal 1.

The most precise bound comes from the analysis of the first line of the matrix, that corresponds to the relation:

$$|V_{ud}|^2 + |V_{us}|^2 + |V_{ub}|^2 = 1 \quad (1.40)$$

As will be explained in a while, to test these relations one has to combine experimental measurements with theoretical calculations to determine the CKM matrix elements.

The value of $|V_{ud}|$ can be very precisely determined from the measurement of nuclear β decays and from leptonic pion decays $\pi \rightarrow \mu, \nu_\mu$, while $|V_{us}|$ can be determined studying

the leptonic and semi-leptonic decays of K mesons. The matrix element $|V_{ub}|$, which can be determined studying the leptonic and semi-leptonic decays of B mesons, is however largely suppressed (see eq. (1.38)) respect to the other quantities in eq. (1.40). Therefore at the current level of precision, when we test the unitarity of the first row of the CKM matrix the determination of $|V_{ub}|$ is at the level of the errors of $|V_{ud}|$ and $|V_{us}|$ and it is therefore irrelevant.

Part of this thesis work is dedicated to the calculation of leptonic decay constants which are used in the determination of the CKM matrix elements, and in next sections we will discuss how lattice computations help in performing such tasks.

Thanks to the increasing precision reached both in experimental measures and by lattice calculation, it is possible to verify rather accurately also the unitarity relation for the second row which reads

$$|V_{cd}|^2 + |V_{cs}|^2 + |V_{cb}|^2 = 1. \quad (1.41)$$

In particular the first two entries can be determined combining experimental measurements of the purely leptonic decays with the D and D_s leptonic decay constants which have been computed in the present work.

The six orthogonality relations, on the other hand, can be represented as six triangles in a complex plane, all having the same area $A = J_{CP}/2$. It is convenient to consider a triangle with sides that are of the same order of magnitude. Using Wolfenstein's parametrization for CKM elements it can be realized that this is obtained by considering the triangle coming from the orthogonality of first and third row (or first and third column, which can be shown to be equivalent at order $\mathcal{O}(\lambda^3)$).

The corresponding orthogonality relation reads

$$V_{ud}V_{ub}^* + V_{cd}V_{cb}^* + V_{td}V_{tb}^* = 0. \quad (1.42)$$

It is convenient to rescale the unitarity triangle (UT), relation (1.42) by dividing for $V_{cd}V_{cb}^*$

$$\frac{V_{ud}V_{ub}^*}{V_{cd}V_{cb}^*} + 1 + \frac{V_{td}V_{tb}^*}{V_{cd}V_{cb}^*} = 0. \quad (1.43)$$

In this way the vertices are $(0,0)$, $(1,0)$ and $(\bar{\rho}, \bar{\eta})$, where the *barred* parameters are related to ρ and η by

$$\rho + i\eta = \sqrt{\frac{1 - A^2\lambda^4}{1 - \lambda^2}} \frac{\bar{\rho} + i\bar{\eta}}{1 - A^2\lambda^4(\bar{\rho} + i\bar{\eta})} = \left(1 - \frac{\lambda^2}{2}\right) (\bar{\rho} + i\bar{\eta}) + \mathcal{O}(\lambda^4). \quad (1.44)$$

The unitarity triangle is shown in fig. 1.2 in the $(\bar{\rho}, \bar{\eta})$ plane

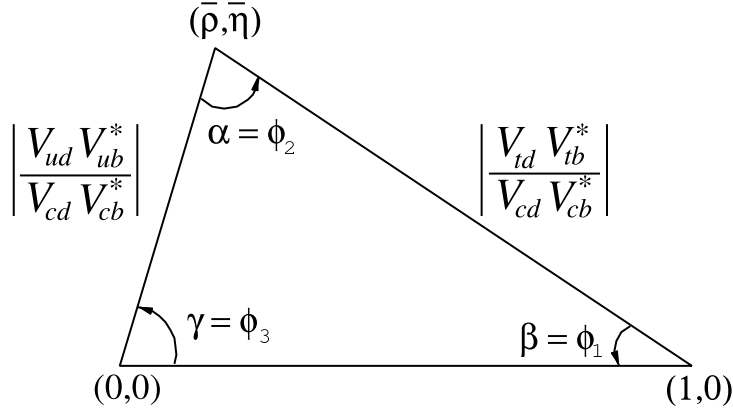


Figure 1.2: *The unitarity triangle.*

where the angles are defined as follows

$$\alpha = \phi_2 = \arg \left(-\frac{V_{td}V_{tb}^*}{V_{ud}V_{ub}^*} \right), \quad (1.45)$$

$$\beta = \phi_1 = \arg \left(-\frac{V_{cd}V_{cb}^*}{V_{td}V_{tb}^*} \right), \quad (1.46)$$

$$\gamma = \phi_3 = \arg \left(-\frac{V_{ud}V_{ub}^*}{V_{cd}V_{cb}^*} \right), \quad (1.47)$$

while the two non trivial sides are

$$R_b = \frac{|V_{ud}V_{ub}^*|}{|V_{cd}V_{cb}^*|} \simeq \left(1 - \frac{\lambda^2}{2}\right) \frac{1}{\lambda} \left| \frac{V_{ub}}{V_{cb}} \right|, \quad (1.48)$$

$$R_t = \frac{|V_{td}V_{tb}^*|}{|V_{cd}V_{cb}^*|} \simeq \frac{1}{\lambda} \left| \frac{V_{td}}{V_{cb}} \right|. \quad (1.49)$$

Various experimental results combined with theoretical determination can study different properties of this triangle, such as side lengths, angles amplitudes, etc. In general

it is convenient to show the various bounds coming from the CKM matrix constraints as bands in the $(\bar{\rho}, \bar{\eta})$ plain which must intersect on the apex of the triangle. In Fig. 1.3 we show the fit of all the present bounds to the values of $(\bar{\rho}$ and $\bar{\eta})$ performed by UTfit collaboration.

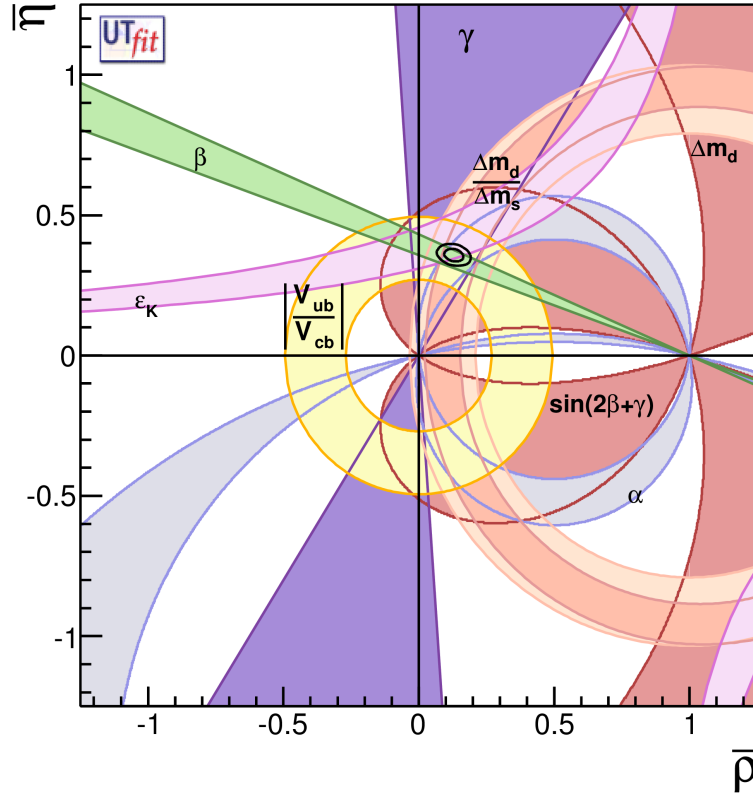


Figure 1.3: Results of the UT analysis within the SM from the UTfit collaboration.

All the constraints to the triangle intersect in the same region, thus indicating quite a good agreement between SM predictions and experiments. The increasing precision both on the theoretical and experimental sides will allow in the future to perform more and more stringent fit and possibly highlight the presence of New Physics.

1.3 Leptonic decay constants

Among the most simple hadronic quantities measurable on lattice are the leptonic decay constants of mesons. A large part of our work has been devoted to the determination

of the decay constants for various pseudo-scalar mesons. The results combined with experimental measurements, provides some of the most precise determination of the CKM matrix elements, and is therefore of great relevance in flavor physics. A charged pseudo-scalar meson, composed by an up-type and down-type quark, can decay into a lepton-neutrino pair through the emission of a W meson. These class of decays, being characterized by a purely leptonic final states, are called leptonic decay. Is worth mentioning that semi-leptonic decays can also be considered for the determination of the CKM matrix elements but, since they have not been studied in the present work, they will not be discussed.

At the energy scale characteristic of an hadronic decay process, strong interaction cannot be treated with perturbative methods because $\alpha_s \gtrsim 1$. Therefore the hadronic quantities involved in the decay widths must be evaluated using non perturbative techniques. In this contest lattice QCD plays a primary role being a non perturbative approach based only on first principles.

A leptonic decay of a meson M can be diagrammatically represented as shown in fig. 1.4

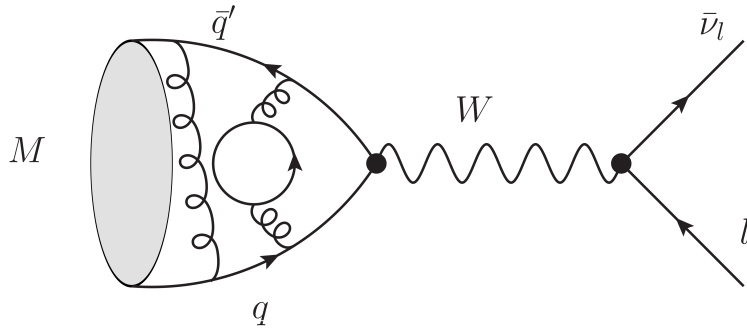


Figure 1.4: *Example of Feynman diagram which contribute to a leptonic decay of a general meson M . The hadronic part must be evaluated by means of non perturbative methods.*

The corresponding decay rate at leading order is given by

$$\Gamma(P_S \rightarrow l, \nu_l) = \frac{G_F^2}{8\pi} |V_{qq'}|^2 f_{PS}^2 M_{PS} M_l^2 \left(1 - \frac{M_l^2}{M_{PS}^2}\right)^2 \quad (1.50)$$

where G_F is the Fermi constant, M_l and M_{PS} are the charged lepton and pseudo-scalar particle masses, $V_{qq'}$ is the CKM matrix element appropriate for the decay, and f_{PS}

parameterize the hadronic matrix element of the axial current between the pseudo-scalar meson state and the vacuum

$$\langle 0 | \bar{u} \gamma_\mu \gamma_5 d | M_{PS} \rangle = -i f_{PS} p_\mu, \quad (1.51)$$

where p_μ is the meson momentum.

Using eq. (1.50) one can obtain the matrix element $V_{qq'}$ by combining the experimental measurement of the decay rate and the lattice calculation of the leptonic decay constant. In the next sessions we will discuss the various decay constants which have been evaluated in the present work by explaining their role in the determination of the CKM matrix parameters.

1.3.1 f_K/f_π and f_K

In the kaon and pion case it is convenient to consider the ratios of leptonic decay rates. In particular, one of the most precise determination of the value of the ratio $|V_{us}/V_{ud}|$ comes from the study of the following ratio

$$\frac{\Gamma(K \rightarrow \mu, \nu_\mu)}{\Gamma(\pi \rightarrow \mu, \nu_\mu)} = \frac{|V_{us}|^2 f_K^2 M_K \left(1 - \frac{M_l^2}{M_K^2}\right)^2}{|V_{ud}|^2 f_\pi^2 M_\pi \left(1 - \frac{M_l^2}{M_\pi^2}\right)^2} (1 + \delta_{EM}), \quad (1.52)$$

where f_K and f_π are the kaon and pion decay constants and δ_{EM} denotes the effect of (long distance) electromagnetic corrections. These corrections are currently estimated using Chiral Perturbation Theory (ChPT) supplemented by large- N model, which provide $\delta_{EM} = 0.0070(35)$ [23].

Experimental measurements on kaon and pion decays have reached a remarkable level of precision allowing to accurately determine the ratio [24]

$$\left| \frac{V_{us}}{V_{ud}} \right| \frac{f_{K^+}}{f_{\pi^+}} = 0.2758(5), \quad (1.53)$$

Therefore to obtain from this measure the ratio $|V_{us}/V_{ud}|$ a determination of f_K/f_π is needed. Lattice QCD calculations is the only method that allows to determine the value of the decay constants non-perturbatively based only on first principles. Our calculation of the ratio f_K/f_π will be presented in chapter 4.

Once $|V_{us}/V_{ud}|$ has been determined, in order to extract the two separate matrix elements

$|V_{us}|$ and $|V_{ud}|$ are considered both the precise determination of $|V_{ud}|$, from superallowed nuclear β transition,

$$|V_{ud}| = 0.97425(22), \quad (1.54)$$

and the determination of $|V_{us}|$ from the kaon semileptonic decays

$$|V_{us}| f_+(0) = 0.2163(5). \quad (1.55)$$

In the latter case the semileptonic form factor $f_+(t)$ relevant for the semileptonic decay $K^0 \rightarrow \pi^-, l, \nu_l$, function of momentum t transferred between the two mesons, must be calculated on the lattice.

It is useful for flavor physics phenomenology to provide not only the ratio of f_K/f_π , but also the value of the decay constant f_K . In particular the knowledge of f_K is relevant for the precise theoretical determination of the parameter ϵ_K , which regulates the amount of CP violation in neutral kaon mixing, and helps us constraining the apex of the CKM unitarity triangle.

In the SM, $K - \bar{K}$ oscillations take place, at the second order in the weak interaction through the exchange of two W 's. At the leading order in $1/M_W^2$ the corresponding box diagram can be contracted to a point resulting in an effective four-fermion interaction controlled by the operator

$$Q_1 = \frac{1}{4} [\bar{s}\gamma_\mu(1 - \gamma_5)d] [\bar{s}\gamma_\mu(1 - \gamma_5)d] \quad (1.56)$$

It is useful to parametrize the matrix element of the operator in terms of its *vacuum insertion approximation* (VIA) (i.e. inserting, in all possible ways, only the vacuum instead of a complete set of states) times the deviation from this approximation represented by the so called bag parameter B_K . This leads to

$$\langle \bar{K}^0 | Q_1 | K^0 \rangle = \langle \bar{K}^0 | Q_1 | K^0 \rangle_{VIA} B_K = \left[\frac{8}{3} \langle \bar{K}^0 | \bar{s}\gamma_0\gamma_5 d | 0 \rangle^2 \right] B_K = \left[\frac{8}{3} f_K^2 M_K^2 \right] B_K \quad (1.57)$$

From equation 1.57 it is clear that f_K , as well as B_K , which must also be calculated on the lattice, is relevant in the determination of the $\Delta S = 2$ operator responsible for neutral kaon oscillations, and therefore in the determination of the ϵ_K parameter.

It is worth mentioning that in New Physics models a larger set of operators can mediate the kaon mixing. Their matrix elements in the VIA still involve f_K but different B -parameters. The lattice determination of these B -parameters together with f_K can be used to put bounds on New Physics models.

The details and the result of our calculation of the kaon decay constant f_K will be presented in chapter 4.

1.3.2 f_D and f_{D_s}

Leptonic and semileptonic decays of D and D_s mesons, which occur via charged W boson exchange, are sensitive probes of $c \rightarrow d$ and $c \rightarrow s$ transitions. Given experimental measurements of the branching fractions combined with sufficiently precise theoretical calculations of the hadronic matrix elements, they enable the determination of the CKM matrix elements $|V_{cd}|$ and $|V_{cs}|$. As already mentioned in sec. 1.2.2 their knowledge is required for a precise test of the unitarity of the second row of the CKM matrix.

In the present work we limited ourself to the calculation of the leptonic decay constants of D and D_s mesons.

The leptonic decays width follows eq. 1.50, which in this case reads

$$\Gamma(D_{(s)} \rightarrow l, \nu_l) = \frac{G_F^2}{8\pi} |V_{cq}|^2 f_{D_{(s)}}^2 M_{D_{(s)}} M_l^2 \left(1 - \frac{M_l^2}{M_{D_{(s)}}^2}\right)^2 \quad (1.58)$$

The branching fractions have been measured by CLEO, BELLE and Babar with a precision around 5 – 6% for the D_s -meson, while the uncertainties are approximately twice as large for the Cabibbo suppressed D -meson decay modes.

The latest experimental averages from the Particle Data Group [25], where electromagnetic corrections estimated to be of the order of 1% have been removed, reads

$$\begin{aligned} |V_{cd}| f_D &= 46.40(1.98) \text{ MeV} \\ |V_{cs}| f_{D_s} &= 253.1(5.3) \text{ MeV} \end{aligned} \quad (1.59)$$

When combined with lattice results for the decay constants, which for the present study are reported in chapter 4, these results allow for determinations of $|V_{cs}|$ and $|V_{cd}|$.

Chapter 2

Lattice QCD

2.1 Lattice regularization

LQCD is a first principle non perturbative implementation of field theory using the Feynman path integral approach. The starting point for the path integral formalism is the partition function in the Minkowski space

$$Z = \int \mathcal{D}\Phi e^{iS[\Phi]}. \quad (2.1)$$

By replacing the continuum space-time by a discrete grid of spacing a and extension aL (aT) in the spatial (time) directions the infinite degrees of freedom of the continuum theory are reduced to a discrete set of degrees of freedom which can be numerically computed.

In the Minkowski space, the paths are weighted with an highly oscillating function $e^{iS[\phi]}$. For this reason, this path integral representation is not suited for numerical calculations. In spite, it is customarily to use the euclidean action in which the paths are weighted by a Boltzmann factor. The euclidean action is obtained from the Minkowskian one by performing a Wick rotation to imaginary time. Under this rotation the partition function transforms as

$$\left(Z = \int \mathcal{D}\Phi e^{iS[\Phi]} \right)_{\text{Minkowski}} \rightarrow \left(Z = \int \mathcal{D}\Phi e^{-S[\Phi]} \right)_{\text{Euclidean}}. \quad (2.2)$$

Lattice regularization provides the only known non-perturbative and mathematically well defined formulation of QCD from first principles.

In addition, the inverse of the lattice spacing provides an intrinsic cutoff scale, regularizing ultraviolet divergences. Therefore, the lattice provides a regularization scheme as dimensional regularization can be, suitable for analytical treatment and compatible with the perturbative approach.

Different actions on the lattice are possible. The basic requirement that any lattice action should fulfil is that it must reproduce the correct expression in the continuum limit ($a \rightarrow 0$).

2.1.1 Fermionic Action

In what follows, we will give a lagrangian formulation of the fermionic action on the lattice and we will show the solution of the so called *fermion doubling* problem. The fermionic lagrangian density in euclidean space-time can be written in the following way, omitting for the sake of readability, the sum over the flavour of the quark involved

$$\mathcal{L}_F = \bar{\psi}(x) (\not{\partial} + M_0) \psi(x). \quad (2.3)$$

From this expression it is straightforward to write the fermionic action

$$S_F = \int d^4x d^4y \bar{\psi}(x)_\alpha K(x, y)_{\alpha\beta} \psi_\beta(y), \quad (2.4)$$

with $K(x, y)_{\alpha\beta} = (i\not{\partial} + M_0)_{\alpha\beta} \delta(x - y)$. Symmetrizing derivative operators and imposing that fermionic fields are zero at spatial infinity in (2.4), one gets

$$S_F = \int d^4x \bar{\psi}(x) \left(-\frac{1}{2} \gamma_\mu \overleftarrow{\partial}^\mu + \frac{1}{2} \gamma_\mu \overrightarrow{\partial}^\mu + M_0 \right) \psi(x). \quad (2.5)$$

Equation(2.5) can be put on the lattice using the following substitutions

$$\left\{ \begin{array}{l} \psi_\alpha(x) \rightarrow \psi_\alpha(x) \\ \overrightarrow{\partial}_\mu \psi(x) \rightarrow D_\mu \psi(x) = \frac{\psi(x+a\hat{\mu}) - \psi(x)}{a} \\ \overleftarrow{\partial}_\mu \psi(x) \rightarrow D_\mu^* \psi(x) = \frac{\psi(x) - \psi(x-a\hat{\mu})}{a} \\ \int d^4x \rightarrow \sum_x a^4 \end{array} \right. \quad \text{with } x \in \Lambda \quad (2.6)$$

where we have indicated with Λ the hypercubical lattice of spacing a and side L . Substituting (2.6) in (2.5) one finds the so called naive regularization

$$S_F^N = a^4 \sum_{x,y} \bar{\psi}(x) Q(x,y) \psi(y) \quad (2.7)$$

where

$$Q(x,y) = \left[M_0 \delta(x-y) + \left(\frac{1}{2a} \sum_{\mu=1}^4 \gamma_\mu \delta(y - (x + \hat{\mu})) - \frac{1}{2a} \sum_{\mu=1}^4 \gamma_\mu \delta(y - (x - \hat{\mu})) \right) \right] \quad (2.8)$$

This minimal approach used to translate the continuum action on the lattice, however, introduces in the theory new and unwanted degrees of freedom. This can be shown explicitly computing the fermion propagator, $S(x,y) = \langle \psi(x) \bar{\psi}(y) \rangle$, associated with the action (2.7). To do so notice that $S(x,y) = Q^{-1}$ where Q^{-1} is determined from the equation

$$\sum_z Q(x,z) Q^{-1}(z,y) = \delta_{xy}. \quad (2.9)$$

The inverse matrix Q^{-1} is easily computed using the Fourier transform formalism in momentum space. Imposing periodic boundary conditions on the lattice, $S(x,y)$ can be written as

$$\frac{1}{a} S(x,y) = \int_{\pi/a}^{-\pi/a} \frac{d^4 p}{(2\pi)^4} \frac{\left[-i \sum_{\mu} \gamma_{\mu} \sin(p_{\mu} a) + M_0 a \right]}{\sum_{\mu} \sin^2(p_{\mu} a) + M_0^2 a^2} e^{ip(x-y)}. \quad (2.10)$$

Recovering the limit $a \rightarrow 0$ one obtains

$$S(x,y) = \lim_{a \rightarrow 0} \int_{-\pi/a}^{\pi/a} \frac{d^4 p}{(2\pi)^4} \frac{\left[-i \sum_{\mu} \gamma_{\mu} \tilde{p}_{\mu} + M_0 \right]}{\sum_{\mu} \tilde{p}_{\mu}^2 + M_0^2} e^{ip(x-y)}, \quad (2.11)$$

with $\tilde{p}_{\mu} = \frac{\sin(p_{\mu} a)}{a}$.

This propagator indeed keeps the physical pole associated with the particle mass. However one must be very careful in taking the continuum limit near the Brillouin zone

boundary. In fact, when p_μ takes the value π/a the function $\sin ap_\mu$ in (2.11) becomes null (as it happens for $p_\mu = 0$). This, in turn, implies that near the point $p_\mu = 0$ or $p_\mu = \pi/a$ the propagator will have extra divergences. These, fifteen regions are pure lattice artifacts having no continuum analog. In conclusion, discretizing the theory with this naive approach one obtains 16 different fermionic species with degenerate mass. This is the so called *fermion doubling* problem.

The doubling problem can be solved by adding to the action a second order derivative term proportional to the lattice spacing a , which therefore vanishes in the continuum limit, called the Wilson term as it was introduced for first time in [26] :

$$S_F^W = S_F + a^4 \sum_x a \frac{r}{2} \bar{\psi}(x) D_\mu^* D_\mu \psi(x) = a^4 \sum_x \bar{\psi}(x) [D_W + M_0] \psi(x), \quad (2.12)$$

where r is the Wilson parameter and the *Wilson-Dirac operator* can be defined as

$$D_W = \sum_\mu \frac{1}{2} \gamma_\mu (D_\mu + D_\mu^*) + a \frac{r}{2} D_\mu^* D_\mu. \quad (2.13)$$

If we calculate the propagator for $S^W(x, y)$, we find that it has been modified in the following way

$$S^W(x, y) = \int_{-\infty}^{\infty} \frac{d^4 p}{(2\pi)^4} \frac{\left[-i \sum_\mu \gamma_\mu \tilde{p}_\mu + M(p) \right]}{\sum_\mu \tilde{p}_\mu^2 + M(p)^2} e^{ip(x-y)}, \quad (2.14)$$

where

$$M(p) = M_0 + \frac{2r}{a} \sin \left(\frac{p_\mu a}{2} \right). \quad (2.15)$$

What happens now is that for any finite value of r the mass of these 15 additional particles, known as doublers, gets larger and larger with the decreasing of the lattice spacing, and eventually decouples from the system in the continuum. In particular setting $r = 1$, in a typical lattice simulation with an inverse lattice spacing of roughly 2 GeV the 15 doublers have a mass of at least 4 GeV, so their presence can be safely ignored in the computation.

The presence of this term in an interacting theory such as QCD has a bad side effect: the chiral symmetry is broken at finite lattice spacing. This comes from a more general

property of QCD, expressed by the No-Go Nielsen and Ninomiya theorem [27], which states that it is impossible to define a discretization of QCD simultaneously free from the fermion doubling problem which reproduces the correct chiral limit when the mass parameter m is set to zero.

Though chiral symmetry is restored in the continuum limit, the fact that it is broken on the lattice has important consequences. First of all it introduces $O(a)$ errors, while the original naive formulation is affected only by $O(a^2)$ errors. Moreover, the quark mass term is not protected against additive renormalization. The renormalized quark mass takes the form $m_R = Z_m(M_0 - M_{cr})$ where M_{cr} is called the critical mass.

2.1.2 Regularization of Yang-Mills theory

Once the problem of unphysical zero modes is solved one can discretize the QCD continuum action to obtain the lattice version.

In order to regularize the QCD we have to make the lattice Lagrangian for fermionic field described in the previous chapter gauge invariant. Let us define a lattice SU(3) gauge transformation $\Omega(x)$, being x the coordinate of a generic lattice site. Fermionic fields must transform according to the fundamental representation of the transformation

$$\begin{aligned}\psi(x) &\rightarrow \Omega(x)\psi(x) \\ \bar{\psi}(x) &\rightarrow \bar{\psi}(x)\Omega^\dagger(x).\end{aligned}\tag{2.16}$$

While the mass lagrangian term is automatically invariant under gauge transformations

$$M\bar{\psi}(x)\psi(x) \rightarrow M\bar{\psi}(x)\Omega^\dagger(x)\Omega(x)\psi(x),\tag{2.17}$$

for the discretized derivative this is not true, consider for example

$$\bar{\psi}(x)\psi(x + \hat{\mu}) \rightarrow \bar{\psi}(x)\Omega^\dagger(x)\Omega(x + \hat{\mu})\psi(x + \hat{\mu})\tag{2.18}$$

As in the continuum case, in order to make the whole lagrangian gauge invariant we have to introduce some kind of covariant derivative. This can be achieved by defining, for each link connecting two nearest neighbour lattice sites n , $n + \hat{\mu}$, a link variable U_μ , element of SU(3), transforming under the gauge transformation Ω as:

$$\begin{aligned}U_\mu(x) &\rightarrow \Omega(x)U_\mu(x)\Omega^\dagger(x + \hat{\mu}) \\ U_\mu^\dagger(x) &\rightarrow \Omega(x + \hat{\mu})U_\mu^\dagger(x)\Omega^\dagger(x),\end{aligned}\tag{2.19}$$

Then, replacing the derivatives D_μ and D_μ^* in eq. (2.13) with ∇_μ and ∇_μ^* which are the forward and the backward covariant lattice derivatives, respectively, defined by

$$\nabla_\mu \psi(x) = \frac{[U_\mu(x)\psi(x + a\hat{\mu}) - \psi(x)]}{a} \quad (2.20)$$

$$\nabla_\mu^* \psi(x) = \frac{[\psi(x) - U_\mu^{-1}(x - a\hat{\mu})\psi(x - a\hat{\mu})]}{a} \quad (2.21)$$

we obtain an action which is gauge invariant under the defined transformation Ω

$$S_F^W[\psi, \bar{\psi}, U] = a^4 \sum_x \bar{\psi}(x) [D_W[U] + M] \psi(x). \quad (2.22)$$

Notice that the link variable $U_\mu(x)$ can be written in terms of a generating element $A_\mu = A^a T^a$ of the algebra of SU(3)

$$U_\mu(x) = e^{ig_0 a A_\mu(x)}, \quad (2.23)$$

where g_0 is the bare coupling constant.

For the gauge fields introduced in the covariant derivative we have also to introduce a kinetic term S_G .

The simplest gauge-invariant quantity that can be built from the group elements U_μ is the trace of the plaquette P , defined as the ordered product of the four links variables lying over the border of the square defined by the points x and $x + \hat{\mu} + \hat{\nu}$:

$$U_P \equiv U_{\mu\nu} = U_\mu(x)U_\nu(x + \hat{\mu})U_\mu^\dagger(x + \hat{\mu} + \hat{\nu})U_\nu^\dagger(x). \quad (2.24)$$

In particular the expression found by Wilson for the gauge action which in the continuum limit correctly reduces to

$$S_G^{cont} = \frac{1}{2} \int d^4x \text{Tr}(F_{\mu\nu}F^{\mu\nu}), \quad (2.25)$$

is given by

$$S_G^W = \sum_P \beta \left(1 - \frac{1}{3} \text{Re}\{\text{Tr}[U_P]\} \right), \quad (2.26)$$

where the sum is intended over the plaquette, which means indicating with n the generic lattice site

$$\sum_P \equiv \sum_n \sum_{\nu < \mu}. \quad (2.27)$$

Indeed, making use of the expansion

$$A_\nu(x + a\hat{\mu}) = A_\nu(x) + a\partial_\mu A_\nu(x) + O(a^2), \quad (2.28)$$

and of the Baker-Campbell-Hausdorff formula

$$e^A e^B = e^{A+B+\frac{1}{2}[A,B]+\dots}, \quad (2.29)$$

it is possible to express the plaquette as

$$U_{\mu\nu} = e^{ig_0 a^2 F_{\mu\nu}}, \quad (2.30)$$

where we have defined $F_{\mu\nu}$ as

$$F_{\mu\nu} = \partial_\mu A_\nu(x) - \partial_\nu A_\mu(x) + ig_0[A_\mu(x), A_\nu(x)] + O(a^2). \quad (2.31)$$

Taking the continuum limit of eq. (2.31) one finds the well known expression for the field tensor in QCD. Then simply substituting eq. (2.30) in eq. (2.26) one finds

$$S_G^W \xrightarrow{a \rightarrow 0} -\frac{\beta}{12} \int d^4x F_{\mu\nu} F^{\mu\nu} + O(a^2). \quad (2.32)$$

This means that the action S_G^W correctly reproduces to the continuum one up to $O(a^2)$ terms, assuming the following relation between β and the bare coupling constant $\beta = \frac{6}{g_0^2}$.

In summary, the lattice QCD action can be written as

$$S_{LQCD} = S_G[U] + \sum_f S_{F,f}^W[U, \psi_f, \bar{\psi}_f], \quad (2.33)$$

with S_G from eq.(2.26) and where for each quark flavor $S_{F,f}^W$ has the form of eq.(2.22).

2.2 Improvement

Being not possible to choose arbitrarily small lattice spacing, it is advisable to use any possible strategy to minimize discretization effects and make the extrapolation to the continuum limit simpler. We have already shown that Wilson gauge action (2.26) reproduces the continuum limit up to terms $O(a^2)$. Wilson regularized fermionic action, defined in eq. (2.22), instead, reproduces the continuum limit up to terms of order $O(a)$. One possibility to improve the approach to the continuum of the discretized action is to add operators of dimension greater than 4, which vanish in the continuum limit. These operators must not modify the symmetries of the regularized action in order not to spoil the continuum limit, but can suppress lattice artifacts and partially remove the discretization effects. If a is small, the S can be expanded in powers of a and the lattice theory can be described by means of a local effective theory with the following action

$$S_{eff} = S_0 + ac_1 S_1 + a^2 c_2 S_2 + O(a^3), \quad (2.34)$$

where S_0 is the continuum QCD action while S_i are irrelevant operators, of dimension $4+i$, suppressed by increasing powers of the cut-off a . Among all the possible operators, the allowed ones are the ones which share the same symmetry of the lattice action.

It is not only the lattice action which is responsible for the cut-off effects, but also the composite local operators which enter the Green functions of interest. Consider the renormalized n -point correlation function

$$G_n(x_1, \dots, x_n) = (Z_\Phi)^n \langle \Phi(x_1) \dots \Phi(x_n) \rangle_{cont}, \quad (2.35)$$

where Z_Φ is the renormalization constant and the points x_1, \dots, x_n are kept well separated from each other. In the local effective theory, the renormalized field $Z_\Phi \Phi(x)$ can be represented as the effective field

$$\Phi_{eff}(x) = \Phi_0(x) + a\Phi_1(x) + a^2\Phi_2(x) + O(a^2), \quad (2.36)$$

where again the fields $\Phi_k(x)$ are a linear combination of local fields with the proper dimension and symmetry properties. At $O(a)$, the connected correlation function on the lattice is given by

$$\begin{aligned}
G_n(x_1, \dots, x_n) &= \langle \Phi_0(x_1), \dots, \Phi_0(x_n) \rangle_{cont} \\
&\quad - a \int d^4y \langle \Phi_0(x_1), \dots, \Phi_0(x_n) \mathcal{L}_1(y) \rangle_{cont} \\
&\quad + a \sum_{k=1}^n \langle \Phi_0(x_1), \dots, \Phi_1(x_k), \dots, \Phi_0(x_n) \rangle_{cont} + O(a^2), \quad (2.37)
\end{aligned}$$

where the subscript *cont* indicates that the expectation values on the right hand side must be taken using the action S_0 . Moreover Φ_1 and \mathcal{L}_1 , which are a linear combination of operators, contains a dependencies inside the coefficients. Those coefficients can be calculated in perturbation theory as polynomial expressions in $\log(a)$.

It should be possible to add a set of irrelevant operators explicitly to the action with appropriate coefficients such to cancel at a certain order the lattice artifacts. The addition of these operators is known as Symanzik improvement program [28].

It will be shown in section 2.3 that using a particular formulation for the fermionic lattice action, known as *twisted mass* lattice QCD (tm-LQCD) action, which is the regularization chosen for our analysis, one is able to gain $O(a)$ improvement in an automatic way only by tuning appropriately M_0 to its critical value M_{cr} , instead of improving both the action and the operators involved in the simulation.

The Symanzik improvement program can be also applied to the gauge action. At first order this requires to write the gauge action in terms of all possible length 6 and 4 paths (which means to add rectangle and chair-shaped paths to the simple plaquette). The simplest case is the tree-level Symanzik improved action in which only rectangle contributions are added so that the gauge action reads:

$$S_{Sym} = \frac{2}{g^2} \sum_n \left[c_0 \sum_{\nu < \mu} (3 - \text{Re} \{ \text{Tr} [U_P^{1 \times 1}] \}) + c_1 \sum_{\nu < \mu} (3 - \text{Re} \{ \text{Tr} [U_P^{2 \times 1}] \}) \right], \quad (2.38)$$

where $U_P^{1 \times 1}$ is the usual plaquette defined in eq. (2.24), while $U_P^{2 \times 1}$ is the rectangle defined as

$$U_P^{2 \times 1} = U_\mu(x) U_\nu(x + \hat{\mu}) U_\nu(x + 2\hat{\mu}) U_\mu^\dagger(x + \hat{\mu} + \hat{\nu}) U_\mu^\dagger(x + \hat{\nu}) U_\nu^\dagger(x) \quad (2.39)$$

The coefficients c_0 and c_1 are fixed perturbatively to $c_1 = 1/12$, $c_0 = 18c_1$.

In the Iwazaki improved action [29], which is the one used in our analysis to regularize the gauge sector, also the chair-shaped paths are included, moreover the coefficients are fixed non-perturbatively.

2.3 Twisted Mass Action

In this section we will present the fermionic action employed in the simulations, known as twisted mass lattice QCD action. The choice for this particular kind of regularization is justified, as we have already anticipated and as we will further discuss in section 2.3.1, because it automatically provides the $O(a)$ improvement for the correlation functions [30, 31].

The twisted mass action however, was originally introduced to solve a different problem [32]. The eigenvalues of the Wilson fermionic matrix fluctuate configuration per configuration because of additive renormalization, and at small quark mass exceptional configurations with anomalously low eigenvalues may appear, whose presence put strong practical and conceptual problems in the numerical analysis, and in particular limits the smallness of the quark masses which can be analysed at a fixed lattice spacing. Twisted mass action provides an infrared regulator that allows to obtain substantially smaller quark masses compared to the Wilson fermion action.

We will start introducing the action and investigating its relation with the one presented in the previous sections.

Let us consider two flavors, $N_f = 2$, of degenerate quarks,

$$\chi = \begin{pmatrix} \chi_u \\ \chi_d \end{pmatrix}. \quad (2.40)$$

The action for the two flavor doublet χ reads

$$S_{tm}[\chi, \bar{\chi}, U] = a^4 \sum_x \bar{\chi}(x) [D_W + M_0 + i\mu\gamma_5\tau_3] \chi(x) = a^4 \sum_x \bar{\chi}(x) D_{tm} \chi(x), \quad (2.41)$$

where D_W is the one defined in eq. (2.13). In (2.41) μ is the so called *twisted mass* and τ_3 is the third Pauli matrix of the flavour symmetry group $SU(2)_f$.

It is interesting to take the continuum limit of (2.41)

$$S_{tm}[\chi, \bar{\chi}, U] \xrightarrow{a \rightarrow \delta} \int d^4x \bar{\chi}(x) [\gamma_\mu D_\mu + m_q + i\mu\gamma_5\tau_3] \chi. \quad (2.42)$$

where $m_q = M_0 - M_{cr}$.

Notice that we can write the mass term as

$$m_q + i\mu\gamma_5\tau_3 = Me^{i\alpha\gamma_5\tau_3}, \quad (2.43)$$

where the untwisted m_q and *twisted mass* μ are now related with the so called polar mass M via the following relations

$$\begin{cases} m_q = M \cos\alpha \\ \mu_q = M \sin\alpha \end{cases} \rightarrow \begin{cases} M = \sqrt{m_q^2 + \mu^2} \\ \tan\alpha = \frac{\mu}{m_q} \end{cases} \quad (2.44)$$

Clearly, in the continuum, the Twisted Mass QCD action is just a rewriting of the standard QCD one in a different basis connected to the ψ one by

$$\chi \rightarrow e^{-i\omega\gamma_5\tau_3/2} \chi = \psi, \quad \bar{\chi} \rightarrow \bar{\chi} e^{-i\omega\gamma_5\tau_3/2} = \bar{\psi}, \quad (2.45)$$

provided we have chosen $\omega = \alpha$, *i.e.* $\tan\omega = \mu/m_q$. Indeed, under transformation (2.45), if the operator D_μ is invariant under chiral transformation, the only affected term is the mass term for which

$$Me^{i\alpha\gamma_5\tau_3} \rightarrow Me^{i(\alpha-\omega)\gamma_5\tau_3}, \quad (2.46)$$

so for the proper choice of ω one has

$$S_{tm}^{cont}[\chi, \bar{\chi}, U]_{m_q, \mu} \rightarrow S_W^{cont}[\chi, \bar{\chi}, U]_M = \int d^4x \bar{\psi}(x) (\gamma_\mu D_\mu + M) \psi(x). \quad (2.47)$$

For this reason, $\chi, \bar{\chi}$ is referred to as the *twisted basis* while, $\psi, \bar{\psi}$ is referred to as the *physical basis*.

At finite lattice spacing, however, the situation is different because the term D_W in the Wilson action breaks the chiral symmetry when the mass parameter is set to zero. Thus

the twisted mass term cannot be eliminated with a rotation of the fermionic fields. This means that the Wilson action and the twisted mass action are not equivalent for finite lattice spacings but only when we take the continuum limit.

It can be useful to write the twisted mass action in the physical basis. It can be easily done applying eqs. (2.45) to the Wilson Twisted Mass action and using the definition (2.13) of D_W . The action turns out to be written in the physical basis as

$$S_{tm}[\psi, \bar{\psi}, G] = a^4 \sum_x \bar{\psi}(x) \left[\frac{1}{2} \sum_{\mu} \gamma_{\mu} (\nabla_{\mu}^* + \nabla_{\mu}) + \left(M_0 - \frac{ar}{2} \sum_{\mu} \nabla_{\mu}^* \nabla_{\mu} \right) e^{-i\omega\gamma_5\tau_3} + m_q \right] \psi(x). \quad (2.48)$$

In this basis, the Wilson term is the *twisted* one, while the mass term is left real.

It is of particular relevance the case $m_q = 0$, hence $M_0 = M_{cr}$ which also implies that the only contribution to the continuum fermion mass M comes from the twisted mass μ (see eqs. (2.44)). This corresponds to a rotation of $\omega = \pi/2$ and under this condition the action is called twisted mass action at *maximal twist*. Tuning the action to maximal twist, as we will see in the next section, is sufficient to guarantee an automatic $O(a)$ improvement.

From the other side, the Twisted terms break parity and isospin at finite lattice spacing. The breaking of parity induces mixing between pseudo-scalar and scalar particles, for example mesons. Being scalar heavier than pseudo-scalar mesons, this is not a problem when one is interested in looking at the lighter ones, because scalar mesons appear as excited states whose presence goes away in the continuum, but can be more troublesome if one is interested in looking at the scalar mesons. Isospin breaking instead leads to a breaking of the SU(2) vectorial symmetry of QCD with two degenerate flavors. The lack of this symmetry at finite lattice spacing means for example that $M_{\pi^+} = M_{\pi^-} \neq M_{\pi^0}$ for discretization effects.

Before moving to the automatic $O(a)$ improvement of the twisted mass regularization, it is useful to add some details on the renormalization of the two bare mass parameters, M_0 and μ . As it is well known the Wilson term breaks explicitly the axial symmetry at

finite lattice spacing. Consequently, as we already discussed, the bare untwisted quark mass is subject to an additive renormalization constant in addition to the multiplicative one:

$$m_q^R = Z_m m_q = Z_m (M_0 - M_{cr}). \quad (2.49)$$

M_{cr} is the value of M_0 where the untwisted quark mass vanishes.

On the other hand, the twisted mass μ_q renormalizes only multiplicatively. It can be shown that the product of the twisted mass μ_q and pseudoscalar density \mathcal{P} is renormalization group invariant. Thus Z_P^{-1} renormalizes μ_q

$$\mu^R = Z_\mu \mu = Z_P^{-1} \mu. \quad (2.50)$$

So, another advantage of working at maximal twist is that the twisted mass μ is in this condition the only mass parameter related directly with the physical mass and, unlike the untwisted mass m_0 , it renormalizes multiplicatively.

The use of Twisted Mass regularization at maximal twist has the further advantage of simplifying the renormalization of some hadronic matrix element. In particular the decay constant f_{PS} of a pseudo-scalar meson composed of two quarks of masses m_1 and m_2 in Wilson regularization is computed as

$$f_{PS} p^\mu = \langle 0 | A_\mu^R | PS \rangle \quad (2.51)$$

where A_μ^R is the renormalized axial current, which can be computed on the lattice only through an appropriate renormalization procedure. However, making use of the Partially Conserved Vector Current (PCVC) relation holding at maximal twist, it can be also computed as

$$f_{PS} = (m_1 + m_2) \frac{\langle 0 | P_5 | PS \rangle}{M_{PS}^2} \quad (2.52)$$

without the need of the knowledge of any renormalization constants [30].

2.3.1 Automatic $O(a)$ improvement

At maximal twist, for which $\omega = \pi/2$, the quark mass comes from the twisted term only, and the exponential $e^{(-i\omega\gamma_5\tau_3)}$ reduces to $-i\gamma_5\tau_3$. So that the theory tuned at maximal twist at finite lattice spacing describes two flavors of Wilson fermions regularized with

two opposite values of r , each carrying a non trivial Dirac structure γ_5 .

$$S_{tm}[\psi, \bar{\psi}, G] = a^4 \sum_x \bar{\psi}(x) \left[\frac{1}{2} \sum_{\mu} \gamma_{\mu} (\nabla_{\mu}^* + \nabla_{\mu}) + \right. \\ \left. - i\gamma_5 \tau_3 \left(M_{cr} - \frac{ar}{2} \sum_{\mu} \nabla_{\mu}^* \nabla_{\mu} \right) + \mu \right] \psi(x). \quad (2.53)$$

This situation has a very nice property: parity even correlation functions (which include all the physical correlators) are automatically $O(a)$ improved, and $O(a)$ discretization effects will appear only in parity odd (unphysical) correlation functions. For a detailed proof see [30], in the present letter we will only give a sketch of the argument behind this remarkable features of twisted mass regularization of QCD.

Through Symanzik expansion (presented in section 2.2) it can be shown that $O(a)$ discretization effects in parity even correlation functions computed in Wilson regularized QCD are odd with respect to a transformation that changes the sign of the Wilson parameter r . Therefore it could be possible to get rid of all the $O(a)$ discretization effects by averaging correlation functions computed with $r = +1$ with the same functions computed with $r = -1$. This is exactly what happens in tmQCD at maximal twist, where the average is automatically performed between the two quarks of the doublet.

So, instead of having to improve both the action and the operators involved in the simulation, one is able to gain $O(a)$ improvement in an automatic way only by tuning to maximal twist.

A possible approach to achieve this tuning is presented in the next section.

2.3.2 Tuning to maximal twist

One of the main advantages of the Twisted Mass Action is that automatic $O(a)$ improvement can be achieved, working at maximal twist, by tuning only one parameter, the bare quark mass M_0 , to its critical value M_{cr} . This means that in the full renormalized theory the maximal twist condition is realized by tuning M_0 to a value for which the renormalized Wilson mass m_q^R is 0.

This can be achieved by making use of the Partially Conserved Axial Current (PCAC) relation

$$m_q^R = \frac{Z_A \langle (\partial_\mu A_\mu^a(x)) P^a(0) \rangle}{2Z_P \langle (P^a(x)) P^a(0) \rangle}, \quad (2.54)$$

where A and P are the axial and pseudoscalar currents. This relation descends from the axial untwisted Ward identity [30], and using it the renormalized Wilson mass can be determined. Being interested in getting a null m^R , it is sufficient to tune M_0 to get a null value of the correlation function $\langle (\partial_\mu A_\mu^a(x)) P^a(0) \rangle$.

2.3.3 Twisted mass with non degenerate quarks

The strange and charm quarks can be introduced in the Twisted Mass action by adding a twisted heavy mass-split doublet [33]

$$\chi_h = \begin{pmatrix} \chi_c \\ \chi_s \end{pmatrix}. \quad (2.55)$$

The twisted lattice fermionic action of a SU(2) pair of mass non-degenerate quarks can be written in the form

$$S_{tm}^h = a^4 \sum_x \bar{\chi}_h(x) [D_W + M_0 + i\mu_\sigma \gamma_5 \tau_1 + i\mu_\delta \tau_3] \chi_h(x), \quad (2.56)$$

where h stands for heavy, M_0 is the untwisted bare quark mass for the heavy doublet, μ_σ the bare Twisted Mass and μ_δ the mass splitting along the τ_3 direction. Physical values of the strange and the charm quark mass can be achieved by tuning the parameters μ_σ and μ_δ such that the simulated K and D mesons have their physical masses. The chiral rotation relating the heavy quark doublet in the twisted basis to the one in the physical basis are given by

$$\begin{aligned} \psi_h(x) &= e^{i\omega_h \gamma_5 \tau_1 / 2} \chi_h(x) \\ \bar{\psi}_h(x) &= \bar{\chi}_h(x) e^{i\omega_h \gamma_5 \tau_1 / 2}. \end{aligned} \quad (2.57)$$

The bare parameters μ_σ and μ_δ for the non-degenerate heavy doublet are related to the physical renormalized strange and charm quarks through [31]

$$\begin{aligned}
m_c &= \frac{1}{Z_P} \left(\mu_\sigma + \frac{Z_P}{Z_S} \mu_\delta \right), \\
m_s &= \frac{1}{Z_P} \left(\mu_\sigma - \frac{Z_P}{Z_S} \mu_\delta \right).
\end{aligned} \tag{2.58}$$

2.4 Numerical simulations

The formulation of a field theory on the lattice, besides providing an ultraviolet cut off, represents also an operative definition for calculating vacuum expectation values of operators.

$$\langle 0 | O | 0 \rangle = \frac{1}{Z} \int [\mathcal{D}U] [\mathcal{D}\psi] [\mathcal{D}\bar{\psi}] O(U, \psi, \bar{\psi}) e^{-S(U, \psi, \bar{\psi})}, \tag{2.59}$$

where the partition function Z is defined as

$$Z = \int [\mathcal{D}U] [\mathcal{D}\psi] [\mathcal{D}\bar{\psi}] e^{-S(U, \psi, \bar{\psi})}. \tag{2.60}$$

On the lattice, functional integrals like (2.59) become ordinary multiple integrals which can be numerically evaluated.

In this section we will describe some of the numerical simulation techniques employed in a lattice calculation. In particular we will begin considering how fermionic fields are treated in the integration and then move to the gauge field part.

2.4.1 Integration of the fermionic degrees of freedom

Let us consider eq. (2.59). Fermionic fields are anti-commutating variables, which in order to be treated numerically should be represented in terms of matrices of rank equal to the lattice volume. One can avoid dealing with such representation by analytically perform the integration over the fermionic variables using the following relation which is a particular case of the Wick theorem

$$\int [\mathcal{D}\psi] [\mathcal{D}\bar{\psi}] e^{-\bar{\psi} M \psi} = \det M. \tag{2.61}$$

Thus the partition function can be expressed as the integral over all the configurations of fields U defining an effective action S_{eff} as

$$Z = \int [\mathcal{D}U] e^{-S_G(U) + \ln(\det M)} = \int [\mathcal{D}U] e^{-S_{eff}}, \quad (2.62)$$

and eq. (2.59) can be rewritten as

$$\langle O \rangle = \frac{\int [\mathcal{D}U] O(U) e^{-S_{eff}}}{\int [\mathcal{D}U] e^{-S_{eff}}}, \quad (2.63)$$

with $O(U)$ being expressed in terms of the gauge fields, according to the Wick theorem.

2.4.2 Montecarlo method for the gauge configurations

Once the fermionic degrees of freedom have been analytically integrated out, we are left with the integral over the gauge fields, which has to be computed numerically. It is clear that already with lattice grids of few points per size, the number of degrees of freedom is too large to allow for a direct evaluation of integrals, so one need to rely on Dynamic Monte Carlo techniques.

However, most of the link gauge configurations have an action that takes large values and fortunately only a small fraction of them will make a significant contribution to the integral. That is, the distribution is highly peaked on those configurations that minimize the action.

For this reason in any lattice simulation only a representative set of gauge configurations is used. This method goes by the name of *importance sampling*. The set of gauge configurations is generated according to a probability distribution given by the Boltzmann factor $P(U_i) = e^{S_{eff}}$ and in particular using a Markov chain where each configuration U_i is obtained from the preceding one U_{i-1} .

For each gauge configuration U_i one measures the value of the observable O_i on such configuration, and then an approximate estimate \bar{O} of the observable is given by simple average of the N determinations O_i . How to properly estimate the statistical uncertainties in these conditions will be discussed in the following sections.

2.4.3 Error analysis

In what follows we briefly present two methods used in our analysis to correctly handle statistical errors in a lattice simulation.

Jackknife analysis

Observable quantities like the meson masses and the leptonic decay constants are derived in lattice calculation from correlation functions as will be explained in sec. 2.5. To obtain these correlation functions a numerical evaluation of the path integral, performed according to the techniques briefly presented in sec. 2.4, is needed. All these techniques are based on the general idea that the mean over all gauge configuration can be replaced with a mean over an appropriate subsample of those configurations. These configurations, however have been generated following a Markov chain so the i th configuration depends on the $(i - 1)$ th configuration. This introduces correlations that need to be properly handled. First of all, one should update the algorithm for a sufficiently large number of steps so that thermalization is achieved, i.e until the system has lost all memory of the initial configuration. Once thermalization is reached one has to select a set of gauge configurations U_i separated by an adequate number of Monte Carlo trajectories in order to reduce the autocorrelation between measurements. In our analysis for example we used a block size of 20 trajectories.

Nonetheless observables calculated on these gauge configurations are still partially correlated. Therefore the typical standard deviation is not a realistic error. The Jackknife method is a statistical method for estimating the error propagation from the original data to derived quantities taking correlation into account.

The general idea is to take a subset of n_i gauge configurations and calculate the averages over this subsample. In this way, if n_i is large enough the averages can be considered as single uncorrelated measures and treated with the usual standard deviation. If however, as in most of practical situation, the subset n_j is not large enough a possible solution is the Jackknife method.

Consider a generic observable \mathcal{O} calculated over N gauge configurations. Instead of taking the average \mathcal{O}_i^J over the n_i configurations, the average is performed on the complementary set $N - n_i$ which is larger. The optimum estimate for the expectation value of the observable \mathcal{O} is $\langle \mathcal{O} \rangle_N \pm \sigma_{jack}(\mathcal{O})$, where σ_{jack} takes into account the fact that the $\mathcal{O}_{i=1\dots N}^J$ are calculated over sets that share part of the data. The formula to calculate σ_{jack} reads

$$\sigma_{jack}^2(O) = (N_J - 1) \left(\langle O_J^2 \rangle_{N_J} - \langle O_J \rangle_{N_J}^2 \right), \quad (2.64)$$

with

$$\langle O_J \rangle_{N_J} = \frac{1}{N_J} \sum_{i=1}^{N_J} O_i^J. \quad (2.65)$$

Bootstrap analysis

In many practical situations one is interested in combining quantities coming from different gauge ensembles, for example in a fit. In these cases it is therefore necessary to correctly estimate how the errors on the original quantities propagate in the derived quantities. Let us consider a practical example. We suppose we have to compare two, statistically independent, quantities A and B , to obtain a third quantity, C , which derives from the other two. We have at our disposal for the input quantities N_J jackknife averages, A_i^J and B_i^J , which have been calculated as explained in the previous section. Notice that, as there is no correlation between the two samples A_i^J and B_i^J , we can in principle choose to combine whatever of the N_J^2 couples (A_i^J, B_k^J) with $i, k = 1 \dots N_J$. The bootstrap procedure consists of generating, following a random distribution, a N_{boot} number (high enough) of $(i, k)_b$ couples. Then, one will proceed to evaluate for each couple b the dependent quantity C_b^B . The mean value C will be equal to the ensemble average. The bootstrap error for that quantity will be given by

$$\sigma_b^2(O) = (N_J - 1) \left(\langle C_B^2 \rangle_{N_{boot}} - \langle C_B \rangle_{N_{boot}}^2 \right), \quad (2.66)$$

with

$$\langle O_J \rangle_{N_{boot}} = \frac{1}{N_{boot}} \sum_{i=1}^{N_J} C_b^B. \quad (2.67)$$

2.4.4 Systematic effects

In the following section we will analyse the various problems affecting a typical lattice computation and the techniques used to treat them.

Chiral extrapolation

In all regularizations, lower values of the quark mass (m_q) correspond to enhance the density of low eigenvalues of the fermionic matrix, and this makes computations more and more demanding and difficult as m_q is lowered. Generally speaking, the lowest value

of quark masses considerable in a simulation, necessary to avoid the problem of exceptional configuration, decreases with decreasing lattice spacing a . This means that, if we want keep the simulated volume large enough to contain finite size effects, the number of lattice points has to be increased in order to simulate lower quark masses.

Only recently, thanks to the increased computational power, the first computations at physical light quark mass have been presented (For example the MILC collaboration is the only one to have data at the physical points in a four dynamical fermion simulation [34]). However, at present, still a large majority of simulations, including ours, is performed with light quark masses higher than their physical value.

This has to be taken into account by performing an accurate chiral extrapolation $m_{light} \rightarrow m_{physical}$ during the computations, as will be described in details in an appropriate section of each studied quantity.

Finite size effects

When performing computations on the lattice, the volume acts as infrared cut-off on the obtained observable, that has to be removed at the end of the computation.

The effects of the finite volume is to modify the energy levels of the particle described by the theory. The shift of the energy levels can be shown to be related to the scattering length of particles in the box, and thus in general can be computed analytically and removed without performing explicitly the $V \rightarrow \infty$ limit. The relevant scales for determining the finite size effects (FSE) are the side L of the box simulated, and the mass of the lowest particle of the theory, therefore the pion mass M_π which, having a greater propagation length, is the most affected by the presence of borders.

For the observables computed in this analysis, FSE are in general an exponentially suppressed function of the quantity $M_\pi L$, which, for the values of $M_\pi L$ associated with our gauge ensembles (typically $\gtrsim 4$), can be calculated using ChPT.

We checked explicitly the amount of FSE by performing in one case two simulations at the same M_π but different L . This allowed us to check not only the amount of FSE in the raw data but also the efficiency of the analytical correction formula we used.

Discretization effects

The lattice regularized theory reproduces the original theory only in the continuum limit $a \rightarrow 0$. Observables computed at finite lattice spacing will differ from its continuum coun-

terpart for finite terms which vanish in this limit, generally called discretization effects. In order to extract continuum physics it is therefore necessary to compute observables at different values of the lattice spacing and extrapolate them to $a \rightarrow 0$.

In practice, data computed at finite lattice spacing are typically fitted with a polynomial expression in a . Once the a dependence has been studied through the fit the continuum limit is performed numerically.

This extrapolation induces errors on the observables, so one should try to work at lattice spacing that are as small as possible. However the minimal lattice spacing affordable is dictated by the available computational power. Hence the importance of improvement which guarantees that we have to deal only with effects of order a^2 and higher.

Lattice spacing determination

To choose the lattice spacing a at the beginning of the computations, one in practice has to fix the gauge coupling g at the value $g(a)$ that it assumes at the chosen scale. In general it is not possible to fix exactly g to the value required for the chosen lattice spacing, due to the uncertainties of the β -function, which is known only perturbatively up to few orders in g .

This means that at the beginning of the computation one cannot choose exactly the value of the lattice spacing to work with, but can only fix it roughly, by taking a reasonable value of g , with the help of the information coming from previous studies.

On the other hand, all quantities determined on the lattice are known only in units of a . Therefore, in order to convert all quantities to physical units, it is crucial to have a good knowledge of the lattice spacing. For this reason, after performing the computations, one needs to re-determine it.

This can be done by choosing a known quantity G and then confronting its value with the one computed in lattice units $G' = aG$.

In our analysis the scale was set using the pion decay constant f_π .

Quenching effects

Up to the late nineties the available computational power was not sufficient to allow to take into account the contribution of the fermionic determinant in lattice computations. For this reason all lattice calculations were performed neglecting the $\det M$ contribution in the action. This corresponds to perform the $m_{quark} \rightarrow \infty$ limit of the action, so that

sea quarks do not propagate, i.e. to neglect diagrams containing fermionic loops in the computation of the correlation functions. This approximation is known as *quenching* of the fermionic degrees of freedom.

In the last decade the development in algorithms and machines made it possible to start performing calculations taking into account the presence of the fermionic determinant. Nowadays, most of the lattice calculations are performed with either two (up and down) or three (up, down and strange) dynamical sea quarks. The present work, performed using the gauge configurations produced by the European Twisted Mass (ETM) Collaboration is one of the first to include the effects of four flavors of dynamical quarks ($N_f = 2 + 1 + 1$).

Non-perturbative renormalization

Renormalization constants provide the link between matrix element regularized on the lattice, and those renormalized in the continuum. The operators we simulate are bare operators regularized with the lattice spacing a which can be interpreted as an ultraviolet cut-off. Therefore renormalization constants can be computed perturbatively since they enclose only short-distance contributions. In practice, however, perturbation theory on the lattice is much more complex than the one in the continuum so that the computations are rarely extended beyond one loop order. Moreover, lattice perturbation theory usually converges rather slowly and the accuracy of the perturbative renormalization constants is limited. For this reason, one often prefer to rely on non-perturbative methods.

The renormalization constants used in the present work have been calculated non perturbatively in the so called RI-MOM scheme.

2.5 Two-point correlation functions

In this section we will discuss the relation between the quantities extracted from the euclidean theory, which is the one employed in simulations, and the physical ones, introducing the standard procedure used for the calculation of the meson masses and decay constants in a given regularization of the fermionic action.

The euclidean two-point Green function, for two generic operators \mathcal{O}_1 and \mathcal{O}_2 , can be written as

$$G(x) = G(t, \vec{x}) = \langle 0 | \mathcal{O}_1(x) \mathcal{O}_2^\dagger(0) | 0 \rangle. \quad (2.68)$$

$G(x)$, once rotated back to Minkowski space-time, gives $\langle 0 | T[\mathcal{O}_1(x) \mathcal{O}_2^\dagger(0)] | 0 \rangle$, with T the time-ordered product. This quantity represents the probability amplitude for the creation of a state sharing the quantum numbers of the \mathcal{O}_2 operator in the space-time point $x = 0$, the propagation of that state up to the point $x = (t, \vec{x})$ and its final annihilation from the \mathcal{O}_1 operator. If we Fourier transform the spacial component we get

$$C^{12}(t, \vec{p}) = \sum_{\vec{x}} \langle 0 | \mathcal{O}_1(x) \mathcal{O}_2(0) | 0 \rangle e^{i\vec{p}\cdot\vec{x}}. \quad (2.69)$$

Let us take $t > 0$ and insert in (3.6) a complete set of covariantly normalized energy eigenstates with well definite momentum $|n, \vec{p}_n\rangle$

$$\langle n, \vec{p}_n | m, \vec{p}_m \rangle = (2\pi)^3 2E_n \delta_{n,m}, \quad (2.70)$$

$$\sum_{n, \vec{p}_n} |n, \vec{p}_n\rangle \frac{1}{(2\pi)^3 2E_n} \langle n, \vec{p}_n | = \mathbb{1}, \quad (2.71)$$

one has

$$\begin{aligned} C^{12}(t, \vec{p}) &= \sum_{\vec{x}} \sum_{n, \vec{p}_n} \frac{\langle 0 | \mathcal{O}_1(x) | n, \vec{p}_n \rangle \langle n, \vec{p}_n | \mathcal{O}_2(0) | 0 \rangle}{(2\pi)^3 2E_n} e^{i\vec{p}\cdot\vec{x}} \\ &= \sum_{\vec{x}} \sum_{n, \vec{p}_n} \frac{\langle 0 | e^{Ht+i\vec{P}\cdot\vec{x}} \mathcal{O}_1(0, \vec{0}) e^{-Ht-i\vec{P}\cdot\vec{x}} | n, \vec{p}_n \rangle \langle n, \vec{p}_n | \mathcal{O}_2(0) | 0 \rangle}{(2\pi)^3 2E_n} e^{i\vec{p}\cdot\vec{x}} \\ &= \sum_{\vec{x}} \sum_{n, \vec{p}_n} \frac{\langle 0 | \mathcal{O}_1(0) | n, \vec{p}_n \rangle \langle n, \vec{p}_n | \mathcal{O}_2(0) | 0 \rangle}{(2\pi)^3 2E_n} e^{-E_n t - i(\vec{p}_n - \vec{p})\cdot\vec{x}} \\ &= \sum_n \frac{\langle 0 | \mathcal{O}_1(0) | n, \vec{p} \rangle \langle n, \vec{p} | \mathcal{O}_2(0) | 0 \rangle}{2E_n} e^{-E_n t} \end{aligned} \quad (2.72)$$

where the translation operator has been used to shift the field in the origin $\mathcal{O}(x) = e^{Ht+i\vec{P}\cdot\vec{x}} \mathcal{O}(0, \vec{0}) e^{-Ht-i\vec{P}\cdot\vec{x}}$ and the Dirac delta $\frac{1}{(2\pi)^3} \sum_{\vec{x}} e^{-i(\vec{p}_n - \vec{p})\cdot\vec{x}} = \delta(\vec{p}_n - \vec{p})$ has been used in performing the spatial “integration”.

Consider single particle states, for them at zero momentum one has $E_n(\vec{p}_n = \vec{0}; M_n) = M_n$, with M_n the mass of the n^{th} state. Then the relation 2.72 becomes

$$C^{12}(t) = \sum_n \frac{\sqrt{\mathcal{Z}_n^1} \sqrt{\mathcal{Z}_n^{2\dagger}}}{2M_n} e^{-M_n t} \quad (2.73)$$

where we have defined

$$\sqrt{\mathcal{Z}_n^i} = \langle 0 | \mathcal{O}_i(0) | n, \vec{p} \rangle. \quad (2.74)$$

So the euclidean 2-point correlation function can be written as a sum, over a lot of possible intermediate states n , of exponentials proportional to the matrix elements $\sqrt{\mathcal{Z}_n^1} \sqrt{\mathcal{Z}_n^{2\dagger}}$. However, for t large enough, only one term will survive because of the exponential suppression, and it will be the single particle state with the lower mass value i.e. the fundamental state:

$$\sum_{\vec{x}} \langle 0 | \mathcal{O}_1(x) \mathcal{O}_2(0) | 0 \rangle \xrightarrow{t \rightarrow \infty} \frac{\sqrt{\mathcal{Z}_0^1} \sqrt{\mathcal{Z}_0^{2\dagger}}}{2M_0} e^{-M_0 t}. \quad (2.75)$$

For fields defined in a finite time interval ($t \in [0, T]$), with periodic boundary conditions, (2.75) is no longer valid and must be modified in order to include contributions from forward and backward propagation. Hence, if we call η the (temporal) parity of the 2-point correlator with respect to the transformation $t \rightarrow T - t$, in the case of zero momentum we will have

$$C^{12}(t) \xrightarrow{t \rightarrow \infty} \frac{\sqrt{\mathcal{Z}_0^1} \sqrt{\mathcal{Z}_0^{2\dagger}}}{2M_0} (e^{-M_0 t} + \eta e^{-M_0(T-t)}). \quad (2.76)$$

In the $\eta = 1$ case, this expression reads

$$C^{12}(t) \xrightarrow{t \rightarrow \infty} \frac{\sqrt{\mathcal{Z}_0^1} \sqrt{\mathcal{Z}_0^{2\dagger}}}{M_0} e^{-M_0 \frac{T}{2}} \cosh \left[\left(t - \frac{T}{2} \right) M_0 \right]. \quad (2.77)$$

In the rest of the chapter our formulae will be always presented, for simplicity, in the infinite (lattice) time extension limit.

In this work we will consider local operators which *interpolate* mesons, i.e. operators with quantum numbers appropriate to create the meson states of interest from the vacuum. Such composite operators can be written as

State	J^{PC}	Dirac Matrix
Scalar	0^{++}	I
	0^{++}	γ_0
Pseudo-scalar	0^{-+}	γ_5
	0^{-+}	$\gamma_5\gamma_0$
Vector	1^{--}	γ_i
	1^{--}	$\gamma_0\gamma_i$
Axial Vector	1^{+-}	$\gamma_5\gamma_i$
Tensor	1^{+-}	$\gamma_i\gamma_k$

Table 2.1: J^{PC} quantum numbers of the 16 Dirac covariants and the Lorentz group transformation properties.

$$\mathcal{O}_\Gamma(x) = \sum_a \bar{q}_1^a(x) \Gamma q_2^a(x), \quad (2.78)$$

where q_1 and q_2 are two valence quarks of different flavour, a is a color index and the spinorial indices have been omitted for the sake of simplicity. Γ is one of the 16 combinations (see tab. 2.1) of Dirac γ matrices which are responsible for the *spin* (J), *parity* (P) and *charge conjugation* (C) quantum numbers of the composite operator $\mathcal{O}_\Gamma(x)$.

For example in this work we considered operators of the form

$$\mathcal{O}_1(x) = \mathcal{O}_2(x) = P_5(x) = \bar{q}_1 \gamma_5 q_2, \quad (2.79)$$

for which it is possible to exploit (2.77) for estimating in LQCD the corresponding meson masses and matrix elements through a simple exponential fit.

However, beside the exponential fit to the large time behaviour of the euclidean lattice correlator, there is another method for estimating meson masses, inspired again by (2.75). It is possible to calculate the so called effective mass (in lattice units), defined by

$$aM_{eff}(t) = \log \left[\frac{C^{12}(t)}{C^{12}(t+1)} \right]. \quad (2.80)$$

This quantity, for large t , will reach a plateau at a value equal to the mass of the ground state.

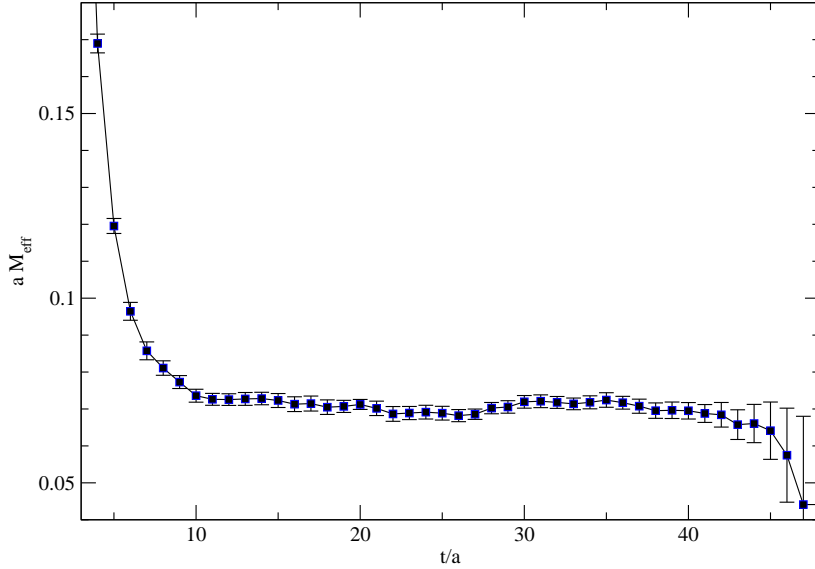


Figure 2.1: *Example of the plateau of the effective mass as a function of time.*

An example of the dependence of the effective mass as a function of time (in lattice units) is shown in fig. 2.1 for a light-light PS meson.

It is crucial to properly choose the time interval $[t_{min}, t_{max}]$ over which the fit has to be performed, so that the fundamental state is isolated. More specifically, t_{min} has to be chosen high enough for the contribution of excited state to be sufficiently suppressed. The lower is the mass difference between the ground state and the first excited states, the higher t_{min} has to be chosen. On the other hand, t_{max} is limited by lattice time extension T , and thus by the available computing power. Moreover the signal we are trying to isolate is exponentially suppressed by the factor $\exp(-M_0 t)$, see eq. 2.75, which lead for large t to noisy data.

Chapter 3

Quark Masses

The precise knowledge of the quark masses and of the hadronic parameters in general plays a fundamental role both in testing the Standard Model (SM) and in the search for new physics (NP). The SM, despite its unquestionable successes in describing experimental data gives neither an explanation nor a prediction for the quark masses. On the theoretical side, explaining and understanding the hierarchical structure of the quark masses remains an open and fascinating challenge. On the phenomenological side, since several important observables depend on the quark masses, a precise determination of these values is crucial to constrain the SM and through comparisons between theory and experiments to search for NP.

In the determination of the quark masses lattice QCD (LQCD) plays a primary role as it is a non perturbative approach based on first principles.

Thanks to the increased computational power as well as to the algorithm and action improvements of the last decade, LQCD simulations have made significant progresses reaching a remarkable level of precision. In particular, this is due to the so-called unquenched calculations, where the contribution of loops of dynamical sea quarks is taken into account. As a matter of fact, most of the recent lattice determinations of quark masses have been performed with either two (up and down) [3, 4] or three (up, down and strange) [5]-[12] dynamical sea quarks.

In this chapter we present an accurate determination of the average up/down, strange and charm quark masses using the gauge configurations produced by the European Twisted Mass (ETM) Collaboration with four flavors of dynamical quarks ($N_f = 2 + 1 + 1$), which include in the sea, besides two light mass degenerate quarks, also the strange

and the charm quarks with masses close to their physical values. Such a setup is the closest one to the real world, adopted till now only by the ETM [13, 14] and the MILC [15] Collaborations.

First we calculated the up/down average quark mass from the analysis of the pion mass and decay constant. Then, using scale setting determined from the pion part of the analysis, we extracted the strange and charm quark masses from the analysis of K - and D -meson correlators, respectively.

3.1 Simulation details

In this section the simulation details will be discussed. We will start presenting the action used in the simulation and then give some details on the gauge ensembles considered in this analysis.

3.1.1 The Action

The present work is based on the $N_f = 2 + 1 + 1$ gauge field configurations generated by the ETMC using the following action

$$S = S_g + S_{tm}^l + S_{tm}^h, \quad (3.1)$$

where the gluon action S_g is the Iwasaki one [29]. For the fermions the Wilson twisted-mass action is adopted, given for the mass-degenerate up/down quark doublet by [35]

$$S_{tm}^l = a^4 \sum_x \bar{\psi}(x) \left\{ \frac{1}{2} \sum_{\mu} \gamma_{\mu} (\nabla_{\mu} + \nabla_{\mu}^*) - i\gamma_5 \tau^3 \left[M_0 - \frac{a}{2} \sum_{\mu} \nabla_{\mu} \nabla_{\mu}^* \right] + \mu_l \right\} \psi(x) \quad (3.2)$$

and for the strange and charm doublet by [33]

$$S_{tm}^h = a^4 \sum_x \bar{\psi}(x) \left\{ \frac{1}{2} \sum_{\mu} \gamma_{\mu} (\nabla_{\mu} + \nabla_{\mu}^*) - i\gamma_5 \tau^1 \left[M_0 - \frac{a}{2} \sum_{\mu} \nabla_{\mu} \nabla_{\mu}^* \right] + \mu_{\sigma} + \mu_{\delta} \tau^3 \right\} \psi(x), \quad (3.3)$$

where ∇_{μ} and ∇_{μ}^* are nearest-neighbor forward and backward covariant derivative, μ_l is the light quark mass and M_0 is the untwisted mass tuned to its critical value M_{cr} as discussed in Ref. [13] in order to guarantee the automatic $\mathcal{O}(a)$ -improvement at maximal twist [30, 31]. Finally in Eq. (3.3) the twisted masses μ_{σ} and μ_{δ} are related to the

renormalized strange and charm sea quark mass via the relation [31]

$$m_{c,s} = \frac{1}{Z_P} \left(\mu_\sigma \pm \frac{Z_P}{Z_S} \mu_\delta \right) \quad (3.4)$$

with Z_P and Z_S being the PS and scalar renormalization constants, respectively.

The twisted-mass action (3.1) is known to lead to a mixing in the strange and charm sectors [14]. In order to avoid the mixing of K - and D -meson states in the correlation functions, we adopted a non-unitary set up in which the valence quarks are regularized as Osterwalder-Seiler (OS) fermions [36]. The action for each valence quark flavor q_f ($f = ll', ss', cc'$) reads as

$$S_{OS}^f = a^4 \sum_x \bar{q}_f(x) \left\{ \frac{1}{2} \sum_\mu \gamma_\mu (\nabla_\mu + \nabla_\mu^*) - i\gamma_5 r_f \left[M_0 - \frac{a}{2} \sum_\mu \nabla_\mu \nabla_\mu^* \right] + \mu_f \right\} q_f(x). \quad (3.5)$$

Each valence doublet is mass-degenerate ($\mu_l = \mu_{l'}$, $\mu_s = \mu_{s'}$ and $\mu_c = \mu_{c'}$), and their Wilson parameters r_f are always chosen such that the two valence quark in a PS meson have opposite r -values. This choice guarantees that the squared PS meson mass, m_{PS}^2 , differs from its continuum counterpart only by terms of $\mathcal{O}(a^2\mu)$ [30].

3.1.2 Lattice set up used in this analysis

The details of our lattice set up are collected in Table 3.1, where the number of gauge configurations correspond to a block size of 20 trajectories. At each lattice spacing, different values of the light sea quark masses have been considered. The light valence and sea quark masses are always taken to be equal. On the contrary the masses of both the strange and the charm sea quarks are fixed at each β to a value chosen to be close to its physical one [13]. To be able to analyse mesons in the strange and charm sectors we have simulated three values of the valence strange quark mass and six values of the valence heavy quark mass, which are needed for the interpolation in the physical charm region as well as to extrapolate possibly to the b -quark sector. In particular, in the light sector the masses were simulated in a range $0.1 m_s^{phys} \lesssim \mu_l \lesssim 0.5 m_s^{phys}$, in the strange sector in $0.7 m_s^{phys} \lesssim \mu_s \lesssim 1.2 m_s^{phys}$, while for the charm sector in $0.7 m_c^{phys} \lesssim \mu_c \lesssim 2.0 m_c^{phys}$. Quark propagators with different valence masses are obtained using the so-called multiple mass solver method [37, 38], which allows to invert the Dirac operator for several quark masses at a relatively low computational cost.

ensemble	β	V/a^4	$a\mu_{sea} = a\mu_l$	$a\mu_\sigma$	$a\mu_\delta$	N_{cfg}	$a\mu_s$	$a\mu_c$		
A30.32	1.90	$32^3 \times 64$	0.0030	0.15	0.19	150	0.0145,	0.1800, 0.2200,		
A40.32			0.0040			90			0.0185,	0.2600, 0.3000,
A50.32			0.0050			150			0.0225	0.3600, 0.4400
A40.24	1.90	$24^3 \times 48$	0.0040	0.15	0.19	150				
A60.24			0.0060			150				
A80.24			0.0080			150				
A100.24			0.0100			150				
B25.32	1.95	$32^3 \times 64$	0.0025	0.135	0.170	150	0.0141,	0.1750, 0.2140,		
B35.32			0.0035			150			0.0180,	0.2530, 0.2920,
B55.32			0.0055			150			0.0219	0.3510, 0.4290
B75.32			0.0075			75				
B85.24	1.95	$24^3 \times 48$	0.0085	0.135	0.170	150				
D15.48	2.10	$48^3 \times 96$	0.0015	0.12	0.1385	60	0.0118,	0.1470, 0.1795,		
D20.48			0.0020			90			0.0151,	0.2120, 0.2450,
D30.48			0.0030			90			0.0184	0.2945, 0.3595

Table 3.1: Values of the simulated sea and valence quark bare masses for each gauge ensemble used in this work.

We studied the dependence of the PS meson masses (and of the pion decay constant) on the (renormalized) light quark mass fitting simultaneously the data at different lattice spacings and volumes. In particular, we anticipate that the values of the lattice spacing we found in our pion analysis are $a = 0.0885(36)$, $0.0815(30)$, $0.0619(18)$ fm at $\beta = 1.90$, 1.95 and 2.10 , respectively, so that the lattice volume goes from $\simeq 2$ to $\simeq 3$ fm. Details of the parameters of the gauge ensembles are reported in Table 3.2. In the same table are also shown the range of pion masses (i.e., $\simeq 210 \div 450$ MeV) and the one of $M_\pi L$, where the values of M_π are already extrapolated to the continuum and infinite volume limits.

The statistical accuracy of the meson correlators is significantly improved by using the so-called ‘‘one-end’’ stochastic method, implemented in [39], which includes spatial stochastic sources at a single time slice chosen randomly. Statistical errors on the meson masses are evaluated using the jackknife procedure, while statistical errors, which are based on data obtained from independent ensembles of gauge configurations, like the errors of the fitting procedures, are evaluated using a bootstrap sampling with 100 events to take properly into account cross-correlations.

ensemble	β	$L(fm)$	$M_\pi(\text{MeV})$	$M_\pi L$
A30.32	1.90	2.84	245	3.53
A40.32			282	4.06
A50.32			314	4.53
A40.24	1.90	2.13	282	3.05
A60.24			344	3.71
A80.24			396	4.27
A100.24			443	4.78
B25.32	1.95	2.61	239	3.16
B35.32			281	3.72
B55.32			350	4.64
B75.32			408	5.41
B85.24	1.95	1.96	435	4.32
D15.48	2.10	2.97	211	3.19
D20.48			243	3.66
D30.48			296	4.46

Table 3.2: Values of the pion mass and of the quantity $M_\pi L$ for the various gauge ensembles used in this work. The values of M_π are already extrapolated to the continuum and infinite volume limits

3.2 Analysis of the 2-point PS correlators

The 2-point PS correlators represent the basic ingredient for the whole analysis. As explained in sec. 2.5 from them it is possible to extract the masses and decay constants of the PS meson analysed in this work.

Considering for example the pion case, for all the gauge ensembles we computed the 2-point PS correlators defined as

$$C(t, \vec{p}) = \sum_{\vec{x}} \langle 0 | \mathcal{P}_5(x) P_5^\dagger(0) | 0 \rangle e^{i\vec{p} \cdot \vec{x}}. \quad (3.6)$$

where $P_5(x) = \bar{u}(x)\gamma_5 d(x)$. As already explained in sec. 2.5, at large time distances one has

$$C(t) \xrightarrow[t \gg a, (T-t) \gg a]{} \frac{\mathcal{Z}_\pi}{2M_\pi} (e^{-M_\pi t} + e^{-M_\pi(T-t)}), \quad (3.7)$$

so that the pion mass and the matrix element $\mathcal{Z}_\pi = |\langle \pi | \bar{u}\gamma_5 d | 0 \rangle|^2$ can be extracted from the simple exponential fit given in the r.h.s. of Eq. (3.7) taken over the appropriate time interval. For maximally twisted fermions the value of \mathcal{Z}_π determines the pion decay constant without the need of the knowledge of any renormalization constant [30], namely

$$af_\pi = 2a\mu_l \frac{\sqrt{a^4 \mathcal{Z}_\pi}}{aM_\pi \sinh(aM_\pi)}. \quad (3.8)$$

Practically, as explained in sec. 2.5, to extract M_π and f_π we used the so called effective mass whose definition is reported here:

$$aM_{eff}(t) = \log \left[\frac{C(t)}{C(t+1)} \right]. \quad (3.9)$$

Once we extracted M_π and f_π we have studied the dependence of the pion mass and decay constant on the renormalized light quark mass

$$m_l = (a\mu_l) \frac{1}{aZ_P} \quad (3.10)$$

through a simultaneous fit.

With the same procedure meson masses and decay constants in the K and D sector can be extracted. In fig. 3.1 three example of 2-point correlators are shown, build up respectively with two light quarks, a light and a strange quark and a light and a charm

quark. The red lines indicate the time intervals in which the plateau was fitted i.e. the region in which the leading exponential contribution can be isolated. As already explained in sec. 2.5, t_{min} has to be chosen large enough for the contribution of excited state to be sufficiently suppressed. The lower is the mass difference between the ground state and the first excited state, the higher t_{min} has to be chosen. This resulted in a different choice of the fitting time intervals for l - l and l - h mesons as can be seen in 3.1.

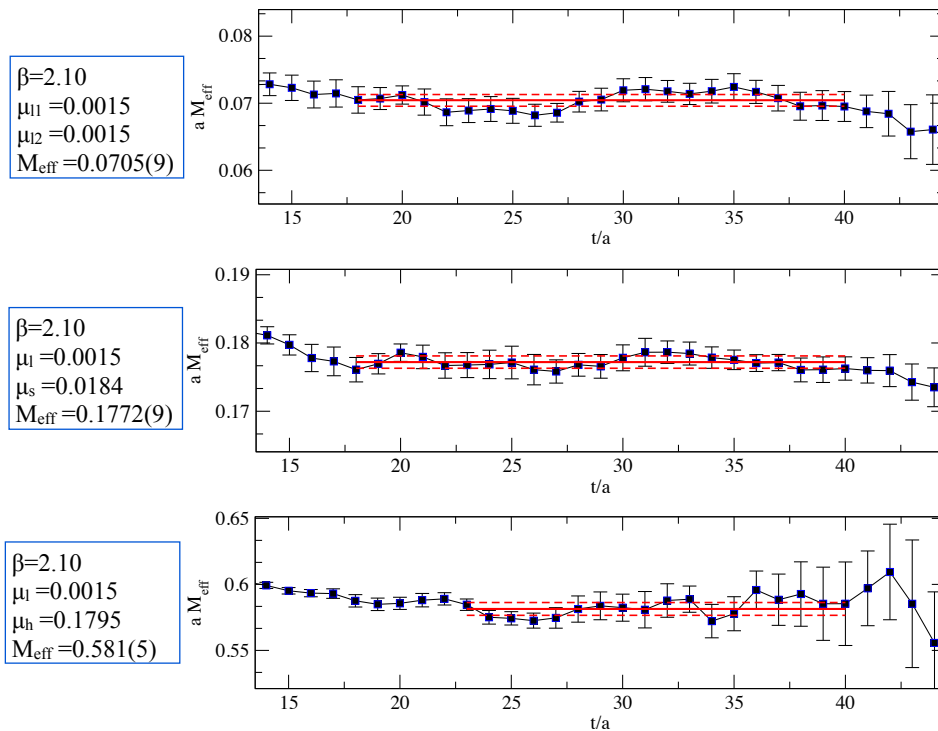


Figure 3.1: Three example of 2-point correlators build up respectively with two light quarks, a light and a strange quark and a light and a charm quark. The red lines indicate the time intervals in which the plateau was fitted.

Before closing this section we have collected for convenience in Table 3.3 the time intervals used for the extraction of the PS meson masses (and of the pion decay constant) from the 2-point correlators at each β and lattice volume in the light, strange and heavy sectors.

β	V/a^4	$\Delta t_{(u,ls)}/a$	$\Delta t_{(lh,sh)}/a$
1.90	$32^3 \times 64$	[12, 31]	[15, 31]
1.90	$24^3 \times 48$	[12, 23]	[16, 23]
1.95	$32^3 \times 64$	[13, 31]	[18, 31]
1.95	$24^3 \times 48$	[13, 23]	[18, 23]
2.10	$48^3 \times 96$	[18, 40]	[23, 40]

Table 3.3: *Time intervals used for the extraction of the PS meson masses (and decay constant) from the 2-point correlators in the light (l), strange (s) and heavy (h) sectors.*

3.3 Average up and down quark mass

In this section we present our determination of the average up/down quark mass. First we will give some details on the general strategy and on the different approaches used to control and estimate the various source of systematic uncertainties related to the chiral extrapolation, the continuum limit and the FSE and the renormalization constants.

Chiral extrapolation

Since the simulation was not performed at the physical value of the light quark mass, a chiral extrapolation is needed. In order to estimate the associated systematic error we studied the dependence on the light quark mass by using different fit formulae based on the predictions of Chiral Perturbation Theory (ChPT) as well as on polynomial expressions.

Discretization effects

As far as the continuum limit is concerned, in order to lower as much as possible the impact of discretization effects and to keep the continuum extrapolation under control we tried two different procedures, which use f_π to ultimately set the scale. The first one involves r_0/a as the intermediate scaling variable, while in the second one we used as a reference mass the one of a fictitious pseudoscalar (PS) meson made of two strange quarks, aM_{ss} , trying to exploit a partial cancellation of discretization effects in the ratios

like M_{ls}/M_{ss} . Of course the continuum limit of M_{ss} has eventually to be performed and this reintroduces non negligible cutoff effects in the determination of the lattice spacing. The fact that we obtain compatible predictions between the two procedures strengthens the validity of our results and shows that we are controlling safely the impact of the discretization effects.

The analysis has thus followed four branches depending on the choice of the scaling variable (either r_0/a or aM_{ss}) as well as on the different fitting procedures (either ChPT or polynomial expansion). The differences among the results obtained within the above-mentioned four branches of the analysis have been used to estimate the systematic uncertainties.

FSE corrections

As far as FSE are concerned, we have considered three different estimators for the corrections: the NLO ChPT predictions of Ref. [40] (which will be labelled as GL), the resummed formulae of Ref. [41] including higher order corrections (labelled as CDH) and finally the formulae developed in Ref. [42] which accounts for the $\pi^0 - \pi^+$ mass splitting (labelled as CWW). Using different approaches gave us a better understanding of how well the corrections are working, what is the size of each contribution on our data and what's the impact of of these FSE on the final results

Renormalization constants and r_0/a

Renormalization constants are a crucial ingredient in the determination of quark masses. Our collaboration calculated the quark mass renormalization constants $Z_m = 1/Z_p$ in the RI-MOM scheme using two different methods, labelled as M1 and M2. The first method M1 tries to remove $\mathcal{O}(a^2p^2)$ effects, while in the second method M2 the renormalization constant are taken at a fixed reference value of p^2 , so that the use of the two sets of renormalization constants should lead to the same final results once the continuum limit is performed. The differences due to the different choice of the values of Z_P are included in the systematic error. In Table 3.4 the values of Z_P used in this work are presented. In the same table are also shown the values of r_0/a that we used to convert the data at different values of lattice spacing to a common scale given in units of the Sommer parameter r_0 . For each β the values of r_0/a have been calculated at the various values

of the light quark mass [13, 43] and then extrapolated to the chiral limit using either a linear or a quadratic dependence in $a\mu_{sea}$. The errors reported in Table 3.4 represent the sum in quadrature of the statistical uncertainty and of the systematic error associated to the two different chiral extrapolations. Notice that in the branches of our analysis, in which we divide the PS meson masses by the quantity aM_{ss} , the impact of r_0/a is marginal and could in principle be avoided.

β	$Z_P^{\overline{MS}}(2 \text{ GeV})(M_1)$	$Z_P^{\overline{MS}}(2 \text{ GeV})(M_2)$	r_0/a
1.90	0.521(7)	0.564(6)	5.31(8)
1.95	0.506(4)	0.537(4)	5.77(6)
2.10	0.513(3)	0.540(2)	7.60(8)

Table 3.4: *Input values for the renormalization constant $Z_P \equiv Z_P^{\overline{MS}}(2 \text{ GeV})$ and the chirally extrapolated values of r_0/a for each values of β (see text).*

Methodology for the external parameter of the analysis

The uncertainties on the renormalization constants Z_P and on the values of r_0/a have been taken into account by including in the definition of the χ^2 the following contribution

$$\sum_{\beta} \frac{\left((r_0/a)_i^{fit} - (r_0/a)_i \right)^2}{\sigma_{r_0/a}^2} + \sum_{\beta} \frac{\left((Z_P)_i^{fit} - (Z_P)_i \right)^2}{\sigma_{Z_P}^2}, \quad (3.11)$$

where $(r_0/a)_i$ and $(Z_P)_i$ stand for the input values corresponding to the bootstrap event i , while $(r_0/a)_i^{fit}$ and $(Z_P)_i^{fit}$ are free parameters of the fit. This procedure is basically equivalent to impose a Bayesian gaussian prior for Z_P and r_0/a . Note that the use of the bootstrap sampling by itself would only propagate correctly the uncertainties of these quantities. Within the single bootstrap event, however, one would assume (arbitrarily) in the fit that these quantities are exactly known. Instead, using Eq. (3.11) we allow the quantities r_0/a and Z_P to change from their central values in the fit for each bootstrap event with a weight in the χ^2 given by their global uncertainties.

3.3.1 Analyses of the pion mass in units of r_0

Since the chiral extrapolation is an important source of uncertainty in our analysis, we tried to fit the dependence of both M_{π}^2 and f_{π} on the renormalized light quark mass

m_l using two different fitting functions: the one predicted by ChPT at NLO and a polynomial expansion. These two choices correspond to expand the squared pion mass and decay constant either around the chiral point $m_l = 0$ up to higher masses, in which case non-analytical chiral logs enter in the expression, or around a non-vanishing mass $m_l = m_l^*$ down to the physical point. The first approach is supposed to be more accurate in the region of very small m_l , but in principle both solutions are legitimate, and one has to look how well the data are fitted by these approaches. Since both fits turn out to be in nice agreement with the lattice data, the differences between the results obtained using the chiral fit and the one obtained using the polynomial expansion reflect our genuine uncertainty on the chiral extrapolation and will be thus used to estimate the corresponding systematics.

Chiral fit in units of r_0

Let us consider the ChPT approach in units of r_0 which hereafter will be referred to as analysis 1A. The ChPT predictions at NLO can be written in the following way

$$(M_\pi r_0)^2 = 2(B_0 r_0)(m_l r_0) \left(1 + \xi_l \log \xi_l + P_1 \xi_l + P_2 \frac{a^2}{r_0^2} + \frac{4c_2}{(4\pi f_0)^2} \frac{a^2}{r_0^2} \log \xi_l \right) \cdot K_M^{FSE} \quad (3.12)$$

$$(f_\pi r_0) = (f_0 r_0) \left(1 - 2\xi_l \log \xi_l + P_3 \xi_l + P_4 \frac{a^2}{r_0^2} - \frac{4c_2}{(4\pi f_0)^2} \frac{a^2}{r_0^2} \log \xi_l \right) \cdot K_f^{FSE} \quad (3.13)$$

where $P_1 - P_4$ are free parameters (P_1 and P_3 are related to the NLO low-energy constants (LECs) $\bar{\ell}_3$ and $\bar{\ell}_4$, respectively) and

$$\xi_l = \frac{2B_0 m_l}{16\pi^2 f_0^2}, \quad (3.14)$$

with B_0 and f_0 being the LECs entering the LO chiral Lagrangian. Both B_0 and f_0 have been left free to vary in our fitting procedures.

The quantities K_M^{FSE} and K_f^{FSE} in eqs. (3.12-3.13) represent the FSE for the pion mass and decay constant, respectively. They will be discussed in a while.

For the moment notice the presence of the terms proportional to $a^2 \log \xi_l$ in Eqs. (3.12-3.13). These terms originate from the mass splitting between the charged and the neutral pions, which is a discretization effect appearing within the twisted mass formulation. The impact of the pion mass splitting on the ChPT expansion of M_π^2 and f_π has been worked out in Ref. [44]. We have expanded the resulting chiral formulae up to $\mathcal{O}(a^2)$, leading

in Eqs. (3.12-3.13) to the presence of the parameter c_2 which is directly related to the neutral and charged pion mass splitting at LO by

$$(M_{\pi^0}^2 - M_{\pi^\pm}^2)_{LO} = 4a^2 c_2 \quad (3.15)$$

Treating c_2 as a free parameter in the χ^2 -minimization procedure leads to quite large uncertainties in the determination of this quantity. Therefore, we choose to give to c_2 a prior based on the values reported in Ref. [45] and to treat it in the same way adopted for the renormalization constants Z_P and the quantity r_0/a in Eq. (3.11). In Ref. [45] two different determinations of c_2 are reported, one in which the chiral limit is performed through a constant fit in M_π^2 and the other one in which the fit was assumed to be linear. In the present work we have used an average of the two values including the spread in the error, namely $r_0^2 c_2 = -1.7 \pm 0.6$.

The dependence of our lattice data for $r_0 M_\pi^2/m_l$ and $r_0 f_\pi$ on the renormalized quark mass $r_0 m_l$ is shown at each lattice spacing in Figs. 3.2 and 3.3, respectively. The behavior of the chiral extrapolation in the continuum limit is also reported.

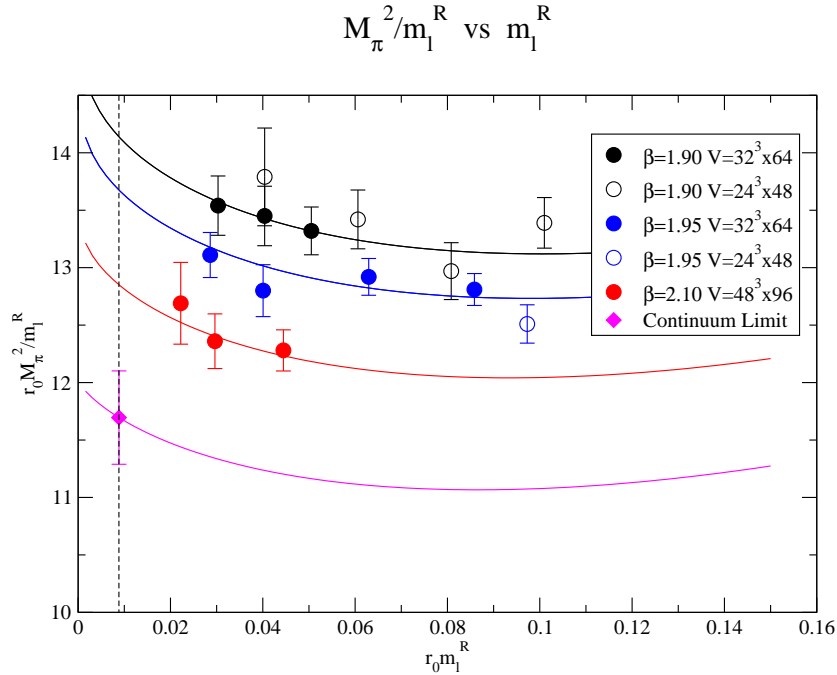


Figure 3.2: Chiral and continuum extrapolation of $r_0 M_\pi^2/m_l$ based on the NLO ChPT fit given by Eq. (3.12). Lattice data have been corrected for FSE using the CWW approach.

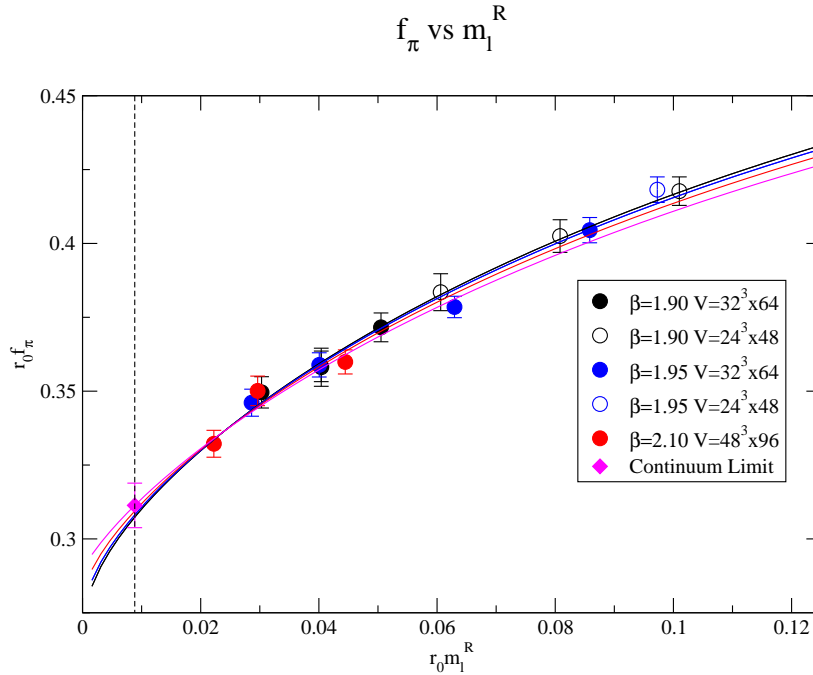


Figure 3.3: *The same as in Fig. 3.2, but for the decay constant $r_0 f_\pi$.*

From Figs. 3.2 and 3.3 it can be seen that the impact of discretization effects using the values of r_0/a is almost completely negligible in the case of $r_0 f_\pi$, while it is at the level of $\simeq 10\%$ in the case of $r_0 M_\pi^2/m_l$ (if estimated from the difference between the continuum results and the ones at the finest lattice spacing).

The value of the physical average up/down quark mass, m_{ud} , can be extracted from the ratio M_π^2/f_π^2 using as input its experimental value obtained using

$$M_{\pi^+}^{exp.} = 135 \text{ MeV} , \quad f_{\pi^+}^{exp.} = 130.41 \text{ MeV} . \quad (3.16)$$

The numerical results for m_{ud} as well as those for the lattice spacing and the relevant LECs will be collected and discussed in Section 3.3.3.

FSE correction in the pion fit

Before moving on to the analysis in which the chiral extrapolation was carried out using a polynomial fit formula, some details will be given on the FSE and on the various approaches we used to address the problem.

On the theoretical side the impact of FSE on M_π and f_π have been studied with ChPT

at NLO in Ref. [40] and using a resummed asymptotic formula in Ref. [41], where both leading and subleading exponential terms are taken into account and the chiral expansion is applied to the $\pi - \pi$ forward scattering amplitude. When the leading chiral representation of the latter is considered, the resummed approach coincides with the NLO result of Ref. [40]. Viceversa at NNLO the resummation technique includes only part of the two-loop effects as well as of higher-loop effects. The resummed approach was positively checked against a full NNLO calculation of the pion mass in Ref. [46], showing that the missing two-loop contributions are actually negligible. Finally, the cutoff effects that within the twisted mass formulation can give rise to a splitting between charged and neutral pions, may in turn enter also the determination of FSE, as explicitly worked out within the resummed approach in Ref. [42].

Thus, as far as FSE are concerned, we have employed three different approaches: the NLO ChPT predictions of Ref. [40] (which will be labelled hereafter as GL), the resummed formulae of Ref. [41] including higher order corrections (labelled as CDH) and finally the formulae developed in Ref. [42] which accounts for the $\pi^0 - \pi^+$ mass splitting (labelled as CWW).

Beside the lattice volume and the pion mass, the predictions of both CDH and CWW approaches require the knowledge of the LECs $\bar{\ell}_1 - \bar{\ell}_4$ and eventually of the splitting parameter c_2 . The LECs $\bar{\ell}_3$ and $\bar{\ell}_4$, which are related to the ξ_l -dependent NLO terms in M_π^2 and f_π , have been treated as free parameters in our fitting procedures, while for $\bar{\ell}_1$ and $\bar{\ell}_2$ we used the values reported in Ref. [42]. The CWW corrections depend also on the neutral pion mass M_{π^0} , which was estimated at LO through Eq. (3.15) using $(M_{\pi^+})_{LO} = 2B_0 m_l$. We have checked that such values of M_{π^0} are consistent with the corresponding ones extracted directly from the appropriate PS correlator in Ref. [47].

To check how well the finite volume corrections are working and what is the relative weight of each contribution we can use the two ensembles A40.32 A40.24 (see Table 3.1), which correspond to the same quark mass and lattice spacing, but different lattice volumes. Moreover, we stress that the ensemble A40.24 has both the lowest value of the quantity $M_\pi L$ (see Table 3.2) and the largest pion mass splitting, being $M_{\pi^0}/M_\pi^+ \approx 0.5$ [47]. Therefore FSE are expected to be maximal for this gauge ensemble.

The terms K_M^{FSE} and K_f^{FSE} , appearing in the ChPT formulae (3.12-3.13), relate the squared pion mass and decay constant calculated at finite volume with their infinite volume counterparts. For the gauge ensemble A40.32 and A40.24 we can write

$$M_{[32]} = M_{[\infty]} K_{M,[32]}^{FSE} ,$$

$$M_{[24]} = M_{[\infty]} K_{M,[24]}^{FSE} \quad (3.17)$$

and in analogous way for $K_{f,[32]}^{FSE}$ and $K_{f,[24]}^{FSE}$ in the case of the decay constant f_π . Taking the ratio of the above relations we see that for an ideal correction the ratio of the multiplicative factors K^{FSE} should match exactly the ratio of the uncorrected lattice data without any knowledge of the infinite volume values. The more accurate the correction is, the more the prediction for $(K_{M,[32]}^{FSE}/K_{M,[24]}^{FSE})$ matches the lattice data $(M_{[32]}/M_{[24]})$. The corresponding numerical results are reported in Tables 3.5 and 3.6 for the pion mass and the decay constant, respectively.

	GL	CDH	CWW	Lattice data M_{32}/M_{24}
$K_{M,[32]}^{FSE}/K_{M,[24]}^{FSE}$	0.994	0.985	0.981	0.972(13)

Table 3.5: Values of the ratio of the FSE correction factor K_M^{FSE} for the gauge ensembles $A40.32$ and $A40.24$ obtained within the approaches GL, CDH and CWW (see text).

	GL	CDH	CWW	Lattice data f_{32}/f_{24}
$K_{f,[32]}^{FSE}/K_{f,[24]}^{FSE}$	1.023	1.040	1.054	1.050(19)

Table 3.6: The same as in Table 3.5 but for the decay constant f_π .

From these tables one can see that the corrections calculated using the CWW approach are compatible with the lattice predictions for both the pion mass and the decay constant, working remarkably well on the latter. It is also possible to see how big is the contribution of the various corrections we are adding in the FSE prediction in terms of getting closer to the ratio of uncorrected lattice data.

In table 3.7 we collected the values of the coefficients $(K_{M,[24]}^{FSE} - 1)$ and $(K_{f,[24]}^{FSE} - 1)$, representing the FSE correction in percentage for the ensemble $A40.24$, which, as already stressed, is affected by the largest FSE correction in the whole set of gauge ensembles. Moreover, by comparing CDH and CWW predictions it can be seen that the $\mathcal{O}(a^2)$ term related to the pion mass splitting, though not negligible, appears to be well under control. Thus, in what follows, the lattice data will be corrected for FSE using the CWW formulae unless explicitly stated.

	GL	CDH	CWW
$K_{M,[24]}^{FSE} - 1$	0.0070	0.0187	0.0243
$K_{f,[24]}^{FSE} - 1$	-0.0280	-0.0469	-0.0632

Table 3.7: Values of $K_M^{FSE} - 1$ and $K_f^{FSE} - 1$ for the gauge ensembles $A40.24$ obtained within the various FSE approaches *GL*, *CDH* and *CWW* (see text).

Polynomial fit in units of r_0

As anticipated in Section 3.3, we studied the chiral extrapolation by replacing the NLO ChPT predictions with a simple polynomial expansion in the renormalized light quark mass (analysis 1*B*), namely

$$(M_\pi r_0)^2 = P_1(m_l r_0) \left(1 + P_2(m_l r_0) + P_3 \frac{a^2}{r_0^2} + P_4(m_l r_0)^2 \right) \cdot K_M^{FSE} \quad (3.18)$$

$$(f_\pi r_0) = P_5 \left(1 + P_6(m_l r_0) + P_7 \frac{a^2}{r_0^2} + P_8(m_l r_0)^2 \right) \cdot K_f^{FSE}, \quad (3.19)$$

where $P_1 - P_8$ are free parameters. Since the calculation of K_M^{FSE} and K_f^{FSE} may require the use of LECs that are only meaningful in a ChPT fit, the FSE corrections have been taken from the ChPT analysis in units of r_0 (analysis 1*A*) and applied directly to the lattice data.

The dependence of $r_0 M_\pi^2/m_l$ and $r_0 f_\pi$ on $r_0 m_l$ at each lattice spacing and in the continuum limit obtained using Eqs. (3.18-3.19) is shown in Figs. 3.4 and 3.5, respectively.

Notice that the impact of discretization effects on $r_0 M_\pi^2/m_l$ obtained using the polynomial fit (see Fig. 3.4) is very similar to the one found in the case of the NLO ChPT prediction (see Fig. 3.2). Finally, as it can clearly be seen from Figs. 3.2-3.5, both the NLO ChPT and the polynomial fits describe quite well the lattice data for the pion mass as well as for the decay constant, yielding slightly different results only at the physical pion point.

3.3.2 Analyses of the pion mass in units of M_{ss}

The results shown in Figs. 3.2 and 3.4 confirms that the impact of discretization effects using r_0 as the scaling variable is at the level of $\simeq 10\%$ for the squared pion mass. In order to keep the extrapolation to the continuum limit under better control we repeated

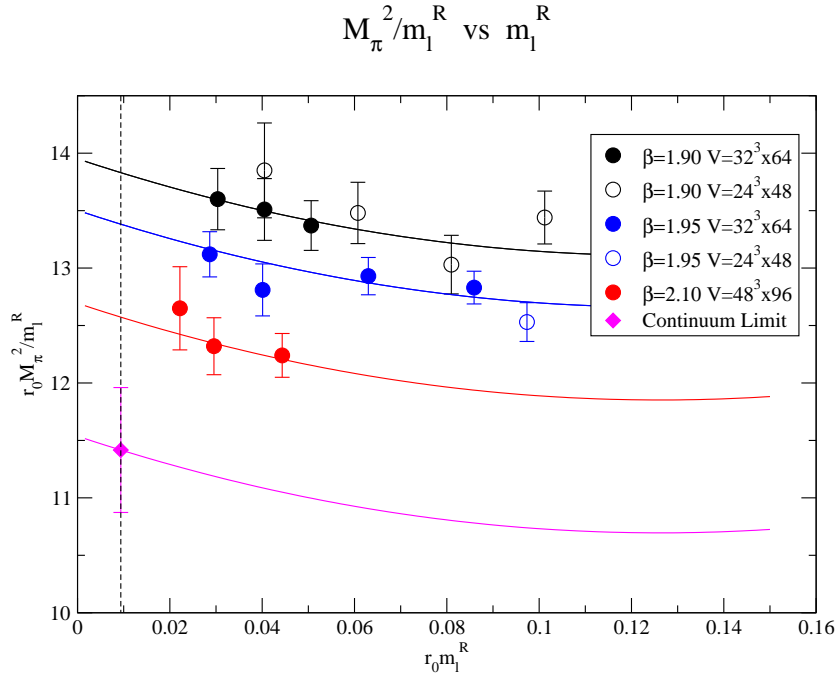


Figure 3.4: Chiral and continuum extrapolation of $r_0 M_\pi^2 / m_l$ obtained using the polynomial fit given by Eq. (3.18). Lattice data are corrected for FSE using the CWW approach.

the analyses 1A and 1B adopting a different choice for the scaling variable, namely instead of r_0 we introduced the mass M_{ss} of a fictitious PS meson made of two strange valence quarks. The PS mass M_{ss} is affected by non-negligible cutoff effects, similar to the ones of a K meson, without however any significant dependence on the light-quark mass. Thus, we tried to improve the continuum extrapolation by considering the ratio M_π^2 / M_{ss}^2 which may exploit a (partial) cancellation of discretization effects.

Extracting the reference mass M_{ss}

To construct the meson mass ratio we first performed a slight interpolation in the strange valence quark mass to get the quantity aM_{ss} at a common (but arbitrary) value $r_0 m_s = 0.22$ for each β and light quark mass. Since, as expected, we found no significant dependence of aM_{ss} on the light quark mass, we performed a constant fit in am_l to obtain the values of aM_{ss} at each β and for each bootstrap event an example of this fit is reported in fig. 3.6

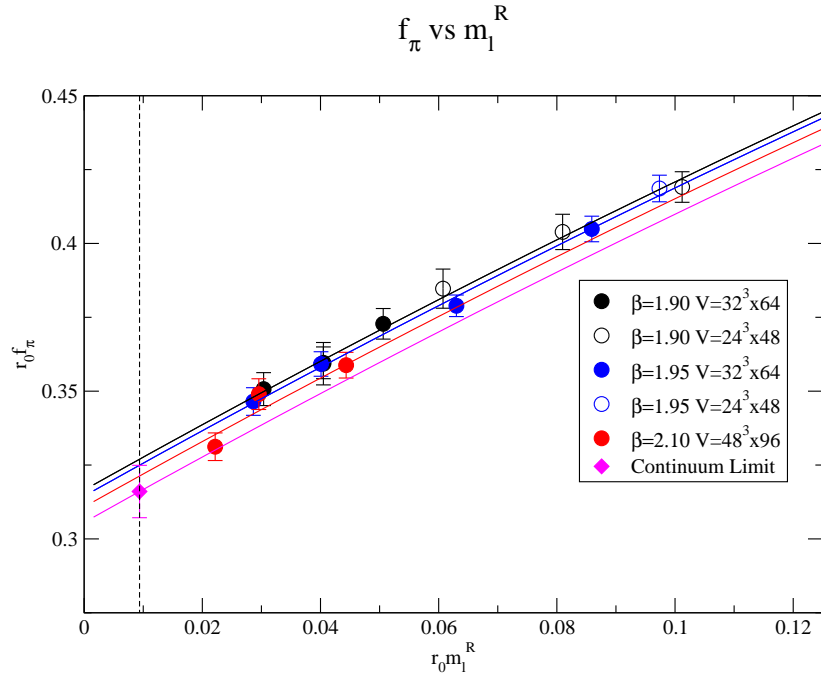


Figure 3.5: *The same as in Fig. 3.4, but for the decay constant $r_0 f_\pi$.*

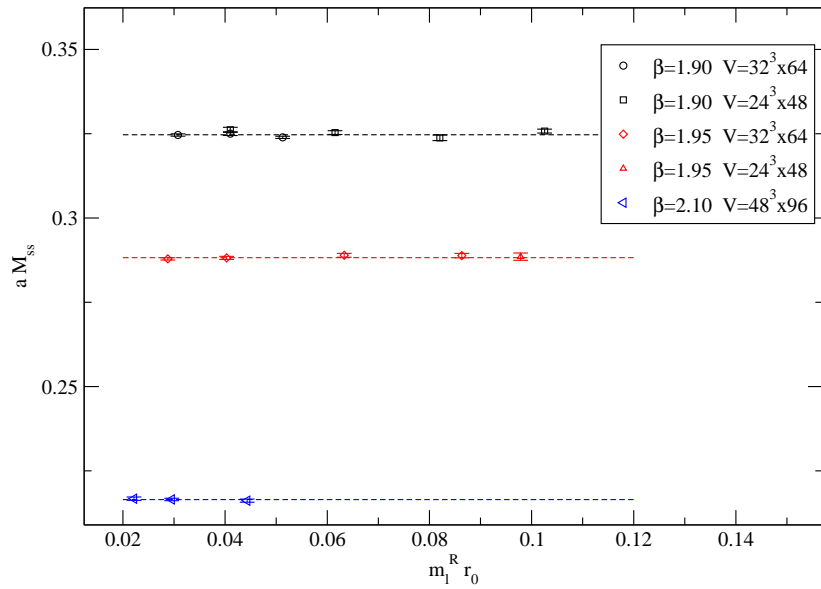


Figure 3.6: *Dependence of $a M_{ss}$ on the light quark mass fitted with a constant.*

The averages over our bootstrap sample read as

$$aM_{ss}|_{\beta=1.90, 1.95, 2.10} = \{0.3258(2), 0.2896(2), 0.2162(3)\} . \quad (3.20)$$

The values for aM_{ss} have been used to bring to a common scale all the lattice quantities simulated at different β , covering the role that in analysis 1A and 1B was played by r_0/a . Notice however that while r_0/a was obtained by an independent analysis, this is not the case for the quantity aM_{ss} , because it is derived directly from the same gauge configurations used in our analysis. Because of that we decided to keep the exact correlations of aM_{ss} with other quantities in the analysis and so we treated its errors not through a contribution in the χ^2 , but simply via the bootstrap sampling.

Chiral and polynomial fit in units of M_{ss}

The analysis 2 proceeds in the same way as in the previous Section, namely in the case of the NLO ChPT fit (analysis 2A) one has

$$\frac{M_\pi^2}{M_{ss}^2} = \frac{2B_0 m_l}{M_{ss}^2} \left(1 + \xi_l \log \xi_l + P_1 \xi_l + P_2 (aM_{ss})^2 + \frac{4c_2}{(4\pi f_0)^2} (aM_{ss})^2 \log \xi_l \right) \cdot K_M^{FSE} \quad (3.21)$$

$$\frac{f_\pi}{M_{ss}} = \frac{f_0}{M_{ss}} \left(1 - 2\xi_l \log \xi_l + P_3 \xi_l + P_4 (aM_{ss})^2 - \frac{4c_2}{(4\pi f_0)^2} (aM_{ss})^2 \log \xi_l \right) \cdot K_f^{FSE} \quad (3.22)$$

and in the case of the polynomial fit (analysis 2B) one has the analogous of Eqs. (3.18) and (3.19) expressed in units of M_{ss} .

$$\frac{M_\pi^2}{M_{ss}^2} = P_1 \frac{m_l}{M_{ss}} \left(1 + P_2 \frac{m_l}{M_{ss}} + P_3 (aM_{ss})^2 + P_4 \left(\frac{m_l}{M_{ss}} \right)^2 \right) \cdot K_M^{FSE} \quad (3.23)$$

$$(f_\pi r_0) = P_5 \left(1 + P_6 \frac{m_l}{M_{ss}} + P_7 (aM_{ss})^2 + P_8 \left(\frac{m_l}{M_{ss}} \right)^2 \right) \cdot K_f^{FSE} , \quad (3.24)$$

Once again the results from both the ChPT and polynomial fits have been considered to get the final result and to estimate the systematics.

In Fig. 3.7 we show the dependence of $M_\pi^2/(m_l M_{ss})$ on m_l/M_{ss} at each lattice spacing and in the continuum limit within the analysis 2A (ChPT fit). Similar results have been obtained within the analysis 2B (polynomial fit) and are shown in fig. 3.8.

The comparison of Figs. 3.2 and 3.7 clearly shows that, when M_{ss} is chosen as the scaling variable, discretization effects on the squared pion mass are significantly reduced

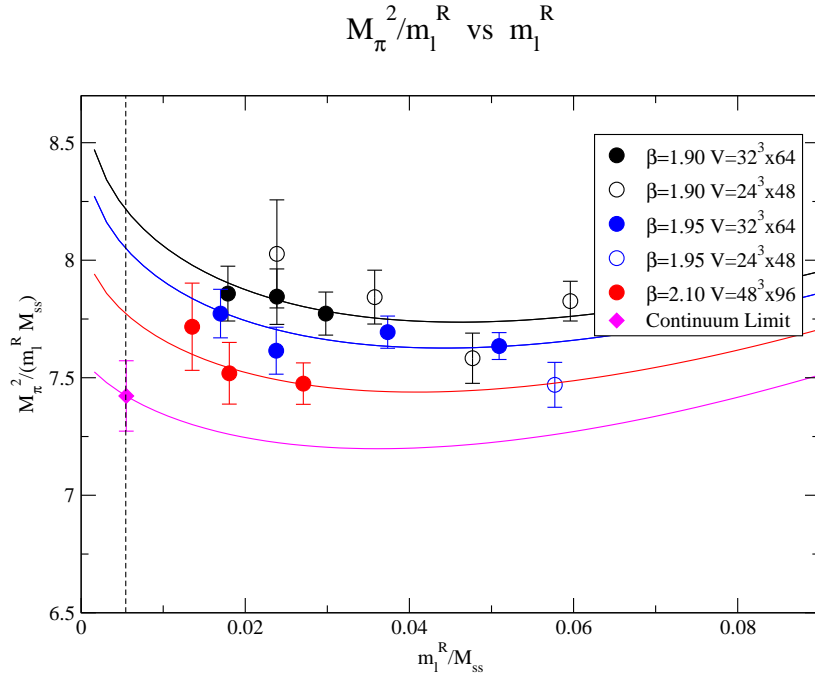


Figure 3.7: *Chiral and continuum extrapolation of $M_\pi^2/(m_l M_{ss})$ performed using the NLO ChPT fit (3.21). Lattice data have been corrected for FSE using the CWW approach.*

from $\simeq 10\%$ down to $\simeq 4.5\%$.

As will be seen in a while, an even stronger reduction will be observed in the case of the kaon or the D -meson mass.

3.3.3 Results in the pion sector.

In this section we present the results for all the four analyses 1A, 1B, 2A and 2B carried out in the pion sector.

Using the experimental value of the ratio M_π^2/f_π^2 the average up/down quark mass m_{ud} can be determined, while using the experimental value of f_π the Sommer parameter r_0 can be obtained within the analyses 1A and 1B. In turn, the latter allows to get the values of the lattice spacing at each β using the values of r_0/a .

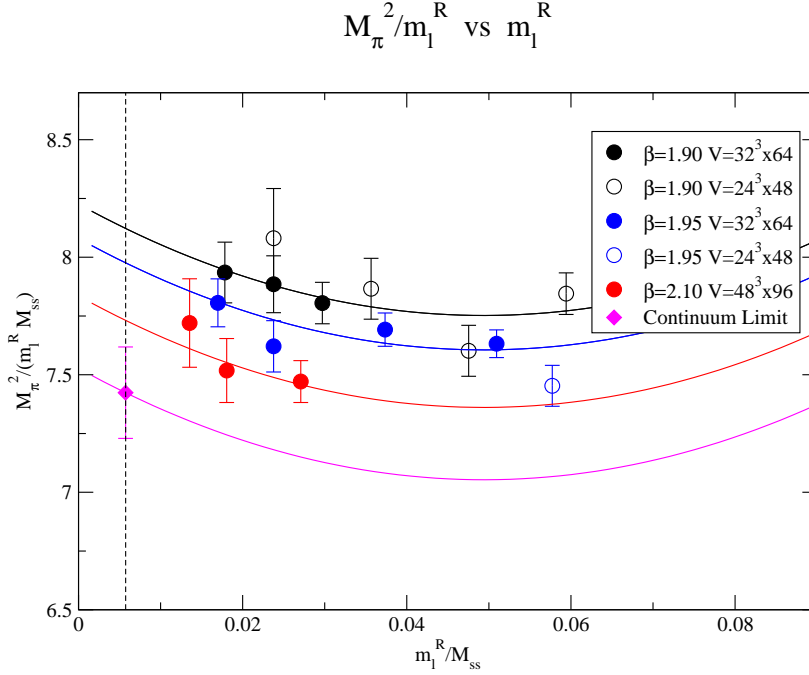


Figure 3.8: *Chiral and continuum extrapolation of $M_\pi^2/(m_l M_{ss})$ performed using the polynomial fit formula. Lattice data have been corrected for FSE using the CWW approach.*

The scale setting for the analyses in M_{ss} units

As far as the scale setting is concerned, the analyses in units of M_{ss} , i.e. analyses 2A and 2B, require a slightly more involved procedure. One could naively think that is sufficient to extract the quantity M_{ss} using the experimental value of the pion decay constant and then to combine this mass with the quantities aM_{ss} given by Eq. (3.20) to get the values of the lattice spacing at each β . However this is not the case, because discretization effects in aM_{ss} are large and a continuum extrapolation of M_{ss} is required. Therefore, we have first converted the quantity aM_{ss} to r_0M_{ss} (using the values of r_0/a) and then performed a simple fit of the form $(r_0M_{ss})^2 = \bar{P}_1 + \bar{P}_2 a^2/r_0^2$.

Combining the continuum extrapolation of r_0M_{ss} with the experimental input of the pion decay constant and the values of r_0/a one can determine the three values of the lattice spacing at each β .

The extrapolation to the continuum limit of the quantity $(r_0M_{ss})^2$ is reported in fig. 3.9

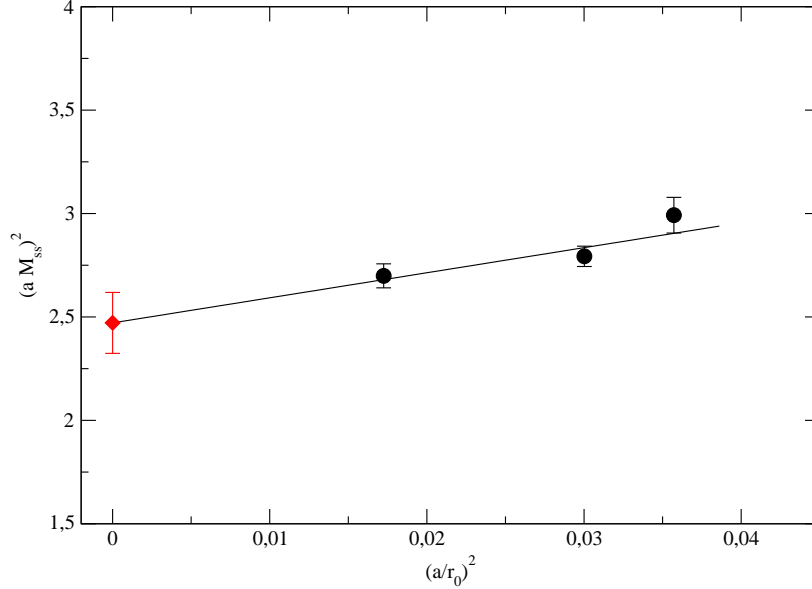


Figure 3.9: *Continuum extrapolation of $(r_0 M_{ss})^2$ performed in order to set the scale in those analyses that uses aM_{ss} as a scaling variable.*

Collection of results from the various analyses

All the results obtained for m_{ud} , for the scaling variables r_0 and M_{ss} , for the values of the lattice spacing at each β and for the LECs B_0 , f_0 , $\bar{\ell}_3$ and $\bar{\ell}_4$ are collected in Table 3.8.

We stress that it is quite reassuring to observe that different ways to handle the chiral extrapolation as well as the discretization effects produce fully consistent results, demonstrating the solidity of our determinations.

Methodology used to combine results from different analyses

Combining all results reported in Table 3.8 provides us with the final estimates, including a determination of the various sources of systematic uncertainties. The general procedure followed in this work consist in taking the average of all the results for a specific quantity, eventually weighted with the inverse of the statistical error, and to compute the overall

Quantity	r_0 Analysis		$M_{\langle ss \rangle}$ Analysis	
	Chiral Fit	Polynomial Fit	Chiral Fit	Polynomial Fit
$m_l(\text{MeV})$	3.72(13)	3.87(17)	3.66(10)	3.75(13)
$r_0(\text{GeV}^{-1})$	2.39(6)	2.42(7)	-	-
$r_0(\text{fm})$	0.470(12)	0.477(14)	-	-
$M_{ss}(\text{GeV})$	-	-	0.672(9)	0.654(10)
$a(\beta = 1.90)(\text{fm})$	0.0886(27)	0.0899(31)	0.0868(33)	0.0892(34)
$a(\beta = 1.95)(\text{fm})$	0.0815(21)	0.0827(25)	0.0799(27)	0.0820(28)
$a(\beta = 2.10)(\text{fm})$	0.0619(11)	0.0628(13)	0.0607(14)	0.0623(15)
$B_0(\text{MeV})$	2515(90)	-	2551(73)	-
$f_0(\text{MeV})$	121.1(2)	-	121.3(2)	-
\bar{l}_3	3.24(25)	-	2.94(20)	-
\bar{l}_4	4.69(10)	-	4.65(8)	-

Table 3.8: Summary of the results of the four analysis in the pion sector using the CWW approach to calculate the FSE and the set M1 for the renormalization constants Z_P .

error using the following formula

$$\sigma^2 = \frac{1}{N} \sum \sigma_i^2 + \frac{1}{N} \sum (x_i - \bar{x})^2, \quad (3.25)$$

where x_i and σ_i are the central value and the error for a given quantity x obtained using the analysis i , \bar{x} is the mean value of the quantity over the different analyses and N is the number of analyses. Clearly the second term in the r.h.s. of Eq. (3.25) accounts for the spread of the results of the various analyses. In the specific case it corresponds to a systematic error which is a combination of the chiral extrapolation and the discretization uncertainties. Eventually we have to add to this error other sources of systematic uncertainties which have not been included so far, namely the systematic error associated to the calculation of FSE and to the method used to calculate the renormalization constants Z_P .

Final estimate and systematics

Combining all the uncertainties together we get the following estimate for the average up/down quark mass in the $\overline{\text{MS}}$ scheme at a renormalization scale of 2 GeV:

$$m_{ud} = 3.70(13)_{\text{stat+fit}}(6)_{\text{Chiral}}(5)_{\text{Disc.}}(5)_{Z_P}(4)_{\text{FSE}} \text{ MeV}$$

$$\begin{aligned}
&= 3.70(13)_{stat+fit}(10)_{syst} \text{ MeV} \\
&= 3.70(17) \text{ MeV} .
\end{aligned} \tag{3.26}$$

Decoupling exactly one source of uncertainties from the other is not a trivial task, so let us discuss a bit further how the various components of the systematics have been evaluated.

The first error includes the statistical one as well as the error associated with the fitting procedure. This means that such an error is larger than the typical statistical error of the lattice data, being amplified in a way that depends on the chiral and continuum extrapolation. In total we get a (stat+fit) error equal to $\simeq 3.5\%$.

Additional chiral extrapolation and discretization uncertainties in the second term of the r.h.s. of Eq. (3.25) are evaluated from the differences of the results obtained using r_0 or M_{ss} (labelled as Disc.) and chiral or polynomial fit (labelled as Chiral). We found them to be at the level of 1.6% and 1.4%, respectively.

For the uncertainty due to FSE we considered the difference between the result obtained using the most accurate correction, i.e. the CWW one, and the result obtained without FSE corrections at all. This give rise to an error equal to $\simeq 1.1\%$.

Finally, comparing the values of m_{ud} obtained using the sets M1 and M2 for the renormalization constants Z_P we get an error of $\simeq 1.4\%$.

Comparison with the FLAG averages and other results from the pion fit

Our determination (3.26) for m_{ud} is the first one obtained at $N_f = 2 + 1 + 1$ and it also satisfies the quality criteria proposed by the FLAG group [48] to be eligible for entering the lattice average of m_{ud} . We remind that the recently updated lattice averages provided by FLAG [48] are: $m_{ud} = 3.6(2)$ MeV at $N_f = 2$ and $m_{ud} = 3.42(9)$ MeV at $N_f = 2 + 1$. The comparison of these results with our finding (3.26) shows that the partial quenching of the strange and/or charm sea quarks is not yet visible at the (few percent) level of the present total systematic uncertainty.

For the Sommer scale r_0 we get

$$r_0 = (0.474 \pm 0.014) \text{ fm} , \tag{3.27}$$

while the values of the lattice spacing at each β turn out to be

$$a|_{\beta=1.90, 1.95, 2.10} = \{0.0885(36), 0.0815(30), 0.0619(18)\} \text{ fm} . \tag{3.28}$$

	Our results	FLAG $_{N_f=2}$	FLAG $_{N_f=2+1}$	FLAG $_{N_f=2+1+1}$
$m_{ud}(\text{MeV})$	3.70(17)	3.6(2)	3.42(9)	-

Table 3.9: Comparison of the result we found in this analysis for the average up/down quark mass m_{ud} with corresponding averages performed by FLAG [48] for $N_f = 2$, $N_f = 2 + 1$.

For completeness, the values obtained for the LECs B_0 , f_0 , $\bar{\ell}_3$ and $\bar{\ell}_4$ are reported also in Table 3.10

Quantity	Value
$B_0(\text{MeV})$	2571(80)(55)
$f_0(\text{MeV})$	121.2(2)(3)
$\bar{\ell}_3$	3.11(23)(25)
$\bar{\ell}_4$	4.69(09)(14)

Table 3.10: Results for the LO and NLO LECs. The first error represents the (stat+fit) uncertainty, while the second error is the remaining systematic one (see text).

We emphasize (see also the recent work of Ref. [49]), that a precise determination of the NLO LECs $\bar{\ell}_3$ and $\bar{\ell}_4$ requires a careful study of the impact of the choice of pion mass range considered for the chiral fit as well as of NNLO corrections. Such analyses, which are in progress, are out of the scope of the present work.

FSE impact on the physical quantities

Before closing this Section, it is very interesting to look at the impact of the various formulae used to calculate the FSE for the quantities extracted from the pion analysis. In this respect, the results obtained within the four analyses 1A, 1B, 2A and 2B are quite similar to each other. Therefore in Table 3.11 we have reported the findings corresponding to the analysis 1A.

From Table 3.11 it can be seen that, though the FSE corrections can reach a level equal to 2.4% and 6.3% for the pion mass and decay constant, respectively (see Table 3.7 for the ensemble A40.24), the final impact on m_{ud} , r_0 and the LECs B_0 , f_0 , $\bar{\ell}_3$ and $\bar{\ell}_4$ is limited to be below the (stat+fit) error.

Quantity	No Correction	GL	CDH	CWW
$m_l(\text{MeV})$	3.68(14)	3.76(14)	3.73(13)	3.72(13)
$r_0(fm)$	0.464(12)	0.466(12)	0.468(12)	0.470(12)
\bar{l}_3	3.42(20)	3.35(20)	3.34(21)	3.24(25)
\bar{l}_4	4.83(9)	4.77(9)	4.76(9)	4.69(10)
$B_0(\text{MeV})$	2548(99)	2497(97)	2500(93)	2515(90)
$f_0(\text{MeV})$	120.8(1)	120.9(1)	120.9(1)	121.1(2)

Table 3.11: Comparison between different FSE corrections on the physical quantities extracted by the pion analysis 1A. The errors include the statistical and fitting procedure uncertainties (see text).

3.4 Strange quark mass

In this section we present our determination of the strange quark mass m_s .

General strategy

The analysis follows a strategy similar to the one presented for the pion sector. As a preliminary step, however, we performed an interpolation of the lattice kaon data at a fixed value of the strange quark mass in order to arrive (iteratively) to the physical one (see next Section). Then for the data at the fixed value m_s we studied the dependence of the kaon mass on both the light quark mass and the lattice spacing to performed the chiral extrapolation and the continuum limit. Also in this analysis, in order to control the systematic uncertainties we investigated multiple approaches concerning both the discretization effects and the chiral extrapolation.

Discretization effects

In the kaon sector we handled discretization effects using the approaches explained already for the pion sector. We performed a standard analysis, using r_0/a as scaling variable, and an alternative one in which we used a fictitious PS meson mass aM_{ss} to build the ratios M_{ls}/M_{ss} , which are expected to have milder lattice artifacts. Indeed we find that, since M_{ls} and M_{ss} have very similar discretization effects, their cancellation is much more significant than in the pion case, as it will be shown in a while.

In these analyses, while the kaon masses simulated at different values of the lattice spac-

ing are brought to a common scale using either aM_{ss} or r_0/a , the quark masses are converted directly to physical units using the values of the lattice spacing determined from the pion sector. The reason for this choice is that the quantity aM_{ss} has non-negligible discretization effects, which are used to compensate those of the kaon mass but would introduce large lattice artifacts in the ratios m_l/M_{ss} .

Chiral extrapolation

In both the r_0 and the M_{ss} analyses we considered two different chiral extrapolations in the light quark mass m_l , namely either the predictions of SU(2) ChPT or a polynomial expansion. In such a way, as in the pion sector, there are four different branches of the analysis, labelled as 1A, 1B, 2A and 2B.

Input parameters from previous analysis

To determine the strange quark mass we made use of quantities extracted from the pion sector, like the lattice spacing, the LECs B_0 and f_0 , the Sommer parameter r_0 and the results for the average up/down quark mass, reported in Table 3.8. In order to preserve meaningful correlations between quantities corresponding to the same bootstrap event, in each of the four kaon analyses we used inputs coming from the corresponding pion fit. This is also motivated also by the fact that, for instance, if SU(2) ChPT is used for the pion analysis, then the same theory should be applied to the kaon as well.

Renormalization constants

In the determination of the strange quark mass, as for the other quark masses, the choice of the method to calculate the renormalization constants has an important impact. Thus both sets of Z_P presented in table 3.4 have been used and the different results have been included in the determination of our final estimate and its systematic uncertainties.

Combining the results from all the four analyses we obtain our final result for m_s and an estimate of various sources of systematic uncertainties.

3.4.1 Analyses of the kaon mass in units of r_0

The analysis is performed iteratively. First one starts from an initial guess for the physical strange quark mass m_s . Then, adopting a quadratic spline lattice data are interpolated in the strange quark mass to the physical value m_s and are brought to a common scale using r_0/a . A combined fit is then performed to extrapolate the dependence of M_K^2 on the light quark mass and on the lattice spacing to the physical point and to the continuum limit. Afterwards the value obtained for the kaon mass, converted in physical units using the value of r_0 obtained from the pion analyses, is compared with the experimental one. If the latter is not reproduced, a new guess for m_s is done and the whole process starts again.

The experimental value of the kaon mass to be matched is the one corrected for leading strong and electromagnetic isospin breaking effects according to

$$(M_K^{exp})^2 = \frac{M_{K^+}^2 + M_{K^0}^2}{2} - \frac{(1 + \varepsilon)}{2} (M_{\pi^+}^2 - M_{\pi^0}^2) \simeq (494.4 \text{ MeV})^2, \quad (3.29)$$

where $\varepsilon \simeq 0.7$ [48].

For the analysis 1A we used the SU(2) ChPT predictions at NLO, which assume the chiral symmetry to be satisfied by the up and down quarks only. For the kaon mass no chiral logs are predicted to appear at the leading order and the corresponding formula reads

$$(r_0 M_K)^2 = P_0(m_l + m_s) [1 + P_1 m_l + P_3 a^2] \cdot K_{M_K}^{FSE}. \quad (3.30)$$

For the polynomial fit (analysis 1B) we introduced also a quadratic dependence in the light quark mass

$$(r_0 M_K)^2 = P'_0(m_l + m_s) [1 + P'_1 m_l + P'_2 m_l^2 + P'_3 a^2] \cdot K_{M_K}^{FSE}. \quad (3.31)$$

The uncertainties on the renormalization constants Z_P and the values of r_0/a are accounted for using the same procedure described for the pion, i.e. by including the term (3.11) in the χ^2 definition.

The dependence of M_K^2 on the renormalized quark mass at each lattice spacing as well as its chiral and continuum extrapolation are shown in Figs. 3.10 and 3.11 in the cases of the SU(2) ChPT fit (3.30) and of the polynomial ansatz (3.31), respectively.

In both cases the lattice data are reproduced quite well by the fitting formulae. Notice the typical size of discretization effects which can be quantified at the level of $\simeq 10\%$ by taking the difference between the results at the finest lattice spacing and the ones in

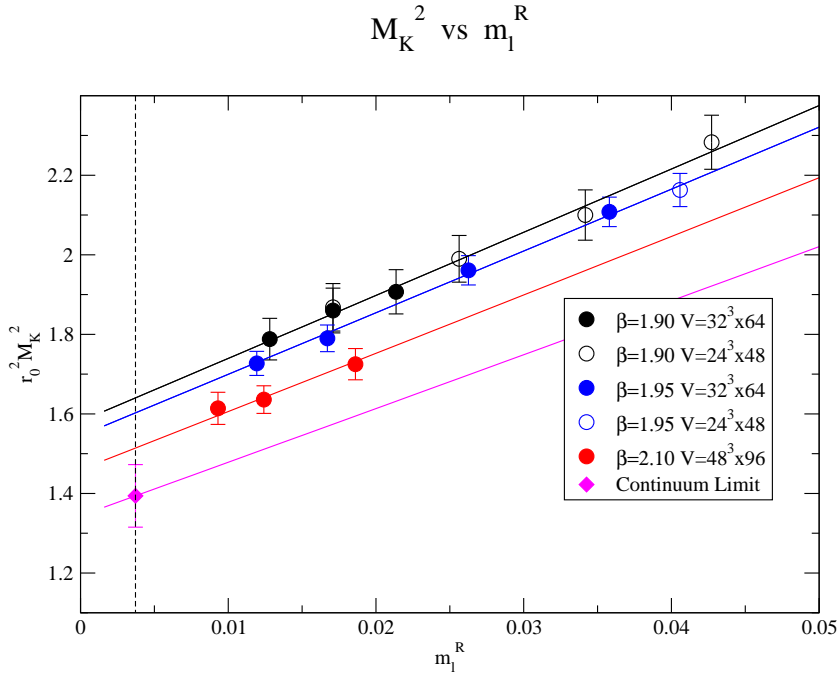


Figure 3.10: Chiral and continuum extrapolation of M_K^2 in units of r_0 using the $SU(2)$ ChPT predictions given by Eq. (3.30). All the data are corrected for FSE using the CDH approach [41].

the continuum limit. As in the pion case, the difference between the results of the two chiral extrapolations represent our estimate of the systematic uncertainties due to the chiral extrapolation.

FSE in the kaon mass

The data for the kaon mass have been corrected for FSE using ChPT formulae. The absence of the chiral log at NLO make the corresponding FSE correction formula, GL, vanishing identically. Thus the first non-vanishing correction appears at NNLO and it was calculated in Ref. [41]. The pion mass splitting is expected to give a contribution to the FSE as for the pion case. However explicit calculations are not available¹. In Table 3.12 we show that: i) FSE on the kaon mass are definitely smaller compared to the pion case (see Table 3.5), and ii) even if the contribution from the pion mass

¹A first step in this direction has appeared recently in Ref. [51], where however the framework adopted differs from the non-unitary setup chosen in this work for the valence and sea strange quarks.

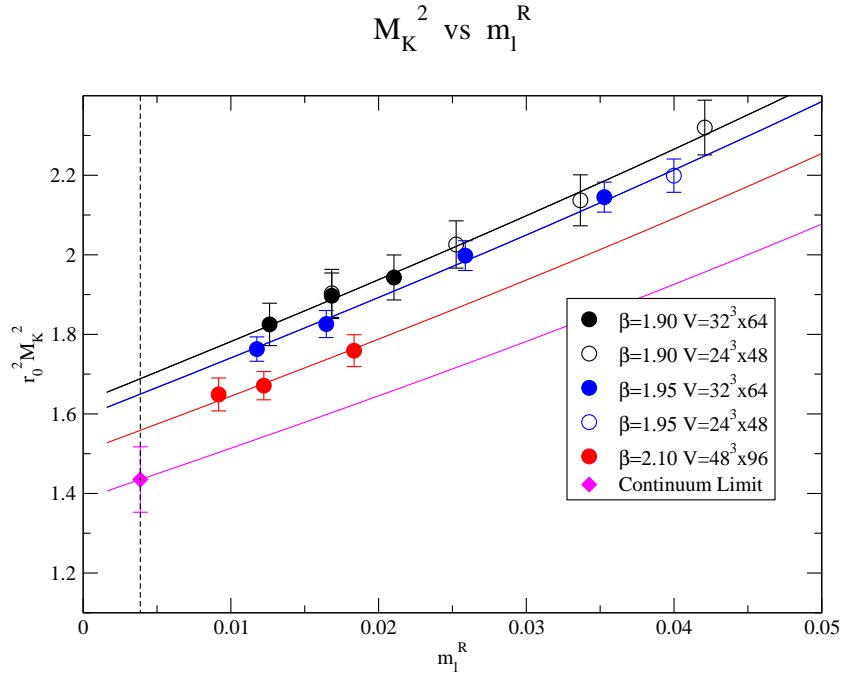


Figure 3.11: The same as in Fig. 3.10, but in the case of the polynomial fit (3.31).

splitting is neglected, the CDH predictions appear to work quite efficiently, reproducing the observed ratio of lattice data evaluated at two different volumes.

	GL	CDH	Lattice data M_{32}/M_{24}
$K_{M_K,[32]}^{FSE}/K_{M_K,[24]}^{FSE}$	1	0.991	0.990(7)

Table 3.12: Values of the ratio of the FSE correction factor $K_{M_K}^{FSE}$ in the case of the kaon mass for the gauge ensembles $A40.32$ and $A40.24$, obtained within the approaches *GL* and *CDH*, compared with the corresponding ratio of lattice data.

As we already did for the pion case, it is interesting to look at the coefficient $K_{M_K,[24]}^{FSE} - 1$, representing the FSE correction in percentage, for the gauge ensemble affected by the largest FSE correction i.e. $A40.24$. These values are collected in in table 3.13.

3.4.2 Analyses of the kaon mass in units of M_{ss}

Following the same strategy adopted in the pion analyses, the kaon masses simulated at different β values can be brought to a common scale by constructing the ratios M_{ls}^2/M_{ss}^2 ,

	GL	CDH
$K_{M_K, [24]}^{FSE} - 1$	0	0.010

Table 3.13: Values of $K_M^{FSE} - 1$ for the gauge ensembles A40.24 obtained within the various FSE approaches GL and CDH.

which are expected to suffer only marginally by discretization effects. Instead, as already pointed out, the light quark mass m_l is not converted in units of M_{ss} in order to avoid the introduction of unwanted lattice artifacts. The mass m_l is directly expressed in physical units by using the values of the lattice spacing found in the pion sector. Let us remind that the quantity aM_{ss} has been extracted for each bootstrap event and that its mean value at each β is reported in Eq. (3.20). Finally, the mass M_{ss} has no experimental counterpart, being just an intermediate hadron scale chosen arbitrarily (see Section 3.3.2).

As for the analyses done in units of r_0 , we used again two different chiral extrapolations, adopting formulae similar to Eqs. (3.30) and (3.31), but expressed in units of M_{ss} . After the chiral extrapolation and the continuum limit are carried out, the result for M_K/M_{ss} can be combined with the continuum limit value of M_{ss} obtained in the corresponding pion analysis in order to eventually compare with the experimental kaon mass (3.29).

The dependencies of M_K^2/M_{ss}^2 on the renormalized light quark mass at each values of β as well as in the continuum limit are shown in Fig. 3.12 using the SU(2) ChPT prediction (analysis 2A).

In the case of the kaon mass the use of the hadron scale M_{ss} turn out to be an extremely efficient tool, for an almost total cancellation of the discretization effects, namely from $\simeq 10\%$ (see Figs. 3.10 and 3.11) to about 0.4% (see Fig. 3.12). This allows us to keep the extrapolation to the continuum limit under a very good control in the whole range of values of the renormalized light quark mass.

Results of the same quality are obtained within the analysis 2B, which makes use of the polynomial fit for the chiral extrapolation, as can be seen from fig. 3.13.

3.4.3 Results for the kaon sector

In this section we collected the results and systematics for the strange quark mass obtained in the analyses presented in the previous sections. At the end of this section we will also

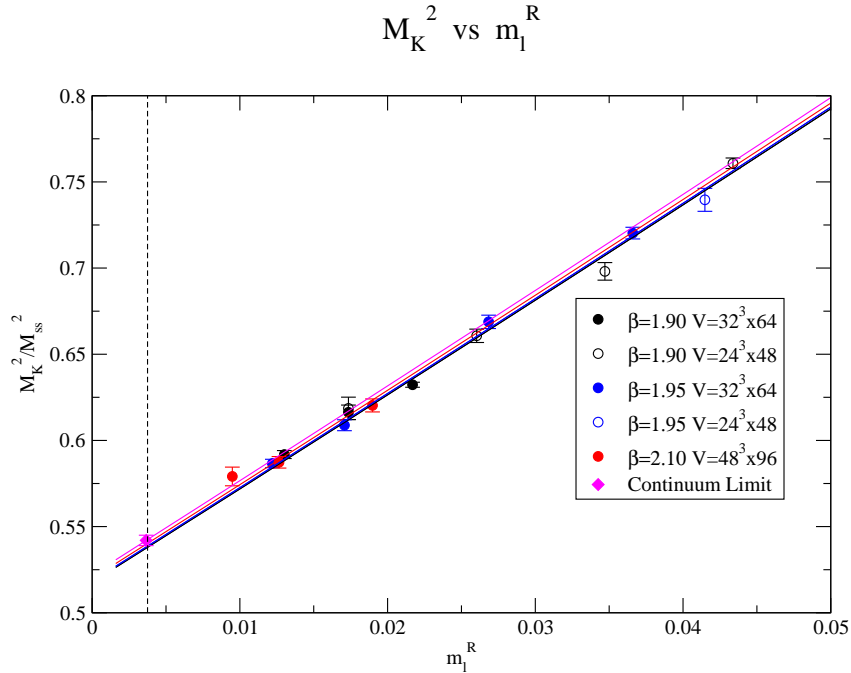


Figure 3.12: *Chiral and continuum extrapolation of M_K^2 in units of M_{ss}^2 using $SU(2)$ ChPT at NLO. All the data are corrected for FSE using the CDH predictions [41].*

present our determination of the ratios m_s/m_{ud} and m_u/m_d .

Collection of results from the various analyses

As explained in the previous sections, our result for the strange quark mass m_s is the one that reproduces after the chiral and continuum limits the experimental value of the K-meson mass, $M_K^{exp} = 494.4$ MeV.

At this point the error on the determination of the strange quark mass has to be estimated from the statistical+fit error obtained for the K meson mass in the fitting procedure. In particular the upper bound in m_s is obtained as the value that reproduces, after the fit, M_K^{exp} plus its fit error while the lower bound is the value that reproduces M_K^{exp} minus its fit error. In practice, this was done scanning a region of the strange quark mass around the central value determined by our analysis, and for each value of m_s a new fit was performed.

The results of the four analyses 1A, 1B, 2A and 2B for the strange quark mass, given in the $\overline{\text{MS}}$ at a renormalization scale of 2 GeV, are shown in Table 3.14, where we used

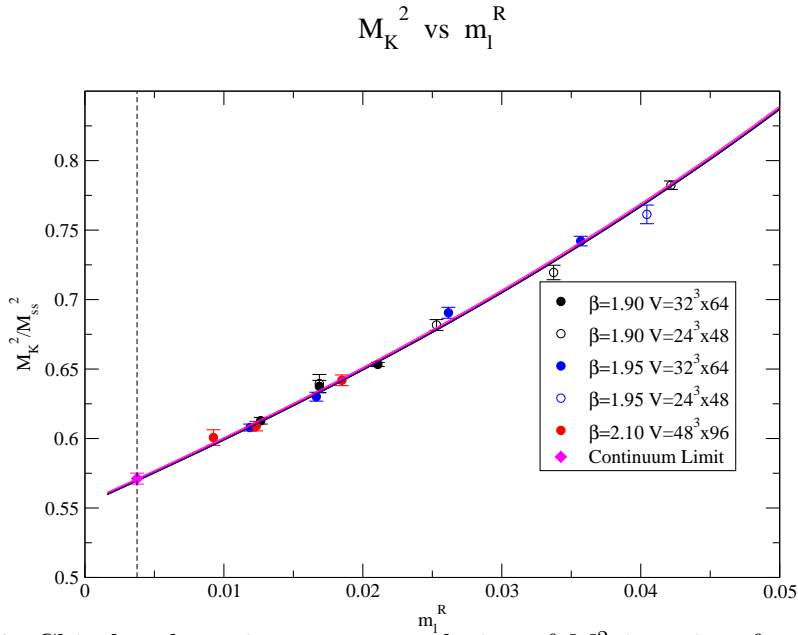


Figure 3.13: Chiral and continuum extrapolation of M_K^2 in units of r_0 using SU(2) ChPT prediction. All the data are corrected for FSE.

the renormalization constants Z_P calculated in the RI-MOM scheme using the method $M1$.

Quantity	r_0 Analysis		M_{ss} Analysis	
	Chiral Fit	Polynomial Fit	Chiral Fit	Polynomial Fit
m_s (MeV)	101.6(4.4)	102.5(3.9)	99.4(2.9)	100.8(3.2)

Table 3.14: Results for the strange quark mass obtained in the four branches of the analysis. The renormalization constants Z_P are those obtained in the RI-MOM scheme within the method $M1$.

Methodology used to combine results from different analyses

The strategy for combining the results from the various analysis used for the strange quark mass is similar to the one presented for the pion fit in Section 3.3.3. However, differently from the pion analysis, the results presented in table 3.14 are associated with wider range of statistical uncertainties. For this reason, the average of the several

analyses was performed weighting the results with the inverse of their statistical errors

$$\bar{x} = \frac{\sum x_i/\sigma_i^2}{\sum 1/\sigma_i^2}. \quad (3.32)$$

Consistently, the formula used to compute the overall error has been modified in the following way

$$\sigma^2 = N \frac{1}{\sum 1/\sigma_i^2} + \frac{\sum (x_i - \bar{x})^2/\sigma_i^2}{\sum 1/\sigma_i^2}. \quad (3.33)$$

This approach is the one used also in the rest of the work.

Final estimate and systematics

Combining the various results, we obtained our final determination of the strange quark mass m_s , namely

$$\begin{aligned} m_s &= 99.2(3.4)_{stat+fit}(0.6)_{Chiral}(1.1)_{Disc.}(1.5)_{Z_P}(0.5)_{FSE} \text{ MeV} , \\ &= 99.2(3.4)_{stat+fit}(2.0)_{syst} \text{ MeV} , \\ &= 99.2(3.9) \text{ MeV} . \end{aligned} \quad (3.34)$$

The largest uncertainty, of about 3.4%, comes from the statistical error plus the uncertainties due to the fitting procedure. The latter is the dominant one, mainly because of the distance between the lowest simulated quark mass and the physical point m_{ud} in the chiral extrapolation.

Additional systematic uncertainty related to the chiral extrapolation has been evaluated using the spread among the results obtained from the chiral and polynomial fit. This corresponds in the error budget to a 0.6% systematic uncertainty.

The discretization error has been calculated using the spread among the results obtained in units of r_0 and those found in units of M_{ss} , representing a 1.1% uncertainty on m_s .

The different sets of values of Z_P , calculated using the methods $M1$ and $M2$, give rise to an uncertainty of 1.5%.

The difference of the strange quark mass obtained in the analysis 1A without correcting for the FSE and the one obtained using the CDH approach [41] has been used to estimate the corresponding systematic uncertainty, which turns out to be of the order 0.5%.

Comparison with the FLAG averages

Closing this section it is interesting to report a comparison of the results we found in this analysis for the strange quark mass m_s with corresponding averages performed by FLAG [48] for $N_f = 2$ and $N_f = 2 + 1$:

	Our results	FLAG $_{N_f=2}$	FLAG $_{N_f=2+1}$	FLAG $_{N_f=2+1+1}$
$m_s(\text{MeV})$	99.2(4.0)	101(3)	93.8(2.4)	-

Table 3.15: Comparison between the result we found in this analysis for the strange quark mass m_s and the corresponding averages performed by FLAG [48] for $N_f = 2$ and $N_f = 2 + 1$.

3.5 Determination of the ratio m_s/m_{ud}

The results for the strange quark mass m_s and for the average up/down quark mass m_{ud} corresponding to each of the four branches of the analysis (see Tables 3.8 and 3.14) can be used to estimate the mass ratio m_s/m_{ud} . One gets

$$\begin{aligned}
\frac{m_s}{m_{ud}} &= 26.98(1.29)_{stat+fit}(0.25)_{Chiral}(0.13)_{Disc.}(0.01)_{Z_P}(0.16)_{FSE} , \\
&= 26.98(1.29)_{stat+fit}(0.32)_{syst} , \\
&= 26.98(1.32) .
\end{aligned} \tag{3.35}$$

The total uncertainty is of 4.9%, coming mainly from the chiral extrapolation.

In order to reduce the uncertainty we considered an alternative strategy.

The squared meson mass M_{12}^2 of a PS meson made of two valence quarks with masses m_1 and m_2 can be written as

$$M_{12}^2 = B_0(m_1 + m_2) [1 + r(m_1, m_2, a^2)] , \tag{3.36}$$

where the quantity $r(m_1, m_2, a^2)$ includes the contributions of all possible mass terms of order higher than the linear one (including also logs).

Therefore one can define the quantity $R(m_s, m_l, a^2)$ as

$$R(m_s, m_l, a^2) \equiv \frac{m_l}{m_s} \frac{2M_K^2 - M_\pi^2}{M_\pi^2} . \tag{3.37}$$

which by construction is independent on the values of Z_P as well as of the lattice spacing. Using eq. 3.36 one gets

$$R(m_s, m_l, a^2) = \frac{1 + (1 + \frac{m_l}{m_s})r(m_s, m_l, a^2) - \frac{m_l}{m_s}r(m_l, m_l, a^2)}{1 + r(m_l, m_l, a^2)}, \quad (3.38)$$

which implies that $R(m_s, m_l, a^2)$ deviates from unity when $r(m_s, m_l, a^2)$ or $r(m_l, m_l, a^2)$ deviates from zero. Moreover in the SU(3) symmetric limit $m_s = m_l$ one has $R(m_l, m_l, a^2) = 1$, which implies that the discretization effects on the ratio $R(m_s, m_l, a^2)$ should start at order $\mathcal{O}[a^2(m_s - m_l)]$.

A useful feature of $R(m_s, m_l, a^2)$ is that the dependence upon the strange and light quark masses is expected to give rise to small corrections only. In particular, the mild dependence on the light quark mass m_l allows to reduce the uncertainty due to the chiral extrapolation, so that a precise determination of the mass ratio m_s/m_{ud} is given by

$$\frac{m_s}{m_{ud}} = \left(\frac{2M_K^2 - M_\pi^2}{M_\pi^2} \right)^{phys} \frac{1}{R^{phys}}, \quad (3.39)$$

where R^{phys} can be precisely evaluated on the lattice.

In Fig. 3.14 the lattice data for $R(m_s, m_l, a^2)$, interpolated at the physical strange mass (3.34) and corrected for FSE using the CWW predictions [42] for M_π and the CDH ones [41] for M_K , are shown versus the light quark mass m_l for all ensembles.

The chiral and continuum extrapolations are performed through a simple linear fit of the form

$$R(m_s, m_l, a^2) = R_0 + R_1 m_l + R_3 a^2, \quad (3.40)$$

The results are presented in Fig. 3.14 as solid lines for each β values and in the continuum. It can be seen that discretization effects are small, being the difference between the result at the finest lattice spacing and the one in the continuum of the order of $\simeq 1\%$. At the physical point we find $R^{phys} = 0.970(11)$ which implies

$$\frac{m_s}{m_{ud}} = 26.65(30). \quad (3.41)$$

The result (3.41) is clearly preliminary because it is based on the bootstrap events of analysis 1A only. It seems however that the use of the quantity R leads to a significant improvement of the precision for the mass ratio m_s/m_{ud} .

A comparison between our result and the corresponding FLAG averages [48] reported in table 3.5.

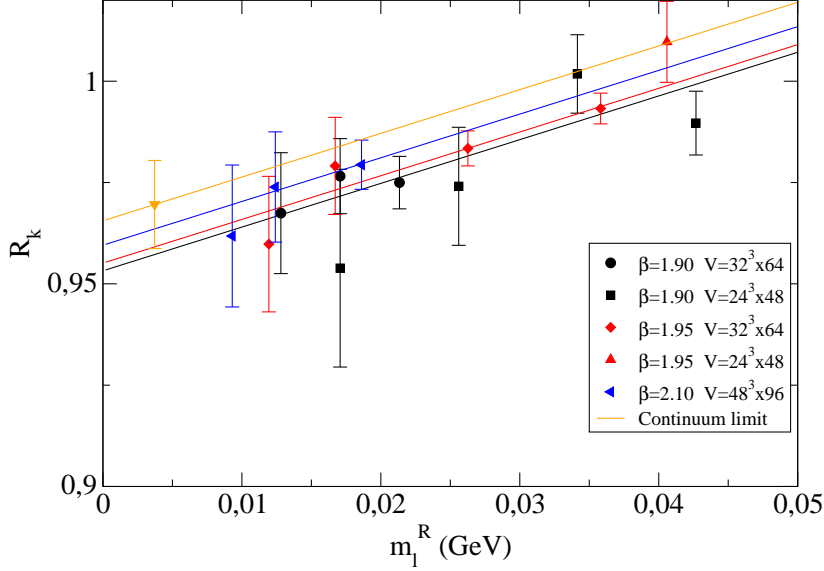


Figure 3.14: Chiral and continuum extrapolation of $R(m_s, m_l, a^2)$, defined in Eq. (3.37), based on a linear fit in m_l . The data are interpolated at the physical strange mass (3.34) and corrected for FSE using the CWW predictions [42] for M_π and the CDH ones [41] for M_K .

3.6 Determination of the ratio m_u/m_d

The light quark mass dependence of the squared kaon mass can be used to evaluate the strong isospin breaking effect due to difference between the u and d quark masses, leading eventually to an estimate of the ratio m_u/m_d . Indeed, in the limit of vanishing electric quark charges the difference between the neutral and charged squared kaon masses can be expanded in powers of the quark mass difference ($m_d - m_u$) as (see Ref. [52] and

	Our results	FLAG $_{N_f=2}$	FLAG $_{N_f=2+1}$	FLAG $_{N_f=2+1+1}$
m_s/m_{ud}	26.7(3)	28.1(1.2)	27.5(4)	-

Table 3.16: Comparison between the result we found in this analysis for the ratio m_s/m_{ud} and the corresponding averages performed by FLAG [48] for $N_f = 2$ and $N_f = 2 + 1$.

references therein)

$$\hat{M}_{K^0}^2 - \hat{M}_{K^+}^2 = (m_d - m_u) \cdot \left(\frac{\partial M_K^2}{\partial m_l} \right)_{m_l=m_{ud}} + \mathcal{O}[(m_d - m_u)^2] . \quad (3.42)$$

The isospin breaking slope $(\partial M_K^2/\partial m_l)_{m_l=m_{ud}}$ is defined in the isospin symmetric limit and therefore it can be computed by applying the derivative to the continuum and infinite volume limits of our fitting formulae, like Eqs. (3.30-3.31), with respect to m_l . The charged and neutral kaon masses, \hat{M}_{K^0} and \hat{M}_{K^+} , are the masses defined in pure QCD. For their values we adopted the recent FLAG estimates $\hat{M}_{K^0} = 497.2(4)$ MeV and $\hat{M}_{K^+} = 491.2(5)$ MeV [48] to obtain from Eq. (3.42) the value of $(m_d - m_u)$ and consequently the one of the ratio m_u/m_d (using also Eq. (3.26) for the average up/down quark mass). After having implemented the above strategy for the four branches of the kaon analysis one gets the result

$$\begin{aligned} \frac{m_u}{m_d} &= 0.486(47)_{stat+fit}(22)_{Chiral}(15)_{Disc.}(3)_{Z_P}(4)_{FSE} \text{ MeV} , \\ &= 0.486(47)_{stat+fit}(27)_{syst} \text{ MeV} , \\ &= 0.486(54) \text{ MeV} , \end{aligned} \quad (3.43)$$

which turns out to be fully consistent with the FLAG averages [48] reported in table 3.6.

	Our results	FLAG $_{N_f=2}$	FLAG $_{N_f=2+1}$	FLAG $_{N_f=2+1+1}$
m_u/m_d	0.49(5)	0.50(4)	0.46(3)	-

Table 3.17: Comparison between the result we found in this analysis for the ratio m_u/m_d and the corresponding averages performed by FLAG [48] for $N_f = 2$ and $N_f = 2 + 1$.

3.7 Charm quark mass

In this Section we present our determination of the mass of the quark charm obtained by analyzing both the D - and D_s -meson masses, following a strategy similar to the one presented for the K -meson.

General strategy

The lattice data for the D - and D_s -meson masses are interpolated to the physical strange and charm quark masses using a quadratic spline. The physical strange quark mass is the one determined in the previous Section, while the physical charm quark mass is defined such that the experimental value of the D - or D_s -meson mass is reproduced. Then the dependence of M_D and M_{D_s} on the light quark mass and on the lattice spacing is studied at fixed strange and charm quark masses, and the continuum limit and the chiral extrapolation to the physical point m_{ud} of the light quark mass is performed. The charm quark mass is determined by fitting either the D - or the D_s -meson mass. The latter, however, is expected to have smaller systematic uncertainty associated to the chiral extrapolation because of the milder light quark dependence, which occurs only through the sea. Because of that our final result for the charm quark mass will be the one coming from the D_s -meson analysis and the value obtained from fitting the D -meson mass is used as a consistency check.

Also in this analysis, in order to control the systematic uncertainties we investigated multiple approaches both on the side of the discretization effects and on the side of chiral extrapolation.

Discretization effects

As in the cases of the pion and kaon analyses, the lattice data for the charmed meson masses are converted in units of either the Sommer parameter r_0 or the mass M_{cs} of a fictitious PS meson made with one valence quark in the strange mass region and one valence quark with mass around charm. Such a reference mass M_{cs} , expected to have discretization effects closer to the ones of M_D or M_{D_s} , has been constructed assuming the arbitrary values $r_0 m_s = 0.22$ and $r_0 m_c = 2.4$ at each β and light quark mass. As in the case of the mass M_{ss} , the continuum limit of M_{cs} is needed and it is calculated after converting the quantities aM_{cs} to $r_0 M_{cs}$ using the values of r_0/a at each β .

Chiral extrapolation

For each choice of the scaling variable we tried different formulae to fit the chiral extrapolation. For the chiral extrapolation in the light quark mass, the Heavy Meson ChPT (HMChPT) predicts no chiral log at NLO for the D -meson mass and therefore we have used either a linear or a quadratic expansion in m_l . In the case of M_{D_s} we have considered also a constant fit because the dependence on m_l , which only comes from the sea, is expected to be very mild.

Input parameters from previous analysis: lattice spacings, light and strange quark masses

Each analysis in the charm sector needs, as input parameters, quantities previously calculated in the pion sector, like the physical value of the light quark mass, the lattice spacings and the value of the Sommer parameter. At variance with the kaon analyses, there is no reason to correlate the results from one specific kind of analysis in the pion sector with its analogue in the charm one. For instance, as far as the chiral extrapolation is concerned, the pion and the $D_{(s)}$ masses don't even share the same chiral theory. However, we want to account for the correlations among other quantities, like m_{ud} and the values of the lattice spacing at each β . Therefore, we have adopted a strategy similar to the one already used to combine the results of the four branches of analysis to get our final results. Namely, for each bootstrap event of the M_D or M_{D_s} fit, all input quantities are taken from one of the pion analyses chosen randomly assuming the same extraction probability (because the corresponding errors obtained from the various analyses on all quantities of the pion sector are very similar to each other). As a matter of fact, we note that the expression (3.25) just corresponds to the variance of a distribution obtained picking up randomly elements from four different distributions of given means \bar{x}_i and variances σ_i^2 .

An important consequence of this strategy is that, when we combine the results of the bootstrap events to obtain the statistical error, the latter automatically includes various sources of uncertainties, the most important of which is the one pertaining to the scale setting. Our final result for the charm quark mass will result from a combination of the

different analyses of the D_s -meson mass, automatically including in this way an estimate of the related systematic uncertainty.

Renormalization constants

Also in the case of the determination of the charm quark mass the choice of the method to calculate the renormalization constants is supposed to have an important impact. Thus both sets of Z_P presented in table 3.4 have been used and the different results have been included in the determination of our final estimate and its systematic uncertainties.

3.7.1 Analyses of D and D_s meson masses in units of r_0

Our analyses follow closely the same strategy already applied to the kaon case. One starts from an initial guess for the physical charm quark mass m_c . Then, after a smooth interpolation in the strange and charm quark masses to their physical values, the D - and D_s -meson masses, extracted in lattice units from the corresponding correlators, are brought to a common scale using r_0/a , while the quark mass is converted in physical units using directly the values of the lattice spacing obtained in the pion sector.

As already explained in the previous Section, the dependence of both r_0M_D and $r_0M_{D_s}$ upon the light quark mass m_l can be described quite well by a simple polynomial formula, namely

$$r_0M_D = P_0 + P_1m_l + P_2m_l^2 + P_3a^2, \quad (3.44)$$

$$r_0M_{D_s} = P'_0 + P'_1m_l + P'_2m_l^2 + P'_3a^2, \quad (3.45)$$

where $P_0 - P_3$ and $P'_0 - P'_3$ are free parameters. In the case of D -meson we have considered either a linear or a quadratic fit, while for the D_s -meson (containing the light quark only in the sea) we have added also a constant fit, i.e. $P'_1 = P'_2 = 0$ in Eq. (3.45).

As in the previous analyses, the errors on Z_P and the r_0/a are accounted for by a contribution to the χ^2 given by Eq. (3.11). Moreover, since the results corresponding to the ensembles A40.24 and A40.32 (differing only because of the lattice volume) almost coincide, we did not apply, in this case, any FSE correction.

The dependencies of M_{D_s} on the light quark mass m_l for each β values and lattice volumes as well as its continuum limit are illustrated in Figs. 3.15-3.16, adopting a constant fit or a quadratic one, respectively. It can be seen that the discretization

effects, which can be estimated through the difference between the results at the finest lattice spacing and those in the continuum limit, are of the order of 3%.

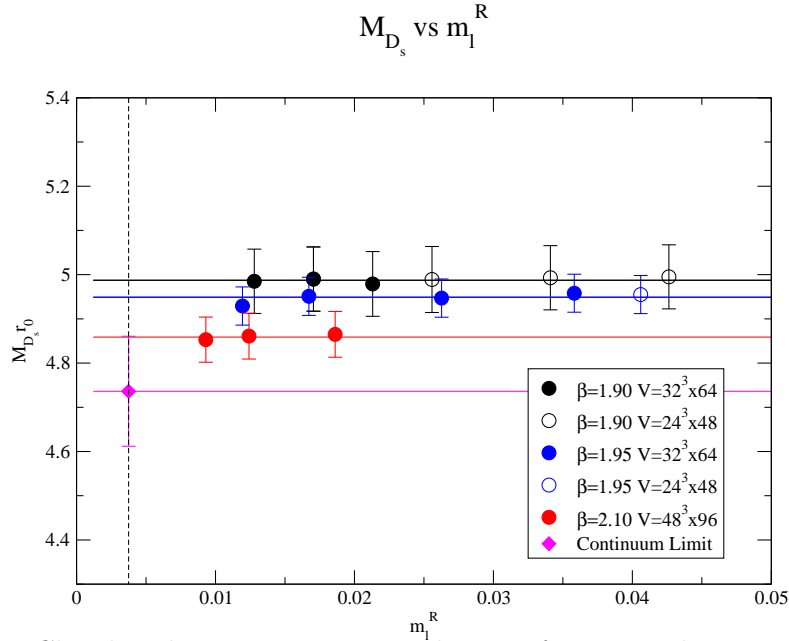


Figure 3.15: Chiral and continuum extrapolation of $r_0 M_{D_s}$ adopting a constant fit in m_l , i.e. $P'_1 = P'_2 = 0$ in Eq. (3.45).

3.7.2 Analyses of D and D_s meson masses in units of M_{c_s}

The size of the discretization effects can be reduced using M_{c_s} as a scaling variable. In this analysis we divide the charmed meson mass aM_{D_s} by the quantity aM_{c_s} , constructed at each β and m_l assuming fixed but arbitrary values for the valence strange and charm quark masses, whereas we convert the quark masses directly to physical units.

Once the continuum limit and the extrapolation to the physical light quark mass has been performed, the mass of the $D(D_s)$ is converted to physical units using the continuum extrapolation of M_{c_s} to be matched with the experimental value.

Extracting the reference mass M_{c_s}

To construct the meson mass M_{c_s} we first performed a slight interpolation in the strange valence quark mass to get the quantity aM_{c_s} at a common (but arbitrary) value $r_0 m_s = 0.22$ for each β and light quark mass. To arbitrarily fix the value of the other valence

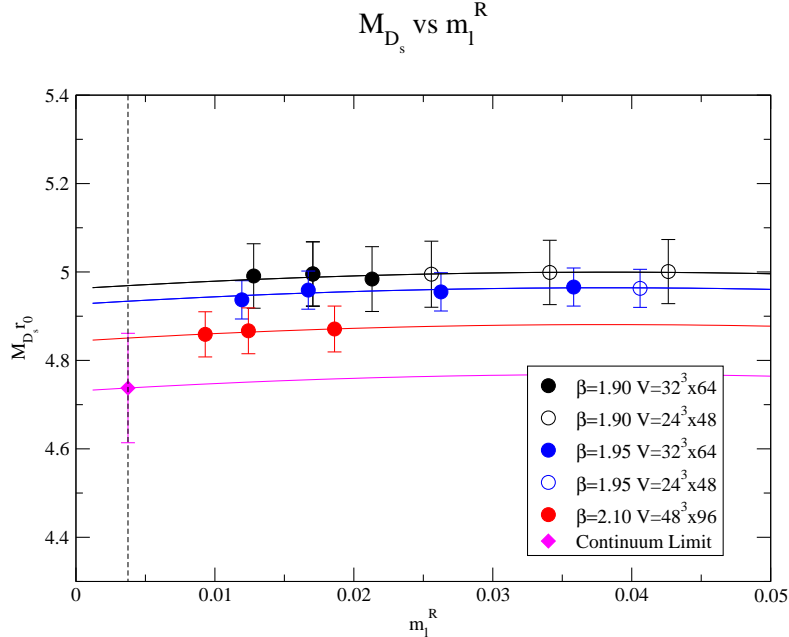


Figure 3.16: The same as in Fig. 3.15, but in case of the quadratic fit of Eq. (3.45).

quark in the charm region we used the relation $r_0 m_c = 2.4$. Finding no significant dependence of aM_{cs} on the light quark mass, we performed a constant fit in $a\mu_l$ to obtain the values of aM_{cs} at each β and for each bootstrap event as can be seen in fig. 3.17.

The averages over our bootstrap sample read as

$$aM_{cs}|_{\beta=1.90, 1.95, 2.10} = \{0.8592(3), 0.7681(4), 0.5779(3)\}. \quad (3.46)$$

Also in this case, the knowledge of the continuum limit of M_{cs} is required.

Therefore, we have first converted the quantity aM_{cs} to $r_0 M_{cs}$ and then performed a simple fit of the form $(r_0 M_{cs})^2 = \bar{P}_1 + \bar{P}_2 a^2 / r_0^2$. The extrapolation to the continuum limit of the quantity $(r_0 M_{cs})^2$ is shown in fig. 3.18

Fit in units of M_{cs}

The chiral extrapolation and the continuum limit of M_{D_s}/M_{cs} is performed using the fitting formula

$$\frac{M_{D_s}}{M_{cs}} = \bar{P}_0 + \bar{P}_1 m_l + \bar{P}_2 m_l^2 + \bar{P}_3 a^2. \quad (3.47)$$

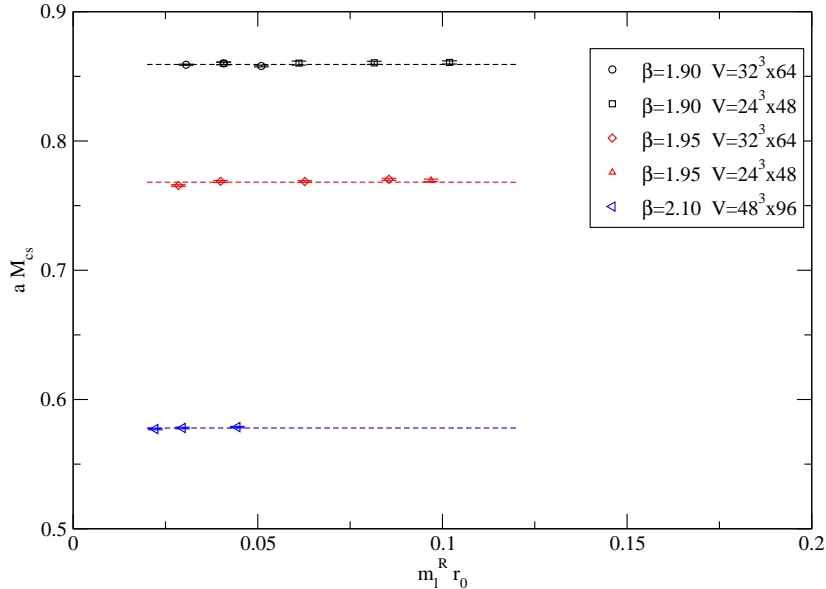


Figure 3.17: *Dependence of aM_{cs} on the light quark mass fitted with a constant.*

The dependence of M_{D_s}/M_{cs} on the light quark mass at each β and in the continuum limit, corresponding to either a constant or a quadratic fit in Eq. (3.47), are shown in Figs. 3.19 and 3.20 respectively.

Comparing the results in units of r_0 presented in Figs. 3.15-3.16, with the ones in units of M_{cs} shown in Figs. 3.19-3.20 one sees that discretization effects are strongly reduced in the ratio M_{D_s}/M_{cs} , so that the gap between the continuum and the finest lattice spacing decreases from 3% down to 0.3%.

3.7.3 Results in the D sector

In this section we collected the results and discuss the systematic uncertainties for the charm quark mass obtained in the analyses presented in the previous sections.

A collection of results from the various analyses of D_s meson

After the continuum limit and the extrapolation to the physical light quark mass m_{ud} are performed, the masses of the D and D_s mesons are converted in physical units using either the value of r_0 obtained from the pion analyses or the continuum extrapolation of

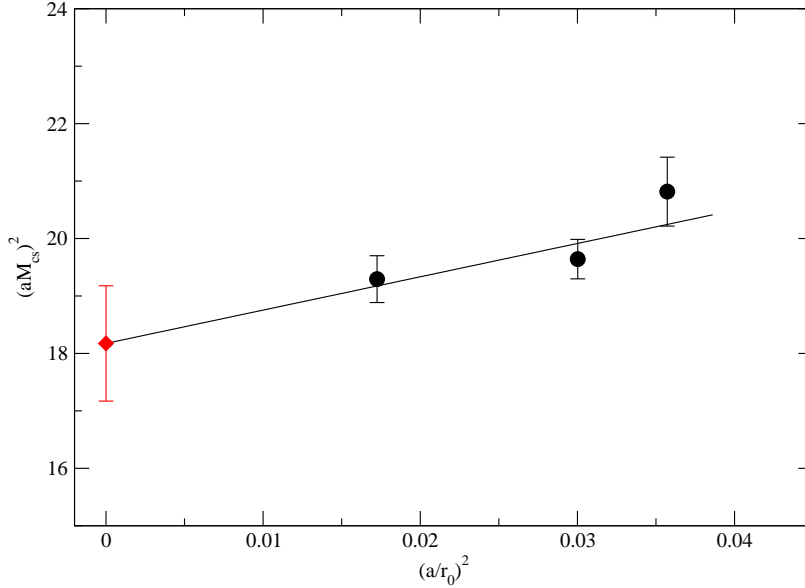


Figure 3.18: Continuum extrapolation of $(r_0 M_{scs})^2$ necessary to set the scale in those analyses that uses aM_{ss} as a scaling variable.

M_{cs} . Then, by successive iterations, the physical charm quark mass m_c is determined by matching the mass of the D - or D_s -meson to the corresponding experimental value [53]

$$M_D^{exp} = 1.870 \text{ GeV} , \quad M_{D_s}^{exp} = 1.969 \text{ GeV} . \quad (3.48)$$

The uncertainty on the physical charm quark mass is estimated from the (stat. + fit) error obtained for the D - or D_s -meson mass at the physical point in the fitting procedure. The uncertainty has been obtained in practice by scanning a region of the physical charm quark mass around the value corresponding to $M_{D_s(D)}^{exp}$ to find the values of m_c that reproduce $M_{D_s(D)}^{exp}$ plus/minus its (stat. + fit) error.

Our findings expressed in the $\overline{\text{MS}}(2 \text{ GeV})$ scheme and corresponding to the various chiral extrapolation formulae discussed in the previous Sections are shown in Table 3.18, where we have used the set of Z_P values of the method M1.

All the analyses have also been performed using the Z_p 's coming from the other calculation method (M2). Our finale estimate is the result of a combination of values obtained from the use of both renormalization constant sets.

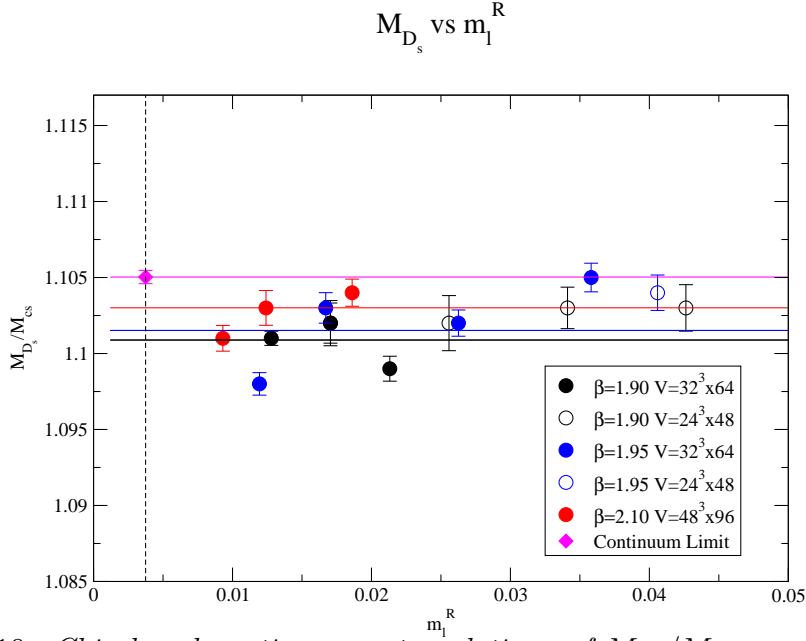


Figure 3.19: Chiral and continuum extrapolations of M_{D_s}/M_{cs} assuming a constant fit in m_l , i.e. $\bar{P}_1 = \bar{P}_2 = 0$ in Eq. (3.47).

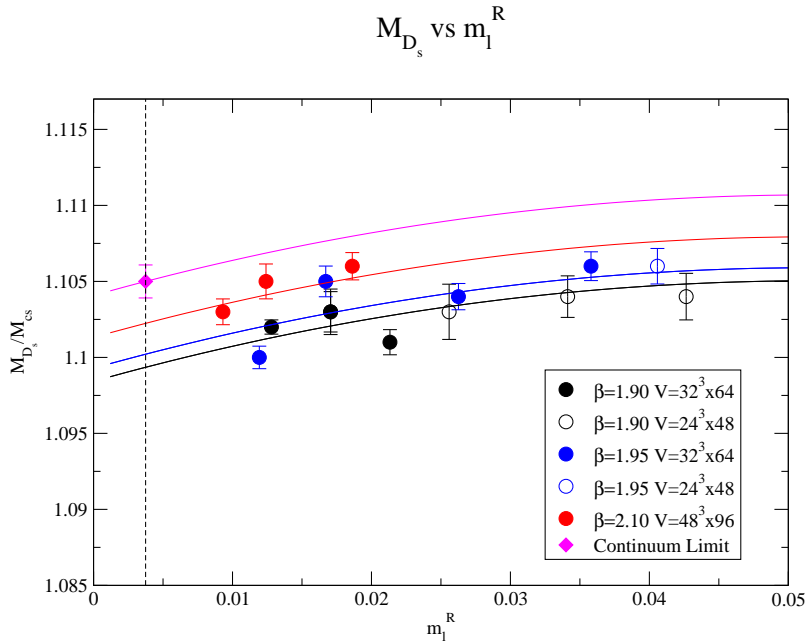


Figure 3.20: The same as in Fig. 3.19, but in case of the quadratic fit of Eq. (3.47).

Comparison with results from the D meson

It is interesting to check the compatibility of the results of Table 3.18 obtained using the D_s -meson mass with the ones corresponding to the analyses of the D -meson mass. The

Quantity	r_0 Analysis			M_{cs} Analysis		
	Const. Fit	Lin. Fit	Quad. Fit	Const. Fit	Lin. Fit	Quad. Fit
$m_c(\text{GeV})$	1.198(37)	1.198(37)	1.201(37)	1.187(38)	1.189(38)	1.190(38)

Table 3.18: Comparison between the results for the physical charm quark mass m_c obtained by different chiral and continuum extrapolations of the D_s meson mass. The results are expressed in the $\overline{\text{MS}}(2\text{ GeV})$ scheme and correspond to the choice of the Z_P values obtained with the method $M1$.

latter ones are reported in Table 3.19, where it can be clearly seen that there is indeed a full compatibility.

Quantity	r_0 Analysis		M_{cs} Analysis	
	Lin. Fit	Quad. Fit	Lin. Fit	Quad. Fit
$m_c(\text{GeV})$	1.187(36)	1.198(40)	1.170(34)	1.181(36)

Table 3.19: Comparison between the results for the charm quark mass m_c obtained by different chiral and continuum extrapolations of the D meson mass. These results are expressed in the $\overline{\text{MS}}(2\text{ GeV})$ scheme and correspond to the choice of the Z_P values corresponding to the method $M1$.

The quality of the chiral and continuum extrapolation performed on the D -meson mass is illustrated in Fig. 3.21 in the case of a quadratic fit in m_l .

Final estimates and systematics

The results from Table 3.18 and the ones obtained using the Z_P values of the method $M2$ have been combined to get our final result for m_c . This was done using the same strategy adopted for the pion case, explained in details in Section 3.3.3, but as for the kaon we used weighted averages (see sec. 3.4.3) After evolving the perturbative scale from 2 GeV to the value of m_c itself using N^3LO perturbation theory with four flavors of sea quarks, one obtains

$$\begin{aligned}
m_c(m_c) &= 1.350(44)_{\text{stat+fit+scale}}(3)_{\text{Chiral}}(8)_{\text{Disc.}}(19)_{Z_P}(5)_{m_s} \text{ GeV} , \\
&= 1.350(44)_{\text{stat+fit+scale}}(22)_{\text{syst}} \text{ GeV} , \\
&= 1.350(49) \text{ GeV}
\end{aligned} \tag{3.49}$$

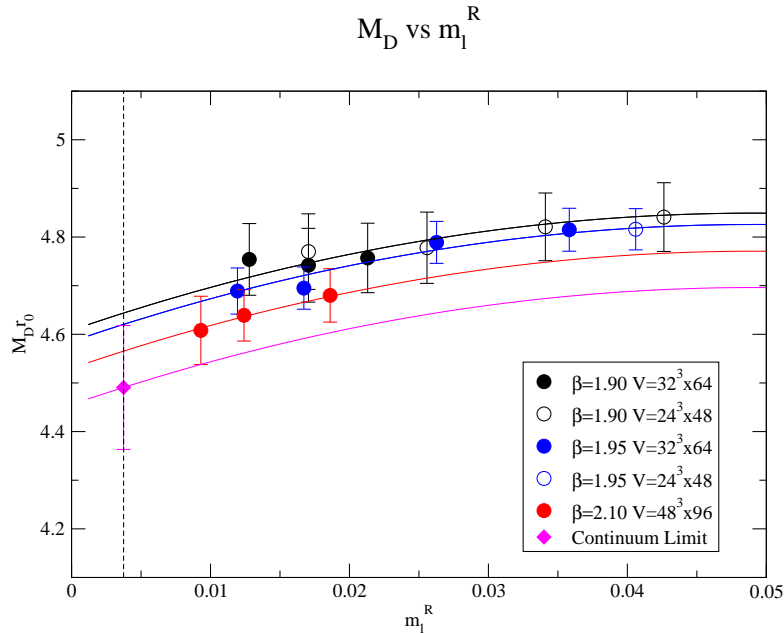


Figure 3.21: *Chiral and continuum extrapolations of $r_0 M_D$ assuming a quadratic fit in m_l .*

with a total uncertainty equal to 3.6% of the central value.

The strategy to separate the various sources of the systematic error is the same as the one used in the previous sections.

In Eq. (3.49) the first error includes not only the statistical uncertainties combined with the one associated with the fitting procedure, but also the uncertainties coming from the setting of the scale (see Section 3.7). This error is the most relevant one and corresponds to a contribution equal to 3.3% of the central value.

The systematic uncertainty due the chiral extrapolation has been estimated from the largest spread amongst the results corresponding to constant, linear or quadratic fits (see Table 3.18) and it turns out to be equal to 0.2%.

The difference among the results obtained using r_0 or M_{cs} can be used to estimate the uncertainty coming from the discretization effects, which results to be of the order of 0.6%.

The effect of the choice of the Z_P values between methods M1 and M2 gives rise to a systematic error of 1.4%.

Finally we have to take into account also the error induced by the total uncertainty of the physical strange quark mass m_s , which has been used to interpolate the lattice

data. This effect results to be equal to 0.3%.

Comparison with other literature results

Our finding (3.49) is consistent with the result $m_c(m_c) = 1.28(4)$ GeV obtained in Ref. [3] at $N_f = 2$, while a very slight tension, at the level of $\simeq 1.5$ standard deviations, occurs with respect to the PDG value $m_c(m_c) = 1.275(25)$ GeV [53] with the largest uncertainty affecting our determination.

3.8 Determination of the ratio m_c/m_s

The results for the strange and charm quark masses reported in Tables 3.14 and 3.18 can be used to estimate the mass ratio m_c/m_s , obtaining

$$\begin{aligned} \frac{m_c}{m_s} &= 11.86(58)_{stat+fit}(6)_{Chiral}(6)_{Disc.}(1)_{Z_P}(6)_{FSE} , \\ &= 11.86(58)_{stat+fit}(10)_{syst} , \\ &= 11.86(59) , \end{aligned} \tag{3.50}$$

which implies a total uncertainty of 5.0%.

In order to improve the precision of our determination of the ratio m_c/m_s we can adapt the approach used in the case of the mass ratio m_s/m_{ud} in Section 3.5.

Using lattice data for the masses of the η_c , D and D_s mesons, we can define the quantity $\bar{R}(m_c, m_s, m_l, a^2)$ as

$$\bar{R}(m_c, m_s, m_l, a^2) \equiv \frac{m_s}{m_c} \frac{(M_{\eta_c} - M_{D_s})(2M_{D_s} - M_{\eta_c})}{M_K^2 - M_\pi^2} . \tag{3.51}$$

which by construction is independent on the values of Z_P as well as of the lattice spacing. In Eq. (3.51) the mass of the η_c meson corresponds to the connected diagram only, or in other words it is the mass of a fictitious $\bar{c}c'$ PS meson with $m_{c'} = m_c$.

For a PS meson made of two valence quarks with masses m_1 and m_2 , in which one of the two quarks is around the charm mass, the meson mass M_{12} can be written as

$$M_{12} \equiv A(1 + Ca^2) + B(1 + Da^2)(m_1 + m_2) [1 + \bar{r}(m_1, m_2, a^2)] , \tag{3.52}$$

while the pion and kaon mass squared can be written as

$$M_{12}^2 = B_0(m_1 + m_2) [1 + r(m_1, m_2, a^2)] , \quad (3.53)$$

where the quantity $\bar{r}(m_1, m_2, a^2)$ includes the contributions of all possible mass terms of order higher than the linear one (including also logs).

Using eqs. (3.52) and (3.53) in eq. (3.51) one can see that the leading contribution in $(M_{\eta_c} - M_{D_s})(2M_{D_s} - M_{\eta_c})$ are proportional to m_c , while the leading contribution in $M_K^2 - M_\pi^2$ are proportional to m_s . Therefore $\bar{R}(m_c, m_s, m_l, a^2)$ is expected to have a mild dependence on the light, strange and charm quark masses. In particular the mild dependence on the light quark mass m_l represent a way to reduce the uncertainty produced by the fitting procedure in the chiral extrapolation, so that a precise determination of the mass ratio m_c/m_s is given by

$$\frac{m_c}{m_s} = \left(\frac{(M_{\eta_c} - M_{D_s})(2M_{D_s} - M_{\eta_c})}{M_K^2 - M_\pi^2} \right)^{phys} \frac{1}{\bar{R}^{phys}} , \quad (3.54)$$

where \bar{R}^{phys} can be computed on the lattice.

In Fig. 3.22 the lattice data for $\bar{R}(m_c, m_s, m_l, a^2)$, interpolated at the physical strange and charm masses, are shown versus the light quark mass m_l for all the gauge ensembles.

The chiral and continuum extrapolations are performed through a simple linear fit of the form

$$R(m_s, m_l, a^2) = R_0 + R_1 m_l + R_3 a^2 , \quad (3.55)$$

The results are reported in Fig. 3.22 as solid lines at each β values and in the continuum. Using this strategy we obtained the following result for the ratio m_s/m_{ud}

$$\frac{m_c}{m_s} = 11.65(9)_{stat+fit}(5)_{m_s}(6)_{m_c} = 11.65(12) . \quad (3.56)$$

The result (3.56) is clearly preliminary because it is based on the bootstrap events of analysis 1A only. It seems however that the use of the quantity \bar{R} leads to a significant improvement of the precision for the mass ratio m_c/m_s .

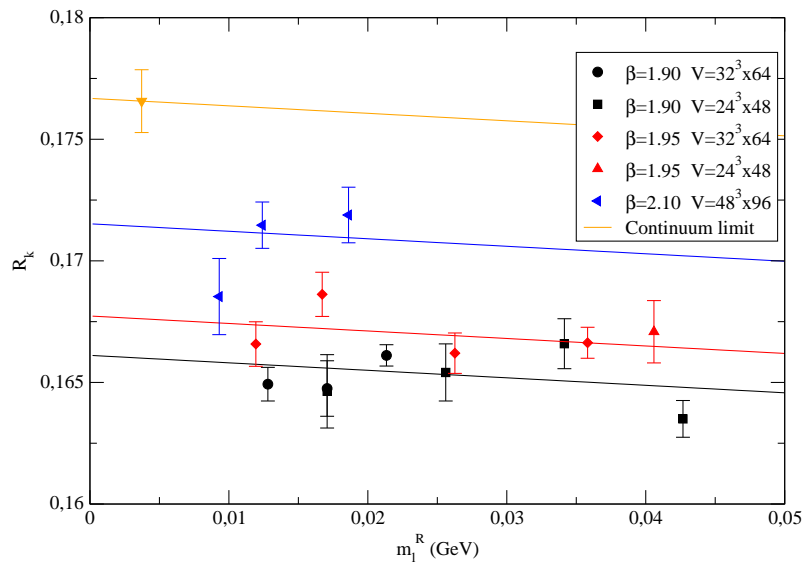


Figure 3.22: Chiral and continuum extrapolation of $\bar{R}(m_c, m_s, m_l, a^2)$, defined in Eq. (3.51), using a linear fit in m_l .

Chapter 4

Leptonic decay constants

4.1 f_{K^+} and the ratio f_{K^+}/f_{π^+}

In this section we present our determination of the leptonic pseudoscalar decay constant f_{K^+} and the ratio f_{K^+}/f_{π^+} . First we will give some details on the general strategy and on the different approaches used to control and estimate the various sources of systematic uncertainties, which are mainly related to the chiral extrapolation, the continuum limit and the FSE.

General strategy

In order to extract the kaon decay constants we first analysed the 2–point correlators for each lattice spacing and volume. As a preliminary step, we performed an interpolation of the lattice data to the physical strange quark mass. In particular, the numerical data for f_K have been interpolated using a quadratic spline to the physical strange quark mass determined as the value for which the experimental K meson mass is reproduced. Then for the data at fixed $m_s = m_s^{phys}$, after correcting for FSE, we studied the dependence of the kaon decay constant on both the light quark mass and the lattice spacing thus performing simultaneously the chiral extrapolation and the continuum limit.

In addition, combining our estimate for the kaon decay constant with the experimental value of f_π , which has been used to set the scale of the entire analysis, we got our determination of the ratio f_{K^+}/f_{π^+} . For this ratio we also tried a direct determination which provided compatible results.

Following a strategy similar to the one explained in details in chapter 3, in which we

computed the up, down, strange and charm quark masses, in the analysis of f_K we investigated different approaches to handle the discretization effects, the chiral extrapolation and the FSE.

Combining the results obtained from the different branches of the analysis we extracted our final determination and assessed the systematic uncertainties.

Discretization effects

To properly control discretization effects we performed both a standard analysis, denominated in the following as analysis 1, in which we used as intermediate scaling variable r_0/a (the final scale was always set using f_π), and second one, in which the quantities calculated at different lattice spacings are set to a common scale by dividing them with a reference meson mass M_{ss} in lattice units. As already explained, since aM_{ss} shows no significant dependence on the light sea quark mass, it was fitted as a constant in m_l for each β value. The ratios f_K/M_{ss} show a partial cancellation of the discretization effects with respect to f_K . On the other hand the scale setting procedure, and in particular the lattice spacing determination, requires, for this kind of analyses, to perform the continuum limit of M_{ss} , reintroducing in this second step the discretization effects removed from the analysis of f_K . For further details on the scale setting for analysis 2 refer to sec. 3.3.3. Thus in this second analysis, with respect to the first one, there is a different interplay between the chiral and continuum extrapolation.

Chiral extrapolation

For both the analyses in units of r_0 and in units of M_{ss} we considered different possibilities for the fitting formula used in the chiral extrapolation, namely, both the prediction of SU(2) ChPT and a polynomial expansion in m_l . We denominated this two cases as analysis *A* and *B*.

Input parameters from previous analysis: lattice spacings, light and strange quark masses

As discussed above the analysis is divided in four main branches denominated as $1A$, $1B$, $2A$ and $2B$.

The same four different approaches have been also considered in the pion analysis in order to determine the average up/down quark mass, the value of the Sommer parameter r_0 (or analogously the value of the reference mass M_{ss} in physical units) and the lattice spacings, and in the study of the kaon mass, to determine the physical strange quark mass. The details and the results of all these analyses are reported in tabs. 3.8 and 3.14. In order to account for existing correlations, and to introduce the same physical assumptions in the various analyses (like the form of the chiral extrapolation), all the input quantities for the kaon decay constants fit have been taken from the corresponding analyses of pion and kaon mass. So, for example, in the fit $1A$ for f_K will use the light quark mass and the lattice spacings from the $1A$ pion fit and the strange quark mass from the $1A$ kaon mass fit.

FSE corrections

In order to correct for FSE we considered two different formulae starting with the NLO prediction of SU(2) ChPT [40], which will be referred to as Gasser Leutwyler (GL) and the higher order correction resummed formula introduced in [41] by Colangelo, Dürr and Haefeli (CDH). The latter, being in principle the most accurate prediction has been used for our central analyses. The comparison with GL, and even even with the absence of FSE corrections, gives useful information and helped us to estimate the correspondent systematic uncertainty.

Renormalization constants

As we already did for the quark mass analysis, we implemented all the different approaches using the two set of quark masses renormalization constants Z_P reported in 3.4. This two sets have been calculated in the RI-MOM scheme by our collaboration using two methods, named $M1$ and $M2$, which differ for the treatment of discretization errors. Thus in principle they should yield the same results for the physical quantities,

after the continuum extrapolation has been taken. Even if the impact of Z_p on the final results of f_K is very limited, it has been nonetheless taken in to account to estimate the corresponding systematics.

4.1.1 Analyses of f_K in units of r_0

In this section we discuss the the analysis of f_K using r_0 as a scaling variable using different assumptions for the chiral extrapolation. As a first step, all the data from different lattice spacings, interpolated at m_s^{phys} have been calculated in a common scale using r_0/a , i.e. in units of the Sommer parameter. The quark masses have been converted directly to physical units using the values of the lattice spacing. The uncertainties on renormalization constants, and those of r_0/a , have been taken into account in the fit using the same procedure described for the quark mass analyses i.e. by including in the definition of the χ^2 , for each bootstrap, the term (3.11). For the lattice spacings errors instead, we used the bootstrap sampling.

Chiral fit of f_K using r_0

We simultaneously studied the dependence of f_K on the light quark mass and on the lattice spacing to perform the chiral and the continuum extrapolation.

In the analysis 1A we used the following fit formula based on SU(2) ChPT prediction

$$(f_K r_0) = P_1 \left(1 - \frac{3}{4} \xi_l \log \xi_l + P_2 \xi_l + P_3 a^2 \right) \cdot K_f^{FSE}, \quad (4.1)$$

where

$$\xi_l = \frac{2B_0 m_l^R}{16\pi^2 f_0^2}. \quad (4.2)$$

and B_0 and f_0 are low energy constants (LECs) entering the LO chiral Lagrangian.

The multiplicative factor K_f^{FSE} is the FSE correction and relates the kaon decay constant calculated at finite volume with its infinite volume counterpart. Some details will be given in a while, for the moment notice that we are using in our main analysis the resummed formula presented in [41] which will be referred to as CDH.

In fig. 4.1 is shown the dependence of $r_0 f_K$ on the renormalized quark mass for each lattice spacing and volume.

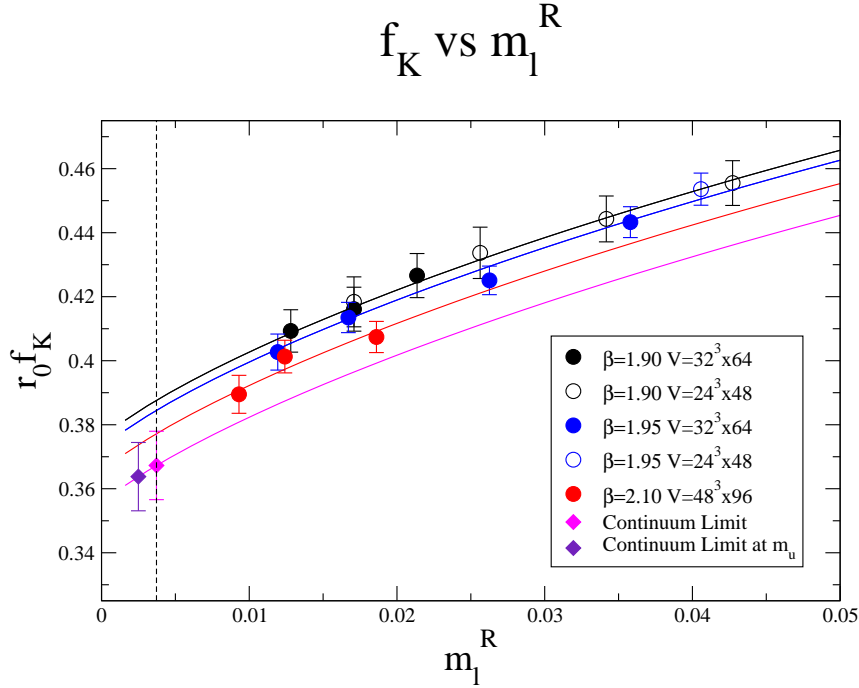


Figure 4.1: Chiral and continuum extrapolation of f_K in units of r_0 using $SU(2)$ ChPT prediction. All data are corrected for FSE.

Notice that after taking the continuum limit the kaon decay constant was extrapolate at two different value of the light quark mass. The first one, presented in the plot in magenta, is the result obtained for f_K in the isospin symmetric limit, and corresponds to the extrapolation at the average up/down quark mass. The second one, represented with a violet symbol, is the value extrapolated to the up quark mass and corresponds to the quantity f_{K^+} corrected for leading isospin breaking effect. In fact, it can be shown that the first order correction of the QCD isospin breaking effects, on a given quantity, only depends on the valence quarks [52]. The effects of the sea quarks enters proportionally to the square of the up/down mass difference, $(m_d - m_u)^2$, an effects which is well below the analysis precision. This means that, for the kaon decay constant, to correct for leading isospin breaking effects, it is sufficient to extrapolate f_K to the up quark mass.

For the pion decay constant, on the other hand, the symmetry under up-down quark exchange guarantees that the first isospin breaking correction coming from the valence quarks is proportional to $(m_d - m_u)^2$. So that, $f_K(m_u)$, $f_\pi(m_{ud})$ and $f_K(m_u)/f_\pi(m_{ud})$

are quantities corrected up to the first order in $m_d - m_u$ for QCD isospin breaking effects. Electromagnetic isospin breaking corrections are a by far more challenging issue and have not been included in the present study.

To perform the extrapolation to the up quark we used the value of m_{ud} calculated from the pion fit presented in 3 and an determination of the ratio $m_u/m_d = 0.5$ taken from [54]. Let me emphasize however that in the quark masses analysis presented in chapter 3 we have also calculated our own determination of the same ratio from the $N_f = 2 + 1 + 1$ lattice data finding completely compatible results. Our determination reads $m_u/m_d = 0.49(5)$, for details on the calculation see section 3.4.3.

Polynomial fit of f_K using r_0

As far as the analysis 1B is concerned, instead of relying on the NLO SU(2) ChPT prediction we performed a polynomial expansion in the renormalized light quark mass. The dependence of the pseudoscalar leptonic decay constant f_K on m_l , and the correspondent chiral extrapolation, have been studied with the following fit formula:

$$(f_K r_0) = P_1 (1 + P_2 m_l + P_3 a^2 + P_4 m_l^2) \cdot K_f^{FSE} \quad (4.3)$$

and the results are shown in fig. 4.2. As for the analysis 1A, both the extrapolation to m_{ud} (f_K), and m_u (f_{K^+}) are shown in the plot.

Both fitting assumptions 1A and 1B provided a good description of the lattice data. We take the differences as a measure of the systematic uncertainties associated to the chiral extrapolation of our analysis.

Having obtained the results for f_K and f_{K^+} one can divide them for the experimental value of the pseudoscalar pion decay constant to obtain the quantities f_K/f_π and f_{K^+}/f_{π^+} which correspond respectively to the SU(2)-symmetric ratio, and the ratio corrected for QCD isospin breaking effect at leading order.

FSE in the leptonic decay constant f_K

Before moving to the second part of the analysis in which we used aM_{ss} as a scaling variable, more details will be given on the FSE corrections.

As already done for the pion case in section 3.3.1, one can look at the two points of

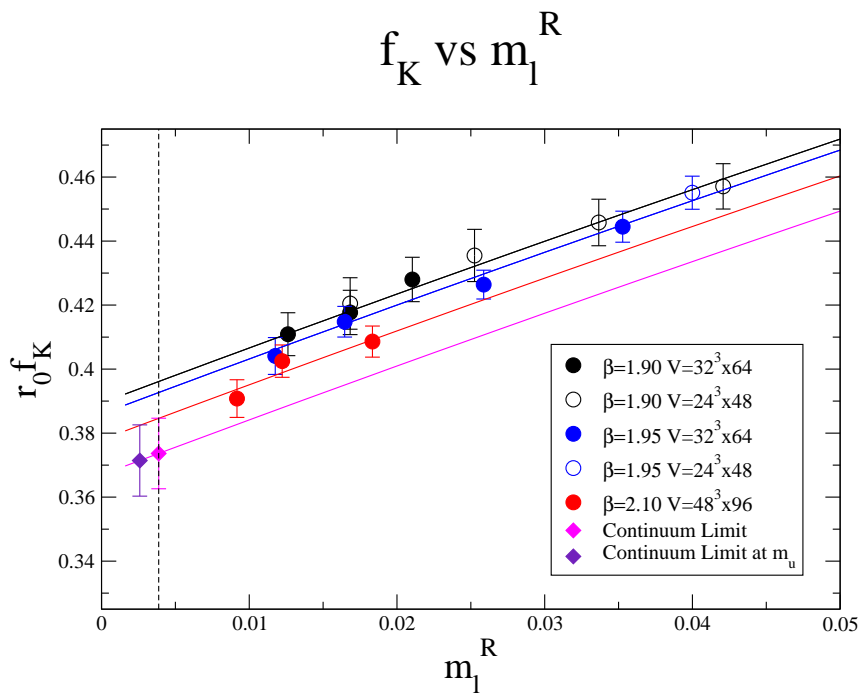


Figure 4.2: Chiral and continuum extrapolation of f_K in units of r_0 using a polynomial formula in m_l . All data are corrected for FSE.

our ensembles sharing the same light quark mass at different simulated volume, i.e. the gauge ensembles $A40.32$ and $A40.24$, to evaluate the magnitude of the FSE and the efficiency of the different correction formulae. By considering the ratio of the analogous of eqs. 3.17 for the kaon decay constant simulated at $L = 32$ and $L = 24$,

$$(f_K)_{[32]} = (f_K)_{[\infty]} K_{f,[32]}^{FSE} \quad (4.4)$$

$$(f_K)_{[24]} = (f_K)_{[\infty]} K_{f,[24]}^{FSE}, \quad (4.5)$$

it is clear that, the more the ratio of the multiplicative correction factors ($K_{f,[32]}^{FSE}/K_{f,[24]}^{FSE}$) is closer to the ratio of the uncorrected lattice data, the better the correction formulae are working. Indeed for an ideal correction an exact equality holds. These values, calculated for both GL and CDH, are reported in table 4.1 and show that the CDH formula is properly estimating the FSE.

	GL	CDH	Lattice data f_{32}/f_{24}
$K_{f,[32]}^{FSE}/K_{f,[24]}^{FSE}$	1.007	1.028	1.020(13)

Table 4.1: Values of the ratio of the FSE correction factor K_f^{FSE} for the gauge ensembles $A40.32$ and $A40.24$ obtained within the approaches GL and CDH (see text).

In table 4.2 are reported the values of $(K_{f,[24]}^{FSE} - 1)$ for the gauge ensemble $A40.24$ which is the one that gets the largest correction in the whole set. For this reason, the values reported in the table, representing the FSE correction in percentage, indicate an upper bound of the magnitude of this effect on the single data point.

	GL	CDH
$K_{f,[24]}^{FSE} - 1$	-0.009	-0.032

Table 4.2: Values of $K_f^{FSE} - 1$ for the gauge ensembles $A40.24$ obtained within the various FSE approaches GL and CDH (see text).

Looking at these tables one see that, even if the FSE are indeed non negligible for the gauge ensemble simulated at small values of $M_\pi L$, the use of the resummed CDH formula keeps them well under control. For this reason, the CDH resummed formula has been used in our main analysis while GL prediction will be used as a way to estimate the associated systematic uncertainty.

It will be shown in section 4.1.3, however, that being the magnitude of the typical correction significantly smaller than the upper limits presented in table 4.2, the impact of FSE on our results is really modest.

4.1.2 Analyses of f_K in units of M_{ss}

In this section we present the analysis 2 which aimed to keep the extrapolation to the continuum limit under better control by reducing the discretization effects in the kaon decay constant building the ratios af_K/aM_{ss} , in line with the strategy presented in chapter 3 for the quark masses.

While the decay constants have been expressed in units of the reference mass M_{ss} , for the quark masses we chose to work in physical units, converting them with our determination of the lattice spacings (see eq. (3.28)). The reason for this is to avoid the introduction of the discretization effects contained in aM_{ss} in the quark masses, which are parameters of the lattice action.

We studied the dependence of f_K/M_{ss} at fixed $m_s = m_s^{phys}$ on the light quark mass for each lattice spacing and volume in order to perform the chiral extrapolation and the continuum limit. This was done either by assuming the fit formula to be based on the prediction of NLO SU(2) ChPT (referred to as analysis 2A)

$$\frac{f_K}{M_{ss}} = P_1 \left(1 - \frac{3}{4} \xi_l \log \xi_l + P_2 \xi_l + P_3 a^2 \right) \cdot [K_f^{FSE}], \quad (4.6)$$

or expanding up to quadratic terms the expression for the kaon decay constant around a non vanishing value of the light quark mass down to the physical point (referred to as analysis 2B). This resulted in a polynomial formula of the form

$$\frac{f_K}{M_{ss}} = P_1 (1 + P_2 m_l + P_3 a^2 + P_4 m_l^2) \cdot [K_f^{FSE}]. \quad (4.7)$$

For both analyses the FSE correction have been calculated using CHD resummed formula.

After the chiral and the continuum extrapolations the value of f_K and f_{K^+} have been converted in physical units using the value of M_{ss} obtained as explained in sec. 3.3.3. The total uncertainties in the determination of M_{ss} have been accounted for using bootstrap sampling.

The results for f_K and f_{K^+} have been finally combined with the experimental value of the pion decay constant to get the ratios f_K/f_π and f_{K^+}/f_{π^+} .

In fig. 4.3 the dependence of f_K in units of M_{ss} on the light quark mass is shown, for each β and volume, together with the extrapolation both at m_{ud} and at m_u in the case of analysis 2A, i.e. by using SU(2) ChPT prediction.

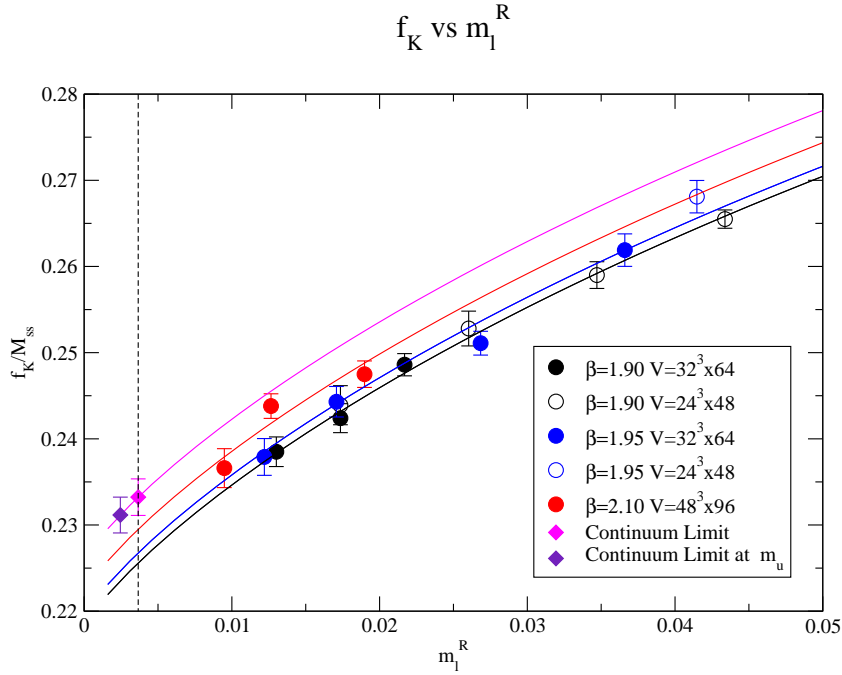


Figure 4.3: *Chiral and continuum extrapolation of f_K in units of M_{ss} using SU(2) ChPT prediction. All data are corrected for FSE using CDH formula.*

A similarly good agreement between the fit formula and the lattice data has been found using eq. (4.7), as can be seen in fig. 4.4. Being the two approaches equally legitimate and capable of providing a satisfying description of our data, both results from analysis 2A and 2B have been used to determine our final results for the kaon decay constant.

Confronting figs. 4.1 and 4.3 one sees that the ratio f_K/M_{ss} exhibits a milder a^2 dependence with respect to the quantity $r_0 f_K$. This reduction, if quantified by taking the difference of the continuum and the finer lattice spacing over the continuum, goes

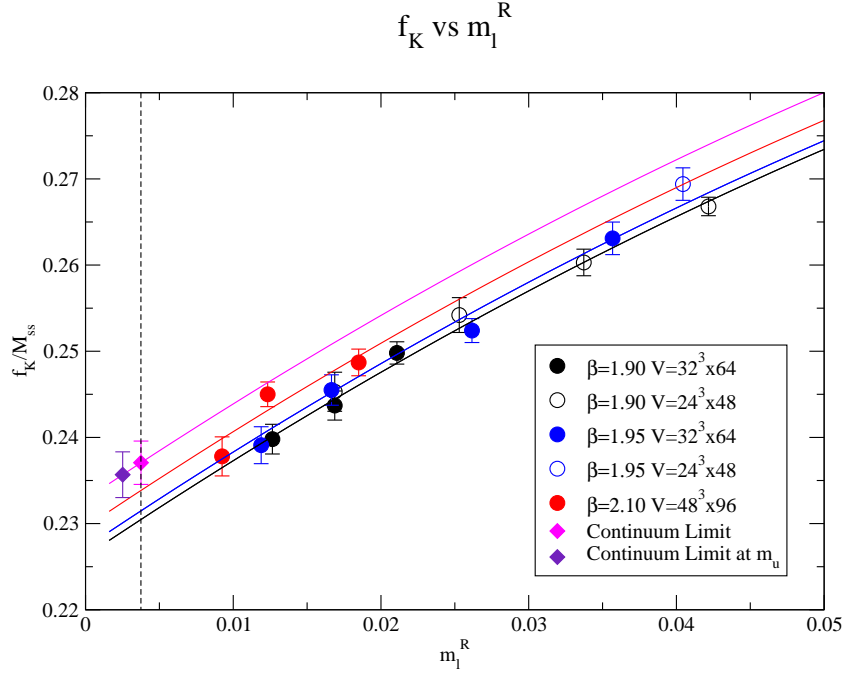


Figure 4.4: Chiral and continuum extrapolation of f_K in units of M_{ss} using a polynomial fit formula. All data are corrected for FSE using CDH formula.

from 3% in the analysis in units of r_0 to -1.5% in the analysis in units of M_{ss} . Both results obtained from the analysis in units of r_0 and in units of M_{ss} will be used to achieve our final determinations and their systematic uncertainties.

4.1.3 Results for f_{K^+} and f_{K^+}/f_{π^+}

In this section we present the results for analyses 1A, 1B, 2A and 2B for the leptonic pseudoscalar decay constant f_K and the ratio f_K/f_π . They include both the quantities calculated in the isospin symmetric limit and the one extrapolated to the up quark mass and thus corrected for isospin breaking effects.

A collection of results from the various analyses

The results reported in table 4.1.3 have been obtained by using the renormalization constants calculated in the RI-MOM scheme with the method $M1$. All these analyses have been also performed using the second set of Z_p , denoted as $M2$, obtaining very similar results. Nonetheless, the results of the analyses performed with both sets of renormalization constants have been combined in our final determination taking this way into account the associated systematic effect.

Quantity	r_0 Analysis		M_{ss} Analysis	
	Chiral Fit	Polynomial Fit	Chiral Fit	Polynomial Fit
f_K (MeV)	153.8(2.5)	154.2(1.9)	156.6(1.3)	155.1(1.6)
f_{K^+} (MeV)	152.3(2.6)	153.3(2.0)	155.2(1.4)	154.2(1.7)
f_K/f_π	1.179(20)	1.182(15)	1.201(09)	1.189(12)
f_{K^+}/f_{π^+}	1.168(20)	1.175(16)	1.190(11)	1.182(13)

Table 4.3: Summary of the results of the four analysis for the decay constant f_K and for the ratio f_K/f_π presented both in the $SU(2)$ -symmetric case, and with QCD isospin breaking effect corrections at leading order. We used the CDH approach to calculate the FSE and the set $M1$ for the renormalization constants Z_P .

Final estimates and systematics

Combining all the results with the same procedure explained in details in sections 3.3.3 and 3.4.3, we obtained our final determination for the quantities of interest and their systematic uncertainties. In particular for f_{K^+} we obtained:

$$\begin{aligned}
 f_{K^+} &= 154.4(1.8)_{stat+fit}(0.5)_{Chiral}(1.0)_{Disc.}(0.4)_{FSE}(0.2)_{Z_P} \text{ MeV} \\
 &= 154.4(1.8)_{stat+fit}(1.2)_{syst} \text{ MeV} \\
 &= 154.4(2.1) \text{ MeV}
 \end{aligned} \tag{4.8}$$

while for ratio of f_{K^+}/f_{π^+} :

Quantity	No Correction	GL	CDH
f_{K^+} (MeV)	151.8(2.6)	152.2(2.6)	152.3(2.6)
f_{K^+}/f_{π^+}	1.164(20)	1.167(20)	1.168(20)

Table 4.4: Results for the kaon decay constant and for the ratio of the kaon over the pion decay constants obtained using different approaches to the FSE correction.

$$\begin{aligned}
f_{K^+}/f_{\pi^+} &= 1.183(14)_{stat+fit}(4)_{Chiral}(8)_{Disc.}(4)_{FSE}(1)_{Z_P} \\
&= 1.183(14)_{stat+fit}(9)_{syst} \\
&= 1.183(17)
\end{aligned} \tag{4.9}$$

Systematic uncertainties due to the chiral extrapolation, besides the fitting errors, have been evaluated using the differences between the results $-A$ and $-B$ from both the analysis in units of r_0 and M_{ss} . This corresponds in the error budget to a 0.3% of the result.

The discretization systematics instead, have been estimated using the differences between the results 1- and 2- and they represent a 0.7% error.

The difference between the results for f_{K^+} and f_{K^+}/f_{π^+} obtained without applying any correction for FSE and the one obtained by correcting with the CDH formula has been used to extract the FSE systematic uncertainty which is 0.3%.

In table 4.4 we show the impact of the different approaches used to treat the FSE (including the choice of applying no correction) on the final results of this part of the analysis. This have been verified for the analysis in units of r_0 and using the chiral fit (analysis 1A) but the effect on the results of all the other analysis are similarly small. As can be seen for this table even if the FSE can be large on some gauge ensemble and clearly needs to be treated carefully the total impact on the physical quantities is less severe.

The different choice of the method to calculate the renormalization constants has for these results a very small impact giving an additional uncertainty of 0.1%.

The largest contribution is the 1.2% of uncertainty coming from the statistical error plus the uncertainties due to the fitting procedure which accounts also for the total error on the determination of m_s (described in sec. 3.4). This error represent a large contribution with respect to the others, but let us emphasize that this is not dominated by the

statistical errors. Comparing the typical error of the data points with the one of the fit results, for example in fig. 4.3, it is clear that the latter have been amplified by the chiral and continuum extrapolation, meaning that it is including a systematic component as well.

Comments on the isospin breaking effects on our results

We now present, the results for f_K and f_K/f_π obtained in the isospin symmetric limit:

$$\begin{aligned}
 f_K &= 155.6(1.6)_{stat+fit}(0.5)_{Chiral}(1.1)_{Disc.}(0.4)_{FSE}(0.2)_{Z_P} \text{ MeV} \\
 &= 155.6(1.6)_{stat+fit}(1.3)_{syst} \text{ MeV} \\
 &= 155.6(2.1) \text{ MeV}
 \end{aligned} \tag{4.10}$$

$$\begin{aligned}
 f_K/f_\pi &= 1.193(13)_{stat+fit}(4)_{Chiral}(8)_{Disc.}(4)_{FSE}(1)_{Z_P} \\
 &= 1.193(13)_{stat+fit}(10)_{syst} \\
 &= 1.193(16)
 \end{aligned} \tag{4.11}$$

From the comparison of the results (4.8-4.9) with those in (4.10-4.11) it is interesting to evaluate the impact of the isospin breaking effects. These effects on f_K (or f_K/f_π) have been also estimated in NLO ChPT (see [23]) to be of the order of 0.21(6)%. A direct lattice calculation presented in [52, 54] obtained the slightly higher value of 0.40(3)%. Although it is beyond the scope of this work to give a precise determination of this effect and its systematic uncertainties, by comparing the result for f_K extrapolated at m_{ud} with the one extrapolated at m_u , we can roughly estimate an effect varying from 0.6% to 0.9%, depending on the form of the chiral extrapolation (a chiral or a polynomial fit). Thus we observe isospin breaking effects which are even larger than the above mentioned results. Let me remark, however, that this estimate clearly suffers from large systematic uncertainties, mostly related to chiral extrapolation. We are trying to infer an effect on the slope in the m_l dependence of f_K at the physical point without data at the physical point.

Comparison with the FLAG averages

Before closing this section it is interesting to present a comparison of the results obtained in our analysis with the corresponding averages quoted by FLAG [48] for $N_f = 2$, $N_f = 2 + 1$ and $N_f = 2 + 1 + 1$:

Quantity	Our Result	FLAG $_{N_f=2}$	FLAG $_{N_f=2+1}$	FLAG $_{N_f=2+1+1}$
f_{K^+} (MeV)	154.4(2.1)	-	-	-
f_K (MeV)	155.6(2.1)	158.1(2.5)	156.3(0.8)	-
f_{K^+}/f_{π^+}	1.183(17)	1.205(6)(17)	1.192(5)	1.195(3)(4)

Table 4.5: Comparison of the results we found in this analysis with corresponding averages quoted by FLAG [48] for $N_f = 2$, $N_f = 2 + 1$ and $N_f = 2 + 1 + 1$

4.1.4 Analyses of the ratio f_K/f_π

In this work we also tried a determination of f_{K^+}/f_{π^+} by analysing directly the ratio. Even if in general studying dimensionless quantities can be useful in order to minimize the uncertainties related to the scale setting, this is not the case here. The reason is that in our analysis the scale was set by using f_π , so that our study of the kaon decay constant, explained in the previous sections, is in fact a study of f_K in units of f_π . Nonetheless the systematic uncertainties associated with an analysis of f_{sl}/f_{ll} will be different, in principle, from the one of f_{sl} . In particular, the fact that the two quantities are known to have a different chiral extrapolation. This motivates the study presented in this section.

Since f_{sl}/f_{ll} is a dimensionless quantity, and no scaling variable is needed, we only considered two approaches: a chiral fit (analysis *A*) and a polynomial one (analysis *B*). In analysis *A* we performed the continuum limit and the chiral extrapolation to the physical point by using the following fit formula:

$$\frac{f_K}{f_\pi} = P_1 \left(1 + \frac{5}{4} \xi_l \log \xi_l + P_2 \xi_l + P_3 a^2 \right) \cdot \frac{[K_{f_K}^{FSE}]}{[K_{f_\pi}^{FSE}]} \quad (4.12)$$

Eq. (4.12) is inspired by SU(2) ChPT predictions for the pion and for the kaon decay constants (see (3.13) and (4.1)) in which we neglected the contribution of the π^0/π^+ mass spitting from the infinite volume expression of f_π . A similar but unknown contribution

is expected in the kaon decay constant as well, and, introducing it only for f_π , would not take into account possible compensation.

To correct f_K/f_π for FSE we used the ratio of the finite size effect corrections for the kaon and the pion decay constants. In particular we used the CDH resummed formula for f_K , and the CWW formula for f_π (see for details sec. 3.3.1 and sec. 4.1.1). The factors $K_{f_K}^{FSE}$ and $K_{f_\pi}^{FSE}$ have been calculated for each bootstrap event in the corresponding chiral analyses (1A) taking into account their errors.

After studying the dependence of f_K/f_π on the lattice spacing and on the light quark mass, the ratio was extrapolated to the average up/down quark mass calculated in the pion fit 3.3.3. For this analysis we took the value of m_{ud} extracted from analysis 1A.

In the second analysis, B, we used, for the chiral and continuum extrapolation, the following polynomial fit formula:

$$\frac{f_K}{f_\pi} = P_1 (1 + P_2 m_l + P_3 m_l^2 + P_4 a^2) \cdot \frac{[K_{f_K}^{FSE}]}{[K_{f_\pi}^{FSE}]} \quad (4.13)$$

For this second case the value of the average up/down quark mass used for the extrapolation has been taken from analysis 2A.

Both eqs. (4.12) and (4.13) describe well the data as it can be seen in fig. 4.5.

In the figure, the dashed line represents the SU(2) ChPT prediction while the continuum line represents the polynomial expression. Combining the two results obtained from the chiral and the polynomial fit, extrapolated to the average up/down quark mass, we get our estimate for the isospin symmetric result f_K/f_π which is:

$$f_K/f_\pi = 1.192(16) \quad (4.14)$$

The determination of f_K/f_π obtained analysing the ratio is thus completely compatible, and shows the same level of precision, with respect to the one obtained analysing f_K (see eq. (4.11)). Thus, this result does not improve but at least strengthen, the solidity of the previous determination.

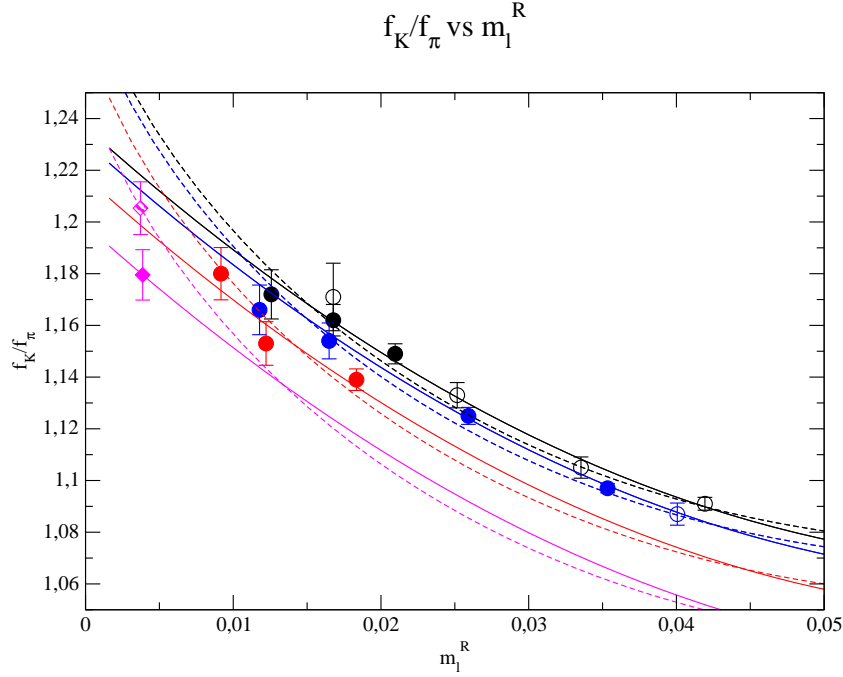


Figure 4.5: Chiral and continuum extrapolation of the ratio f_K/f_π performed using both $SU(2)$ ChPT prediction and polynomial expansion in the light quark mass. All data are corrected for FSE. The numerator has been corrected using CDH formula for the kaon decay constant while the denominator have been corrected with CWW formula for the pion decay constant.

4.2 f_{D_s} , f_D and the ratio f_{D_s}/f_D

In this section we present our determination of the pseudoscalar decay constants of the D and D_s mesons. First we discuss the general strategy and the different approaches used to control and estimate the various sources of systematic uncertainties in f_{D_s} and f_{D_s}/f_D .

General Strategy

The analysis has been performed studying separately f_{D_s} and the ratio f_{D_s}/f_D whose results are then combined to obtain also f_D . The reason for this strategy is that f_{D_s} has a m_l dependence which is milder, occurring only through sea quarks, than the one of f_D ,

while the ratio f_{D_s}/f_D can present a cancellation of some systematic uncertainties. In order to determine f_{D_s} and f_{D_s}/f_D we studied the quantities Φ_{D_s} and Φ_{D_s}/Φ_D defined as follows:

$$\frac{\Phi_{D_s}}{\Phi_D} = \frac{f_{D_s}\sqrt{M_{D_s}}}{f_D\sqrt{M_D}} \quad (4.15)$$

These Φ are well defined in Heavy Meson ChPT since they are finite in the heavy quark static limit.

The analysis closely follows the strategy presented for the K decay constant. First the simulated data for Φ_{D_s} and Φ_{D_s}/Φ_D are slightly interpolated to physical values of the strange and charm quark masses, which have been presented respectively in secs. 3.3 and 3.4, using a quadratic spline. The dependence of Φ_{D_s} and Φ_{D_s}/Φ_D (at fixed m_s and m_c) on the light quark mass and on the lattice spacings is then studied in order to perform the continuum limit and to extrapolate the results to the physical up/down quark mass. We also considered another analysis to determine the ratio f_{D_s}/f_D based on the study of the double ratio $(f_{D_s}/f_D)/(f_K/f_\pi)$. This idea, suggested in [55], provides a more precise determination of the ratio of the D and D_s decay constants thanks to the mild dependence of the double ratio on the light quark mass which greatly reduces the systematic associated with the chiral extrapolation. For this reason we will quote as our final result for f_{D_s}/f_D the determination obtained fitting the double ratio.

Discretization effects and chiral extrapolation

In order to control and estimate the systematic uncertainties due to the chiral and continuum extrapolation, two approaches have been adopted.

For the Φ_{D_s} fit we performed an analysis using r_0 as the scaling variable (analysis 1), and another one in which, as we already did for the D_s meson mass, we tried to reduce discretization effects building the ratios $\Phi_{D_s}/(M_{cs})^{(3/2)}$, making use of the reference PS meson mass introduced in section 3.7.2 (analysis 2). For each choice of the scaling variable we considered two different formulae to fit the chiral extrapolation in the light sea quark mass, i.e. a linear (analysis *A*) or a quadratic (analysis *B*) extrapolation.

For f_{D_s}/f_D , which is a dimensionless quantity, the analysis is only divided in two branches corresponding to different approaches for the chiral extrapolation. One makes use of the Heavy Meson ChPT predictions, while the other, of a polynomial formula in m_l .

Input parameters from previous analysis: lattice spacings, and quark masses

Concerning the quantities needed in this analysis that have been previously calculated in the pion fit, such as the physical values of the light quark mass, the lattice spacings and the value of the Sommer parameter, the strategy is the same explained for the charm quark mass analysis (see sec. 3.7). In each bootstrap event of the fit all the input quantities are taken from the same analysis choosing randomly among the four branches 1A, 1B, 2A and 2B, preserving in this way the correlations. Since the errors obtained from the various strategies on all the quantities determined from the pion fit are very similar, at each analysis the same extraction probability is assigned. In this way, the statistical plus fitting error obtained combining the fit results from the various bootstrap events will actually include also other sources of uncertainties, the most important of which is the uncertainty on the scale. The latter will of course only affect f_{D_s} , while the statistical plus fitting error on f_{D_s}/f_D will only include a small uncertainty on the light quark mass determination.

Our final results will be a combination of all the different branches of the analysis providing at the same time an estimate of the associated systematic uncertainties.

4.2.1 Analyses of Φ_{D_s} in units of r_0

After a small interpolation in the charm and strange quark mass to the physical values, the simulated values of Φ_{D_s} are brought to a common scale using the appropriate power of r_0/a . For the quark masses we chose to work in physical units converting them with the value of the lattice spacings obtained from the pion fit.

The Z_p and the r_0/a 's errors are accounted in the fit through a contribution in the χ^2 as described for the pion fit while the error on the lattice spacings, that are computed on the same gauge configurations used in our analysis, are treated with bootstrap sampling. In order to study the Φ_{D_s} dependence on the average up/down sea quark mass and on the lattice spacings at fixed (physical) strange and charm quark mass, we considered the following formula which turn out to describe well the data:

$$\Phi_{D_s} r_0^{3/2} = P_1(1 + P_2 m_l + P_3 m_l^2 + P_4 a^2). \quad (4.16)$$

We have also performed the chiral extrapolation with a linear dependence on m_l that is dropping the parameter P_3 .

In this analysis we did not correct for FSE. As it will be shown in figs. 4.6 and 4.7, the two points corresponding to the gauge ensembles $A40.32$ and $A40.24$ sharing the same pion mass at different volume are almost exactly overlapped.

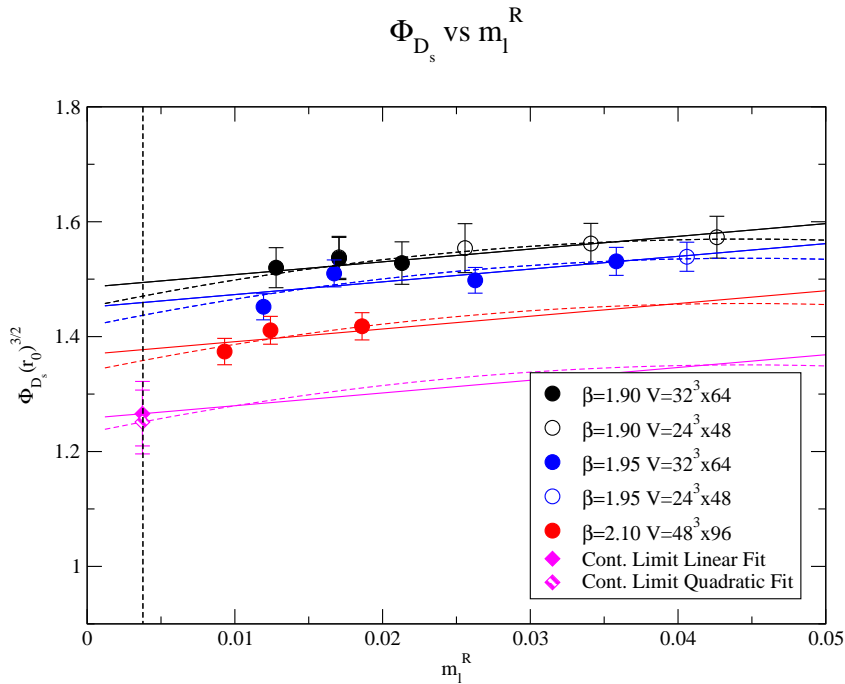


Figure 4.6: *Chiral and continuum extrapolation of Φ_{D_s} in units of r_0 using both a linear and a quadratic expansion in the light quark mass.*

Fig. 4.6 shows the dependence of Φ_{D_s} on the light quark mass for all the different β 's and volumes respectively for a linear and a quadratic fit. Both the linear fit and the quadratic one, depicted respectively as a continuum and a dashed line, provide a good description of the lattice data, and have been used to determine our finale result. Notice that, as expected, the dependence of the Φ_{D_s} meson mass on m_l is mild since the light quark is in the sea only. Finally, f_{D_s} can be easily obtained from the chiral and continuum extrapolated value of Φ_{D_s} , using the experimental value of M_{D_s} .

4.2.2 Analyses of Φ_{D_s} in units of M_{cs}

As far as analysis 2 is concerned, we divided the pseudoscalar decay constants calculated at different lattice spacings and volume by aM_{cs} , the reference PS meson mass already used for the determination of the charm quark mass in sec. 3.7 and converted the quark masses in physical units by means of the lattice spacing calculated in the pion's fit.

Once the continuum limit and the extrapolation to the physical light quark mass have been performed, Φ_{D_s} can be converted in physical units using the continuum extrapolated value of M_{cs} . At this point the result for f_{D_s} can be obtained by using the experimental value of the D_s meson mass. The fits are performed using the same formulae of analysis 1 which in this units reads:

$$\Phi_{D_s}/M_{cs}^{3/2} = P_1(1 + P_2m_l + P_3a^2 + P_4m_l^2) \quad (4.17)$$

In fig. 4.7 is shown the dependence of $\Phi_{D_s}/M_{cs}^{3/2}$ on m_l for all the different lattice spacings and volumes, obtained fitting the data with a linear and a quadratic formula.

Both assumptions provide a good description of the lattice data, and have been combined to get the finale result.

Comparing fig. 4.7 with the same plot where Φ_{D_s} is in units of r_0 , (fig. 4.6), it can be seen that the cancellation of the discretization effects produced by the ratio has brought the gap between the continuum and the finer lattice spacing from 8% down to 3% of the final result.

4.2.3 Analyses of Φ_{D_s}/Φ_D and of the double ratio $(f_{D_s}/f_D)/(f_K/f_\pi)$

In this section we present two different approaches we used for the determination of the ratio f_{D_s}/f_D .

Chiral and Polynomial fit of Φ_{D_s}/Φ_D

In the first one we studied the dependence of Φ_{D_s}/Φ_D on the light quark mass and on the lattice spacing for physical values of the strange and charm quark masses as determined in our analysis and presented in secs. 3.4.3 and 3.7.3.

Heavy Meson ChPT has been used to perform the chiral extrapolation of this quantity to the average up/down quark mass combined, as usual, with the continuum limit according to the formula:

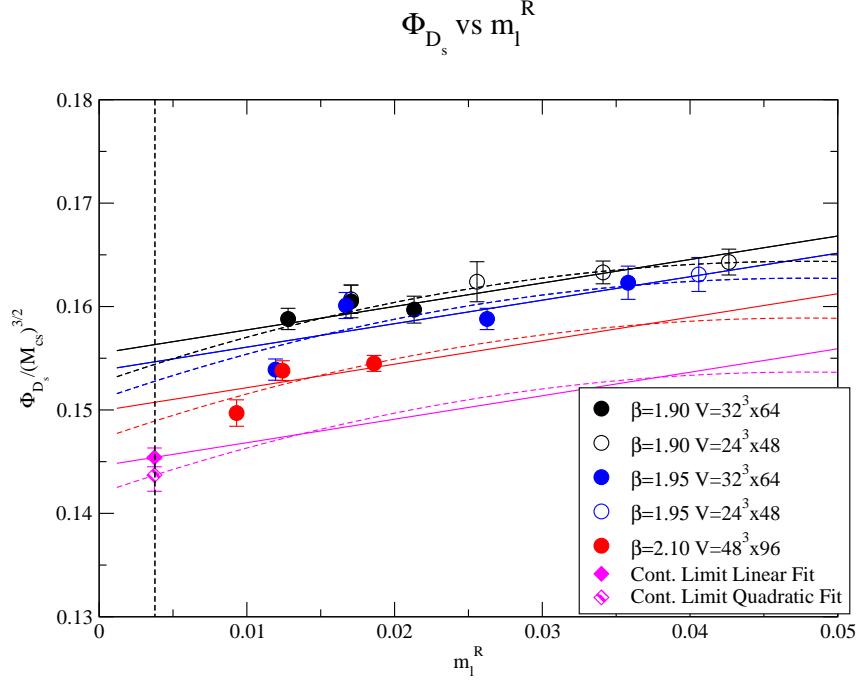


Figure 4.7: Chiral and continuum extrapolation of Φ_{D_s} in units of M_{ss} using both a linear and a quadratic expansion in the light quark mass.

$$\frac{\Phi_{D_s}}{\Phi_D} = P_1 \left(1 + P_2 m_l + P_3 a^2 + \frac{3}{4} (1 + 3\hat{g}^2) \xi_l \log \xi_l \right), \quad (4.18)$$

where \hat{g} is a parameter of Heavy Meson ChPT measuring the axial coupling of a pion to doublets of heavy-light mesons (D, D^*). In our analysis we used the determination of $\hat{g} = 0.61(7)$ reported in [56].

We also tried a second fit dropping the chiral log thus fitting Φ_{D_s}/Φ_D with a simple linear dependence in m_l . The comparison between the two fits also accounts for, other possible input values for \hat{g} .

Both fit assumptions are shown in fig. 4.8, the chiral fit being the dashed line while the linear fit is represented by the continuum one.

We notice that, even if both fits are in good agreement with the data, the values obtained extrapolating at the average up/down quark mass show a difference which is significantly larger than the statistical errors. This of course corresponds to a large systematic error associated with the chiral extrapolation.

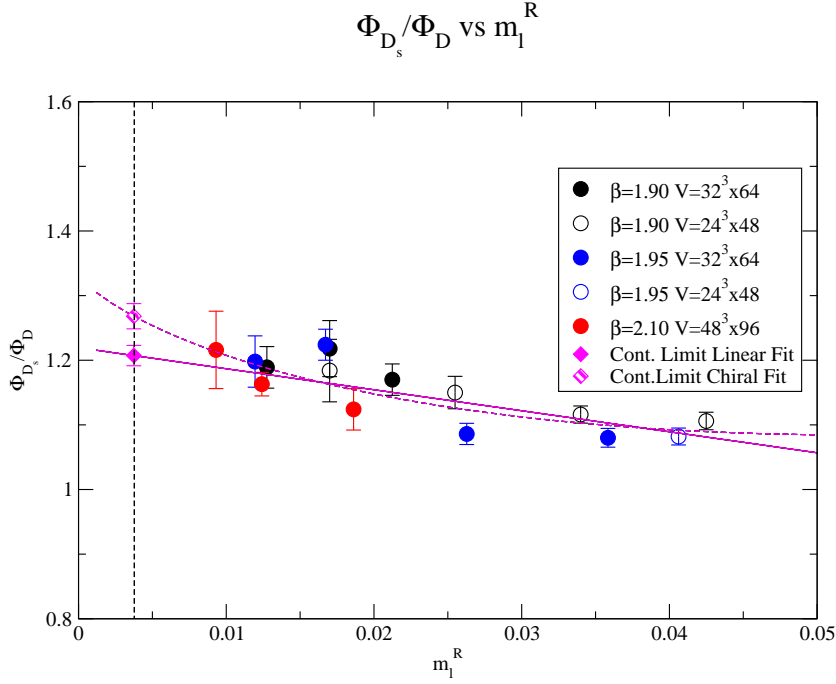


Figure 4.8: *Chiral and continuum extrapolation of Φ_{D_s}/Φ_D using both the prediction from Heavy Meson ChPT and a polynomial expansion in the light quark mass.*

Chiral and Polynomial fit of the double ratio $(f_{D_s}/f_D)/(f_K/f_\pi)$

As suggested in [55], we found that analysing the double ratio $(f_{D_s}/f_D)/(f_K/f_\pi)$ increases the precision on the determination of f_{D_s}/f_D because of the much milder dependence of this quantity on m_l . To fit the double ratio we combined the ChPT predictions for the four decay constant obtaining the following formula:

$$\frac{f_{D_s}/f_D}{f_K/f_\pi} = P_1 \left(1 + P_2 m_l + \left(\frac{9}{4} \hat{g}^2 - \frac{1}{2} \right) \xi_l \log \xi_l \right) \frac{K_{f_\pi}^{FSE}}{K_{f_K}^{FSE}}. \quad (4.19)$$

As we already did in the study of the ratio (f_K/f_π) , we decided to drop the contribution proportional to the π^0/π^+ mass splitting in the pion decay constant. Since a similar but unknown contribution is expected to occur also for the kaon decay constant and including it in the pion only, would not account for possible compensations.

Notice also the presence of the FSE correction for f_π and f_K . We corrected them using CWW and CDH as explained in details in (see secs. 3.3.1 and 4.1.1).

As usual a second fit was performed omitting the chiral log contribution, i.e. using the following linear expression:

$$\frac{f_{D_s}/f_D}{f_K/f_\pi} = P_1 (1 + P_2 m_l) \frac{K_{f_\pi}^{FSE}}{K_{f_K}^{FSE}}. \quad (4.20)$$

Both approaches to the chiral extrapolation are shown in fig. 4.9.

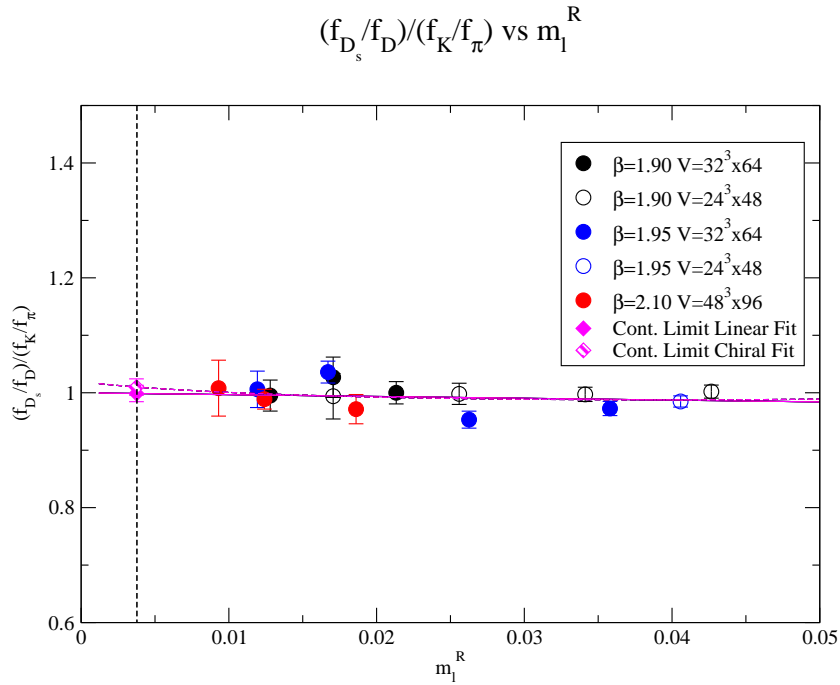


Figure 4.9: *Chiral and continuum extrapolation of the double ratio $(f_{D_s}/f_D)/(f_K/f_\pi)$ using both the prediction from ChPT and a polynomial expansion in the light quark mass.*

We observe that the results for the double ratio obtained from the two different choices of chiral extrapolation are compatible within their statistical uncertainties. As a consequence, the systematic uncertainty on f_{D_s}/f_D , computed from the double ratio and using our determination of f_K/f_π , turns out to be significantly reduced with this second approach. For this reason this determination of f_{D_s}/f_D supersedes the one obtained

from the single ratio Φ_{D_s}/Φ_D and our final result will be the one derived from it. We also observe that our data have been extrapolated to m_{ud} . As a consequence, our results for f_{D_s}/f_D are quoted in the QCD isospin symmetric limit. The impact of the isospin breaking effect on the ratio f_{D_s}/f_D can be estimated looking at the isospin breaking effects of Φ_{D_s}/Φ_D and M_D , evaluated taking the difference between the extrapolation at m_{ud} and the extrapolation at m_d . Since both effects are of the order of 1% but with opposite sign the total impact on f_{D_s}/f_D is expected to be below the per cent level, hence small, in this case, compared to other sources of uncertainties.

4.2.4 Results for f_{D_s} , f_D and f_{D_s}/f_D

In this section we present the results for f_{D_s} , f_D and f_{D_s}/f_D as obtained from the analysis described above. The systematic uncertainties are also collected and discussed.

f_{D_s} : final estimate and systematics

The results collected in the following tables have been obtained using the first set of RI-MOM renormalization constants calculated with the $M1$ method (see table 3.4). All these analyses have been also performed using the Z_P values obtained from the method $M2$ and the results, though not presented here for brevity, have been included in the final determination.

For f_{D_s} we collected in table 4.6 the results from the four branches of the analysis which differ for the different choice of the scaling variable and for the different ansatz in the chiral extrapolation.

	r_0 Analysis		M_{cs} Analysis	
Quantity	Linear Fit	Quadratic Fit	Linear Fit	Quadratic Fit
f_{D_s} (MeV)	241.7(7.3)	239.0(7.1)	246.5(7.8)	243.6(8.0)

Table 4.6: Results for the D_s meson decay constant from the different branches of the analysis. The errors include the statistical error, the error associated to the fitting procedure, the uncertainties related the setting of the scale combined also with the uncertainties in the determination of the strange and charm quark masses.

Combining these results following the strategy explained in secs. 3.3.3 and 3.4.3, we

obtained our final result for f_{D_s}/f_D

$$\begin{aligned}
 f_{D_s} &= 242.1(7.1)_{stat+fit+scale}(1.4)_{Chiral}(2.9)_{Disc.}(2.4)_{m_c}(1.4)_{m_s} \text{ MeV} \\
 &= 242.1(7.1)_{stat+fit+scale}(4.3)_{syst} \text{ MeV} \\
 &= 242.1(8.3) \text{ MeV}
 \end{aligned} \tag{4.21}$$

The strategy to separate the various systematic components is same one used in the rest of this work.

The first contribution, which is the largest one, includes, not only the statistical and fit uncertainties, but also the uncertainties coming from the setting of the scale as explained in 4.2. This contribution correspond to an error of 2.9%

The chiral extrapolation systematic uncertainty has been evaluated using the difference between the results obtained using a linear or a quadratic fit and turns out to be of the order of 0.6%.

The difference between results from analysis 1 and 2, i.e. in units of r_0 or in units of M_{cs} , have been used to estimate the uncertainty coming from discretization effects, which is of the order of 1.2%.

The contributions coming from the uncertainties in the determination of the charm and strange quark masses can be quantified to be respectively of the order of 1.0% and 0.6%. The effect of the systematic uncertainty of renormalization constants, estimated from the comparison M1-M2 has a very small impact corresponding to an effect of 0.1%.

f_{D_s}/f_D : final estimate and systematics

For the ratio f_{D_s}/f_D the results coming from the various analyses are collected in table 4.7

The first two columns correspond to different fits of Φ_{D_s}/Φ_D , while the last two columns are coming from the two different fits of the double ratio $(f_{D_s}/f_D)/(f_K/f_\pi)$. Quoted errors includes the statistical error, the error associated to the fitting procedure combined also with the uncertainties in the determination of the strange and charm quark masses. For the results of the double ratio method the error was also combined with the uncertainty on our determination of the ratio $f_K/f_\pi = 1.193(16)$ presented in section 4.1.3. The latter method shows a smaller systematic effect due to the chiral

	Method 1		Method 2	
Quantity	Chiral Fit	Linear Fit	Chiral Fit	Linear Fit
f_{D_s}/f_D	1.235(20)	1.176(17)	1.204(22)	1.191(22)

Table 4.7: Results for the ratio f_{D_s}/f_D from the different branches of the analysis. The first two columns, referred to as method 1, correspond to different fits of Φ_{D_s}/Φ_D , while the last two columns, referred to as method 2, are coming from the two different fits of the double ratio $(f_{D_s}/f_D)/(f_K/f_\pi)$. The final estimate will be a combination of the results obtained with method 2 which is the procedure that exhibits the smaller chiral systematics.

extrapolation. For this reason our final result has been determined combining columns 3 and 4 only, and reads

$$\begin{aligned}
 f_{D_s}/f_D &= 1.199(17)_{stat+fit(7)Chiral(16)}f_K/f_\pi \\
 f_{D_s}/f_D &= 1.199(17)_{stat+fit(17)_{syst}} \\
 &= 1.199(25)
 \end{aligned} \tag{4.22}$$

The first contribution includes the statistical uncertainties combined with the one associated with the fitting procedure which corresponds to an effect of the 1.4%

The systematic uncertainty due to the chiral extrapolation has been taken as the difference between the results obtained using the prediction from Heavy Meson ChPT and a linear fit. In the double ratio analysis this effect is reduced to 0.5%.

In addition there is the uncertainty coming from the required input f_K/f_π , which is of the order of 1.3%.

The effect of the choice of renormalization constants method of calculation has a very small impact corresponding to an effect of 0.1%.

The double ratio method has the further advantage of having negligible discretization uncertainties. As it can be seen in fig. 4.9, discretization effects are small compared for example to the statistical errors of the data points. The a -dependence is found to be compatible with zero but its inclusion has the effect of increasing the error on the final result. For this reason we removed it from the fit. Moreover, performing the same fit in m_l without the data corresponding to the coarser lattice spacing, which are roughly half of the points, we obtain the same result.

The double ratio proved to be also very stable with respect to changes of the strange

and charm quark masses which if varied within their total error produced no changes in the result at this level of precision.

f_D determination and comparison with the FLAG averages

Combining the results obtained for f_{D_s} and f_{D_s}/f_{D_r} we can estimate f_D from our analysis, which reads:

$$f_D = 201.9(8.0)\text{MeV} \quad (4.23)$$

At the end of this section is reported a collection of the result presented for D and D_s meson decay constants as well as the FLAG's averages for $N_f = 2$, $N_f = 2+1$. Although some results for this quantities calculated in an $N_f = 2+1+1$ simulation have already been presented (see [57]) no FLAG $_{N_f=2+1+1}$ average has been released yet.

Table 4.8: Comparison between different fits

Quantity	Our Result	FLAG $_{N_f=2}$	FLAG $_{N_f=2+1}$	FLAG $_{N_f=2+1+1}$
f_{D_s} (MeV)	242.1(8.3)	248(6)	248.6(2.7)	-
f_{D_s}/f_D	1.199(25)	1.17(5)	1.187(12)	-
f_D (MeV)	201.9(8.0)	212(8)	209.2(3.3)	-

Table 4.9: Comparison of the results we found in this analysis for f_{D_s} , f_D and f_{D_s}/f_D with corresponding averages performed by FLAG [48] for $N_f = 2$, $N_f = 2+1$.

Conclusions

In this thesis we presented an accurate lattice determination of the average up/down, strange and charm quark masses and of the decay constants f_K , f_K/f_π , f_D and f_{D_s} (summarized in the Introduction), using the gauge configurations produced by the European Twisted Mass (ETM) Collaboration with four flavors of dynamical quarks ($N_f = 2+1+1$). These simulations include in the sea, besides two light mass degenerate quarks, also the strange and the charm quarks with masses close to their physical values. Let me emphasize that as far as the quark masses are concerned these are the first results obtained from an $N_f = 2 + 1 + 1$ simulation.

The value of quark masses have been determined by tuning them in such a way to reproduce the observed spectrum of pseudo-scalar mesons. For the average up-down quark mass we have analysed the pion mass, for strange quark the kaon, and for charm we used D and D_s mesons. Quark masses has been renormalized non-perturbatively in the RI-MOM scheme, and converted to physical units by fixing the lattice spacing from the pion decay constant f_π . By performing the continuum limit, the chiral extrapolation and the FSE correction through several approaches, we have been able to present results where the various sources of systematic errors are properly taken into account.

The value of quark masses have been then used as inputs in the lattice calculation of the leptonic decay constants for which a careful continuum limit, chiral extrapolation and the FSE corrections were also implemented. These decay constants in combination with the experimental measurements of appropriate leptonic decay rates provide the knowledge of the CKM matrix elements $|V_{ud}|$, $|V_{us}|$, $|V_{cd}|$ and $|V_{cs}|$ which can be used in particular to test the unitarity constraints of the first two row of the CKM matrix.

In our results, for both the quark masses and the decay constants, the chiral extrapolation, which is the extrapolations from the unphysically higher values of the simulated light quark masses to the physical point, represents an important contribution in the total systematic uncertainty. Thanks to the algorithm and action improvements, simulations

at the physical value of the light quark mass are feasible nowadays, though computationally expensive. The ETM Collaboration has already performed simulations at the physical point with two flavors of dynamical quarks ($N_f = 2$). Analogous simulation with $N_f = 2 + 1 + 1$ are planned for the near future.

Acknowledgements

I would like to thank all the people who helped me during these three years of PhD and made this thesis possible. In particular Vittorio Lubicz, for his advices and patience. I am also very grateful to Cecilia Tarantino and Silvano Simula for their precious comments and suggestions. I would finally like to thank all the people I had the chance to collaborate with during the preparation of this thesis and in particular my colleagues Paolo Lami and Eleonora Picca.

Bibliography

- [1] G. Aad *et al.* [ATLAS Collaboration], Phys. Lett. B **716** (2012) 1 [arXiv:1207.7214 [hep-ex]].
- [2] S. Chatrchyan *et al.* [CMS Collaboration], Phys. Lett. B **716** (2012) 30 [arXiv:1207.7235 [hep-ex]].
- [3] B. Blossier *et al.* [ETM Collaboration], Phys. Rev. D **82** (2010) 114513 [arXiv:1010.3659 [hep-lat]].
- [4] P. Fritzscht, F. Knechtli, B. Leder, M. Marinkovic, S. Schaefer, R. Sommer, F. Virotta and R. Sommer *et al.*, Nucl. Phys. B **865** (2012) 397 [arXiv:1205.5380 [hep-lat]].
- [5] A. Bazavov *et al.*, Rev. Mod. Phys. **82** (2010) 1349 [arXiv:0903.3598 [hep-lat]].
- [6] A. Bazavov, C. Bernard, C. DeTar, X. Du, W. Freeman, S. Gottlieb, U. M. Heller and J. E. Hetrick *et al.*, PoS LATTICE **2010** (2010) 083 [arXiv:1011.1792 [hep-lat]].
- [7] R. Arthur *et al.* [RBC and UKQCD Collaborations], Phys. Rev. D **87** (2013) 094514 [arXiv:1208.4412 [hep-lat]].
- [8] S. Aoki, K. I. Ishikawa, N. Ishizuka, K. Kanaya, Y. Kuramashi, Y. Nakamura, Y. Namekawa and M. Okawa *et al.*, Phys. Rev. D **86** (2012) 034507 [arXiv:1205.2961 [hep-lat]].
- [9] J. Laiho and R. S. Van de Water, PoS LATTICE **2011** (2011) 293 [arXiv:1112.4861 [hep-lat]].
- [10] C. T. H. Davies *et al.*, Phys. Rev. Lett. **104** (2010) 132003 [arXiv:0910.3102 [hep-ph]].

- [11] C. McNeile, C. T. H. Davies, E. Follana, K. Hornbostel and G. P. Lepage, Phys. Rev. D **82** (2010) 034512 [arXiv:1004.4285 [hep-lat]].
- [12] T. Blum, R. Zhou, T. Doi, M. Hayakawa, T. Izubuchi, S. Uno and N. Yamada, Phys. Rev. D **82** (2010) 094508 [arXiv:1006.1311 [hep-lat]].
- [13] R. Baron *et al.* [European Twisted Mass Collaboration], JHEP **1006** (2010) 111 [arXiv:1004.5284 [hep-lat]].
- [14] R. Baron *et al.* [European Twisted Mass Collaboration], Comput. Phys. Commun. **182** (2011) 299 [arXiv:1005.2042 [hep-lat]].
- [15] A. Bazavov *et al.* [MILC Coll.], Phys. Rev. D **82** (2010) 074501 [arXiv:1004.0342].
- [16] P. W. Higgs, Phys. Rev. Lett. **13** (1964) 508.
- [17] F. Englert and R. Brout, Phys. Rev. Lett. **13** (1964) 321.
- [18] N. Cabibbo, Phys. Rev. Lett. **10** (1963) 531.
- [19] M. Kobayashi and T. Maskawa, Prog. Theor. Phys. **49** (1973) 652.
- [20] C. Jarlskog, Phys. Rev. Lett. **55** (1985) 1039.
- [21] The UThit collaboration (summer 2012): <http://www.utfit.org/utfit/results>.
- [22] L. Wolfenstein, Phys. Rev. Lett. **51** (1983) 1945.
- [23] V. Cirigliano and H. Neufeld, Phys. Lett. B **700** (2011) 7 [arXiv:1102.0563 [hep-ph]].
- [24] M. Antonelli, V. Cirigliano, G. Isidori, F. Mescia, M. Moulson, H. Neufeld, E. Passemar and M. Palutan *et al.*, Eur. Phys. J. C **69** (2010) 399 [arXiv:1005.2323 [hep-ph]].
- [25] J. L. Rosner and S. Stone, arXiv:1201.2401 [hep-ex].
- [26] K. G. Wilson, Phys. Rev. D **10** (1974) 2445.
- [27] H. B. Nielsen and M. Ninomiya, Phys. Lett. B **105** (1981) 219.
- [28] K. Symanzik, Nucl. Phys. B **226** (1983) 187.
- [29] Y. Iwasaki, Nucl. Phys. B **258** (1985) 141.

- [30] R. Frezzotti and G. C. Rossi, JHEP **0408** (2004) 007 [hep-lat/0306014].
- [31] R. Frezzotti and G. C. Rossi, JHEP **0410** (2004) 070 [hep-lat/0407002].
- [32] S. Aoki and A. Gocksch, Phys. Lett. B **231** (1989) 449.
- [33] R. Frezzotti and G. C. Rossi, Nucl. Phys. Proc. Suppl. **128** (2004) 193 [hep-lat/0311008].
- [34] A. Bazavov *et al.* [MILC Collaboration], Phys. Rev. D **87** (2013) 054505 [arXiv:1212.4768 [hep-lat]].
- [35] R. Frezzotti *et al.* [Alpha Collaboration], JHEP **0108** (2001) 058 [hep-lat/0101001].
- [36] K. Osterwalder and E. Seiler, Annals Phys. **110** (1978) 440.
- [37] B. Jegerlehner, arXiv:hep-lat/9612014.
- [38] K. Jansen, M. Papinutto, A. Shindler, C. Urbach and I. Wetzorke [XLF Coll.], JHEP **0509** (2005) 071 [arXiv:hep-lat/0507010].
- [39] C. McNeile and C. Michael [UKQCD Coll.], Phys. Rev. D **73** (2006) 074506 [hep-lat/0603007].
- [40] J. Gasser and H. Leutwyler, Phys. Lett. B **184** (1987) 83.
- [41] G. Colangelo, S. Durr and C. Haefeli, Nucl. Phys. B **721** (2005) 136 [arXiv:hep-lat/0503014].
- [42] G. Colangelo, U. Wenger and J. M. S. Wu, Phys. Rev. D **82** (2010) 034502 [arXiv:1003.0847 [hep-lat]].
- [43] R. Baron *et al.* [ETM Collaboration], PoS LATTICE **2010** (2010) 123 [arXiv:1101.0518 [hep-lat]].
- [44] O. Bar, Phys. Rev. D **82** (2010) 094505 [arXiv:1008.0784 [hep-lat]].
- [45] G. Herdoiza, K. Jansen, C. Michael, K. Ottnad and C. Urbach, JHEP **1305** (2013) 038 [arXiv:1303.3516 [hep-lat]].
- [46] G. Colangelo and C. Haefeli, Nucl. Phys. B **744** (2006) 14 [arXiv:hep-lat/0602017].

- [47] K. Ottnad *et al.* [ETM Collaboration], JHEP **1211** (2012) 048 [arXiv:1206.6719 [hep-lat]].
- [48] See the sections of the online version of the update of the FLAG review available at <http://itpwiki.unibe.ch/flag/>.
For the presently published version of the FLAG review see:
G. Colangelo, S. Durr, A. Juttner, L. Lellouch, H. Leutwyler, V. Lubicz, S. Necco and C. T. Sachrajda *et al.*, Eur. Phys. J. C **71** (2011) 1695 [arXiv:1011.4408 [hep-lat]].
- [49] E. E. Scholz, S. Borsanyi, S. Durr, Z. Fodor, S. Krieg, A. Schfer and K. K. Szabo, PoS ConfinementX (2012) 111 [arXiv:1301.7557 [hep-lat]].
- [50] ETM Collaboration, in preparation.
- [51] O. Bar and B. Horz, arXiv:1308.3366 [hep-lat].
- [52] G. M. de Divitiis, P. Dimopoulos, R. Frezzotti, V. Lubicz, G. Martinelli, R. Petronzio, G. C. Rossi and F. Sanfilippo *et al.*, JHEP **1204** (2012) 124 [arXiv:1110.6294 [hep-lat]].
- [53] J. Beringer *et al.* [Particle Data Group], Phys. Rev. D **86** (2012) 010001 and 2013 partial update for the 2014 edition.
- [54] G. M. de Divitiis, R. Frezzotti, V. Lubicz, G. Martinelli, R. Petronzio, G. C. Rossi, F. Sanfilippo and S. Simula *et al.*, Phys. Rev. D **87** (2013) 114505 [arXiv:1303.4896 [hep-lat]].
- [55] D. Becirevic, S. Fajfer, S. Prelovsek and J. Zupan, Phys. Lett. B **563** (2003) 150 [hep-ph/0211271].
- [56] K. Nakamura *et al.* [Particle Data Group Collaboration], J. Phys. G G **37** (2010) 075021.
- [57] A. Bazavov *et al.* [Fermilab Lattice and MILC Collaborations], PoS LATTICE **2012** (2012) 159 [arXiv:1210.8431 [hep-lat]].